Fracture Mechanics

A Collection of Data

Collected and Edited by

Prof. Mordechai Perl

*Griffith's** Fracture Criterion

The Energy Balance Approach

Incipient fracture in ideally brittle materials occurs when the magnitude of the elastic energy supplied at the crack tip during an incremented increase in the crack length is equal to or greater than the magnitude of the elastic-surface energy required to create the new surface area of the crack.

---

* A. A. Griffith, "The Phenomena of Rupture and Flow in Solids," Philosophical Transactions of the Royal Society of London, Series A, Vol. 221, 1921, pp. 163-198.

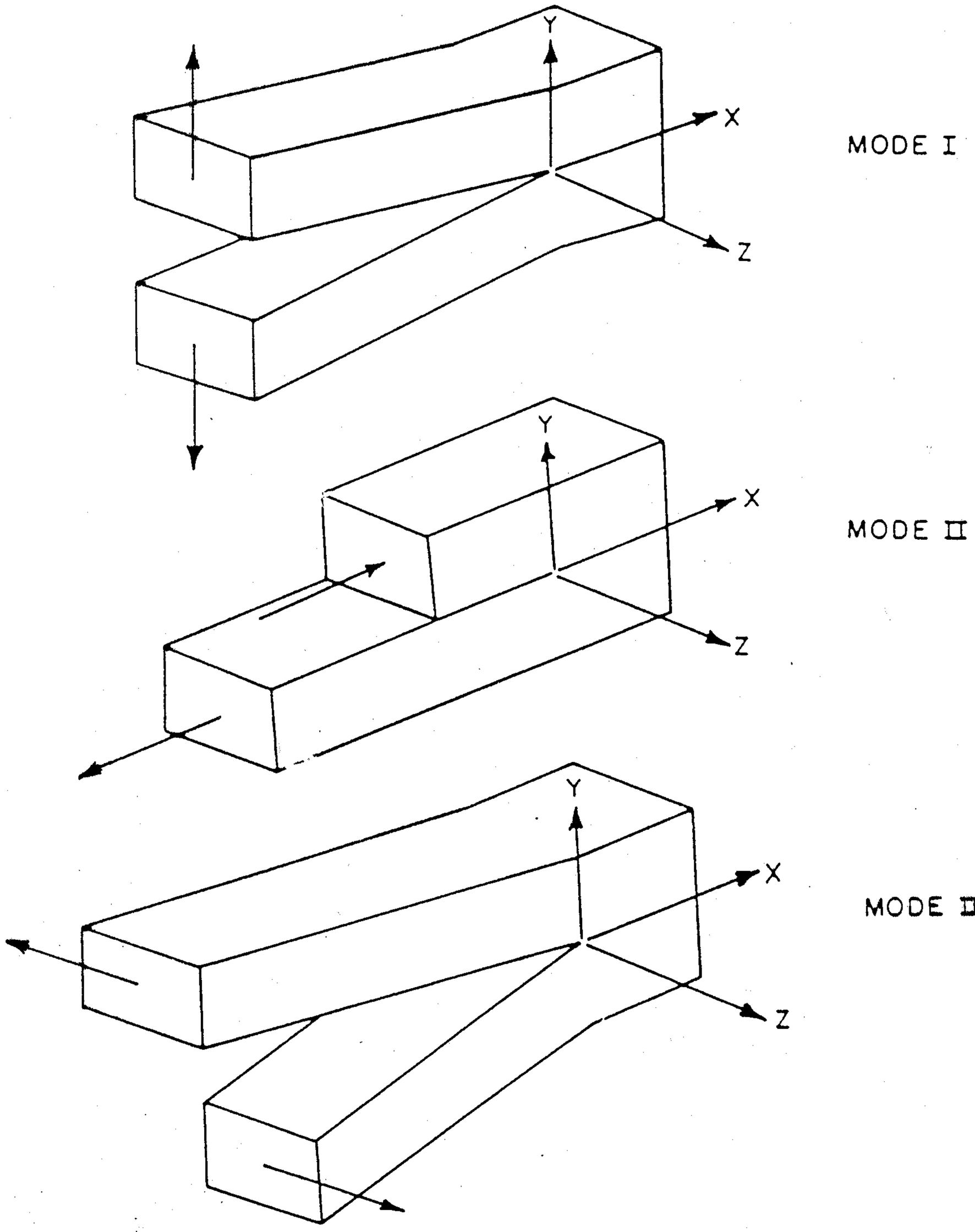


FIG. 2.1. The three basic modes of crack surface displacements

2.2.1. *Modes de sollicitations*

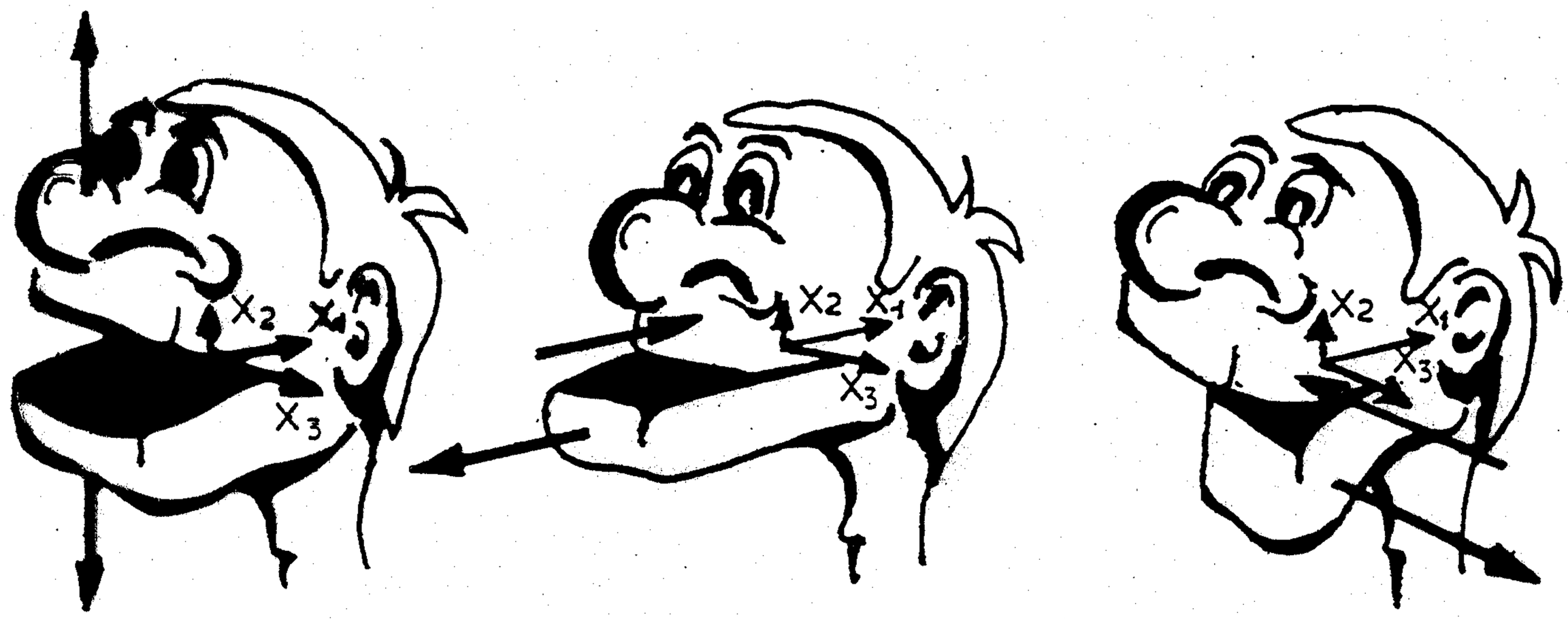


Fig. 2. Modes de sollicitations d'une fissure (dessins de Bill Bocquet).

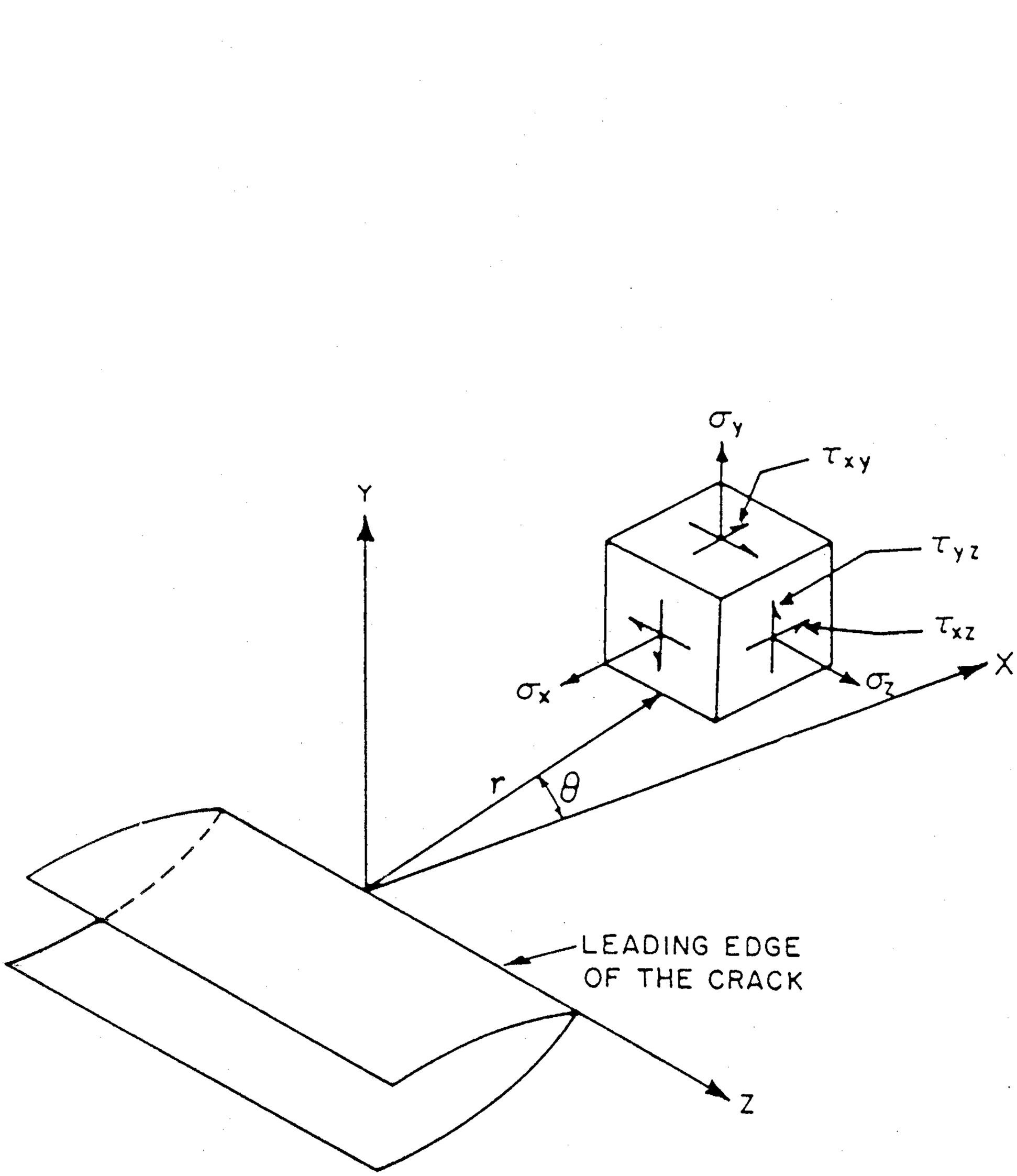


FIG. 2.2. Coordinate system and stress components ahead of a crack tip

Mode I:

$$\sigma_x = \frac{K_I}{(2\pi r)^{1/2}} \cos\frac{\theta}{2}\left[1 - \sin\frac{\theta}{2}\sin\frac{3\theta}{2}\right]$$

$$\sigma_y = \frac{K_I}{(2\pi r)^{1/2}} \cos\frac{\theta}{2}\left[1 + \sin\frac{\theta}{2}\sin\frac{3\theta}{2}\right]$$

$$\tau_{xy} = \frac{K_I}{(2\pi r)^{1/2}} \sin\frac{\theta}{2}\cos\frac{\theta}{2}\cos\frac{3\theta}{2}$$

$$\sigma_z = \nu(\sigma_x + \sigma_y), \qquad \tau_{xz} = \tau_{yz} = 0$$

$$u = \frac{K_I}{G}\left[\frac{r}{2\pi}\right]^{1/2} \cos\frac{\theta}{2}\left[1 - 2\nu + \sin^2\frac{\theta}{2}\right]$$

$$v = \frac{K_I}{G}\left[\frac{r}{2\pi}\right]^{1/2} \sin\frac{\theta}{2}\left[2 - 2\nu - \cos^2\frac{\theta}{2}\right]$$

$$w = 0$$

Mode II:

$$\sigma_x = -\frac{K_{II}}{(2\pi r)^{1/2}} \sin\frac{\theta}{2}\left[2 + \cos\frac{\theta}{2}\cos\frac{3\theta}{2}\right]$$

$$\sigma_y = \frac{K_{II}}{(2\pi r)^{1/2}} \sin\frac{\theta}{2}\cos\frac{\theta}{2}\cos\frac{3\theta}{2}$$

$$\tau_{xy} = \frac{K_{II}}{(2\pi r)^{1/2}} \cos\frac{\theta}{2}\left[1 - \sin\frac{\theta}{2}\sin\frac{3\theta}{2}\right]$$

$$\sigma_z = \nu(\sigma_x + \sigma_y), \qquad \tau_{xz} = \tau_{yz} = 0$$

$$u = \frac{K_{II}}{G}\left[\frac{r}{2\pi}\right]^{1/2} \sin\frac{\theta}{2}\left[2 - 2\nu + \cos^2\frac{\theta}{2}\right]$$

$$v = \frac{K_{II}}{G}\left[\frac{r}{2\pi}\right]^{1/2} \cos\frac{\theta}{2}\left[-1 + 2\nu + \sin^2\frac{\theta}{2}\right]$$

$$w = 0$$

Mode III:

$$\tau_{xz} = -\frac{K_{III}}{(2\pi r)^{1/2}} \sin\frac{\theta}{2}$$

$$\tau_{yz} = \frac{K_{III}}{(2\pi r)^{1/2}} \cos\frac{\theta}{2}$$

$$\sigma_x = \sigma_y = \sigma_z = \tau_{xy} = 0$$

$$w = \frac{K_{III}}{G}\left[\frac{2r}{\pi}\right]^{1/2} \sin\frac{\theta}{2}$$

$$u = v = 0$$

*Irwin's*** Fracture Criterion

The Stress Approach

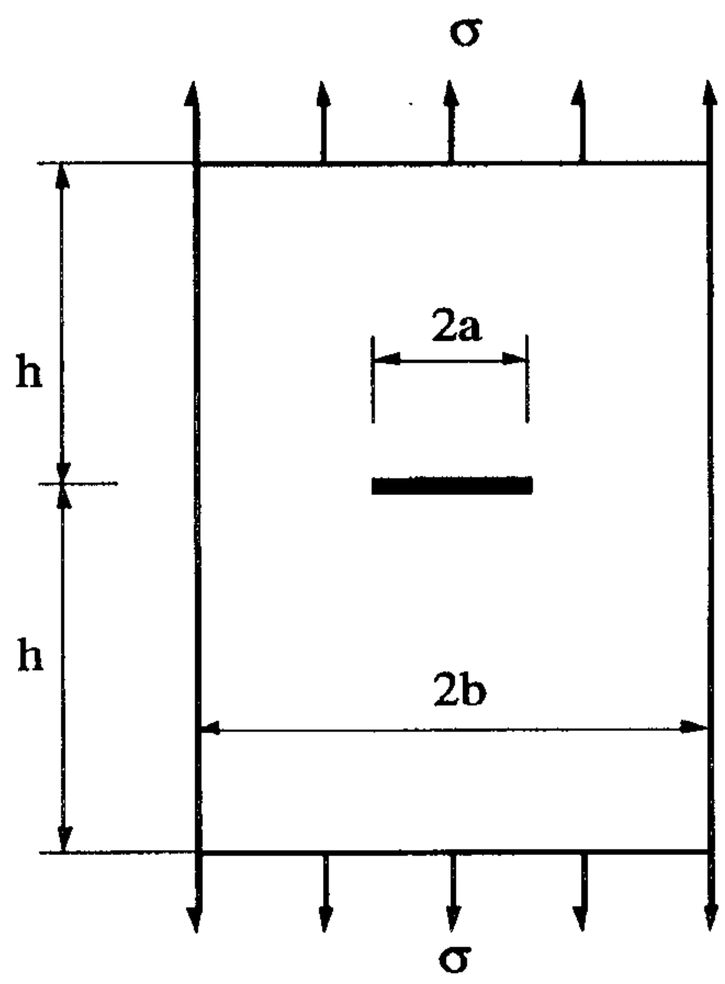
Onset of fracture occurs when the magnitude of the stress intensity factor prevailing at the crack tip reaches its critical value - the material toughness.

** G.R. Irwin "Analysis of Stresses and Strains Near the End of a Crack Traversing a Plate," *Journal of Applied Mechanics*, Vol. 24, 1957, pp. 361-364.

Example #1 – Evaluation of Residual Strength

A centrally cracked steel plate, made of SAE 4340, is loaded in tension as described in the figure. The crack length is 2a=2mm

What is the *residual strength* of the plate?



SAE 4340 Properties

Yield stress: $\sigma_y = 185\,Kg/mm^2$

Fracture Toughness: $K_{Ic} = 150\,Kg/mm^{-3/2}$

Example #2 – Material Selection

Design an aeronautical plate subjected to uniform tensile stress, as shown in example #1. The safety factor of 2, with respect to σ_u, is prescribed. The NDT method used after fabrication is such that the maximum possible crack in the plate is no longer than 2a=0.2". Three candidate materials, of similar specific strength σ_u/ρ, are considered for the plate. The material properties are given in the table below:

Property / Material	$\frac{\sigma_u}{\rho}[in]$	$\sigma_u[ksi]$	$K_{Ic}\left[ksi\sqrt{in}\right]$	$\eta_u = \frac{\sigma_u}{\sigma_w}$	$\eta_f = \frac{\sigma_f}{\sigma_w}$	$\frac{K_{Ic}}{\sigma_u}\left[\sqrt{in}\right]$
Steel	880	250	100	2	1.43	0.40
Aluminum	870	85	30	2	1.25	0.35
Titanium	860	140	80	2	2.09	0.57

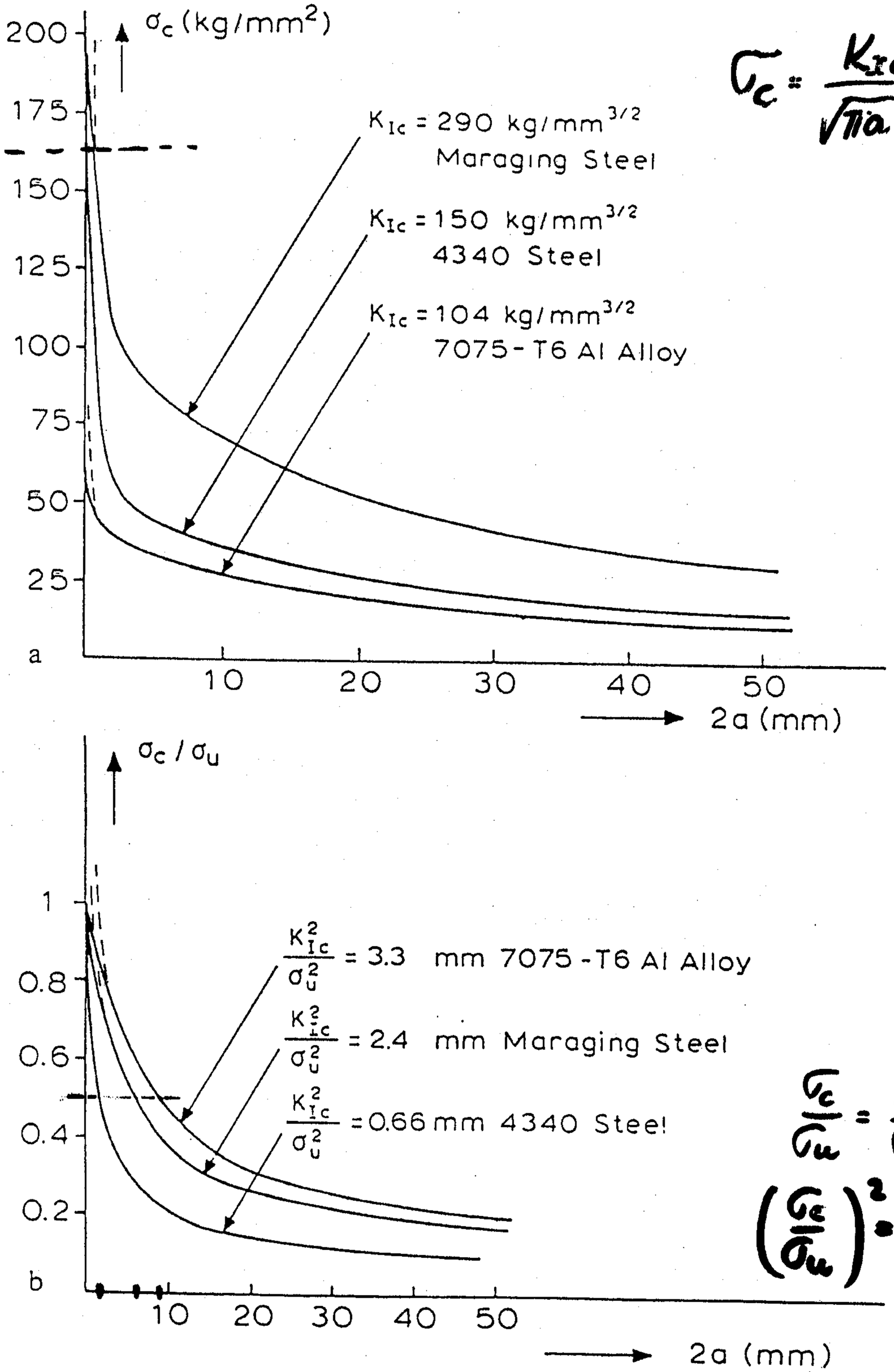
Determine the safety factor for fracture failure for each of the above materials.

Example #3 –Comparison between Materials

Property Material	σ_u [Kg/mm^2]	K_{Ic} [$Kg\ mm^{-3/2}$]
Al 7075-T6	57	104
Mar 300	188	290
SAE 4340	185	150

Example #3 –Comparison between Materials (b)

σ_c σ_u



$$\sigma_c = \frac{K_{Ic}}{\sqrt{\pi a}}$$

$$\frac{\sigma_c}{\sigma_u} = \frac{K_{Ic}}{\sigma_u} \cdot \frac{1}{\sqrt{\pi a}}$$

$$\left(\frac{\sigma_c}{\sigma_u}\right)^2 = \left(\frac{K_{Ic}}{\sigma_u}\right)^2 \frac{1}{\pi a}$$

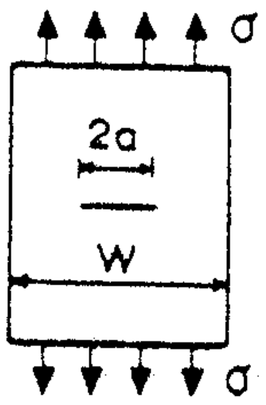
Figure 1.7. Crack toughness of three high strength materials
a. Residual strength as a function of crack size; b. Relative residual strength

EXAMPLE # 4 MAXIMUM TOLERATED CRACK LENGTH

Property / Material	σ_u [Kg/mm²]	K_{IC} [Kg . mm$^{-3/2}$]	Tolerated Crack 2a [mm]
7075-T6 Al alloy	57	104	8.46
Maraging 300 Steel	188	290	6.04
4340 Steel	185	150	1.67

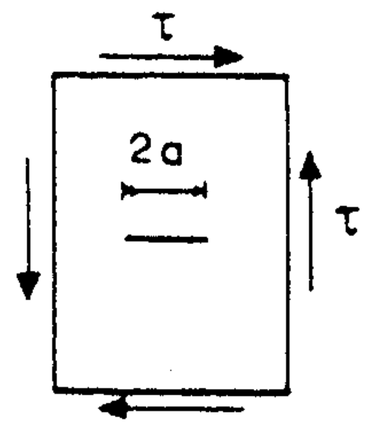
TABLE 3.1

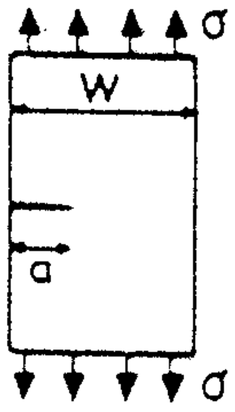
K for practical geometries



$$K_I = \sigma\sqrt{\pi a}\left(\sec\frac{\pi a}{W}\right)^{1/2}$$

$$K_{II} = \tau\sqrt{\pi a}\left(\text{small}\,\frac{a}{W}\right)$$



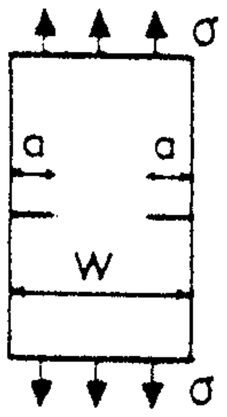


$$K_I = 1.12\,\sigma\sqrt{\pi a}\left(\text{small}\,\frac{a}{W}\right)$$

or $K_I = Y\sigma\sqrt{a}$

with $Y = 1.99 - 0.41\frac{a}{W} + 18.7\left(\frac{a}{W}\right)^2 - 38.48\left(\frac{a}{W}\right)^3 + 53.85\left(\frac{a}{W}\right)^4$

$\left(1.99 = 1.12\sqrt{\pi}\right)$

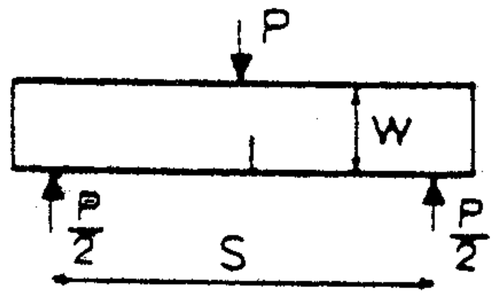


$$K_I = 1.12\,\sigma\sqrt{\pi a}\left(\text{small}\,\frac{a}{W}\right)$$

or $K_I = Y\sigma\sqrt{a}$

with $Y = 1.99 + 0.76\frac{a}{W} - 8.48\left(\frac{a}{W}\right)^2 + 27.36\left(\frac{a}{W}\right)^3$

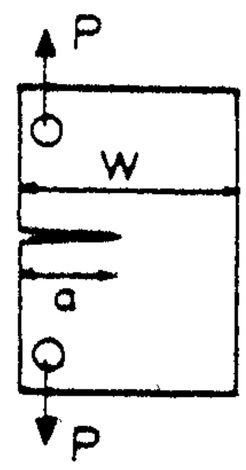
$\left(1.99 = 1.12\sqrt{\pi}\right)$



Thickness B

$$K_I = \frac{PS}{BW^{3/2}}\left[2.9\left(\frac{a}{W}\right)^{1/2} - 4.6\left(\frac{a}{W}\right)^{3/2} + 21.8\left(\frac{a}{W}\right)^{5/2} - \right.$$

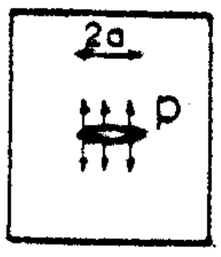
$$\left. - 37.6\left(\frac{a}{W}\right)^{7/2} + 38.7\left(\frac{a}{W}\right)^{9/2}\right]$$



Thickness B

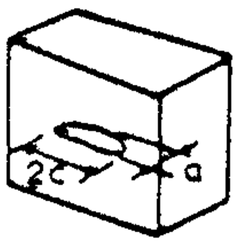
$$K_I = \frac{P}{BW^{1/2}}\left[29.6\left(\frac{a}{W}\right)^{1/2} - 185.5\left(\frac{a}{W}\right)^{3/2} + \right.$$

$$\left. + 655.7\left(\frac{a}{W}\right)^{5/2} - 1017\left(\frac{a}{W}\right)^{7/2} + 63.9\left(\frac{a}{W}\right)^{9/2}\right]$$



p per unit thickness

$K_I = p\sqrt{\pi a}$



$$K_{I_{max}} = 1.12\frac{\sigma}{\Phi}\sqrt{\pi a}$$

$$K_{I_{min}} = 1.12\frac{\sigma}{\Phi}\sqrt{\pi a^2/c}$$

$$\Phi = \int_0^{\pi/2}\left[1 - \frac{c^2 - a^2}{c^2}\sin^2\varphi\right]d\varphi$$

$$\Phi \approx \frac{3\pi}{8} + \frac{\pi}{8}\frac{a^2}{c^2}$$

5.2

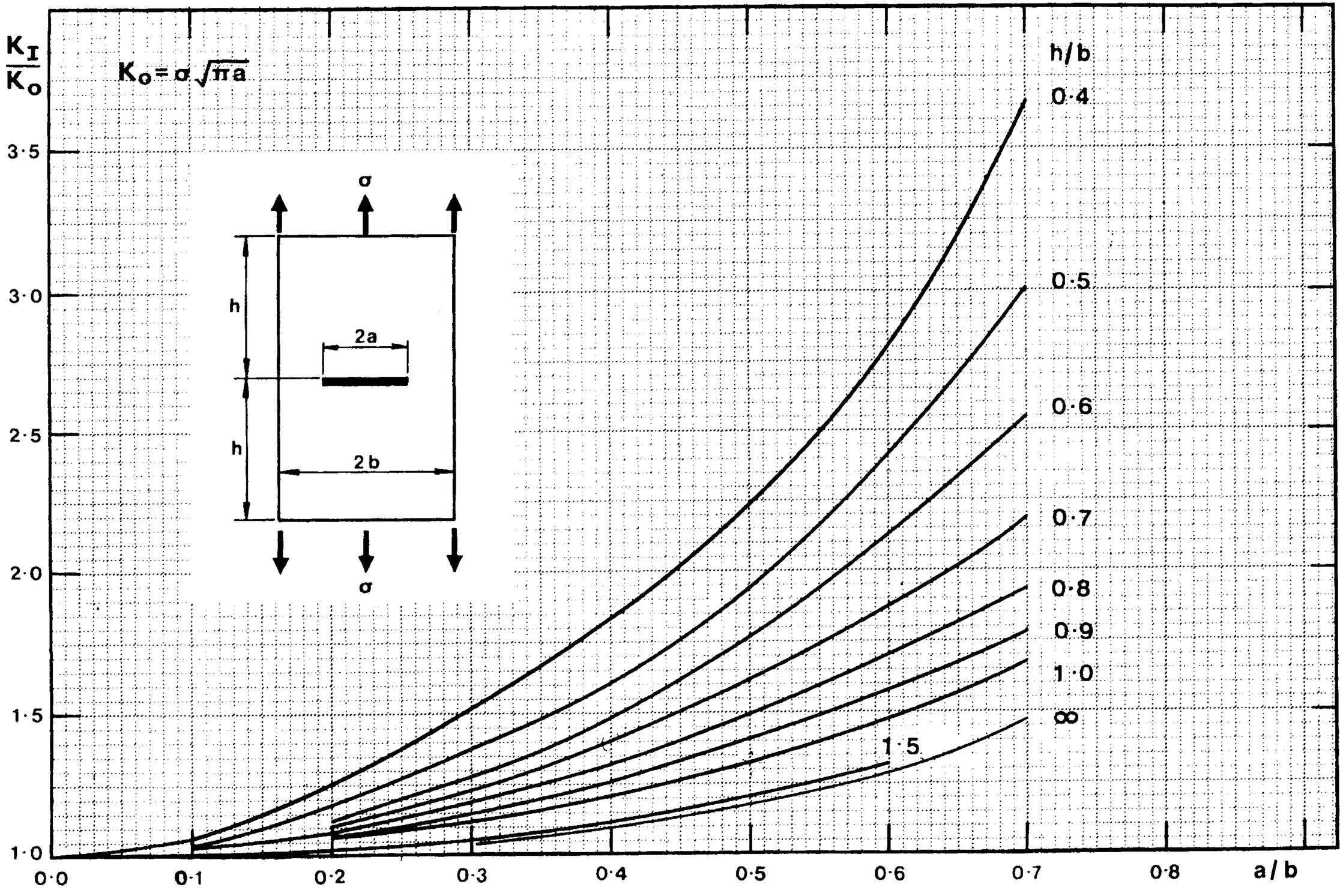


Fig.1 K_I for a central crack in a rectangular sheet subjected to a uniform uniaxial tensile stress

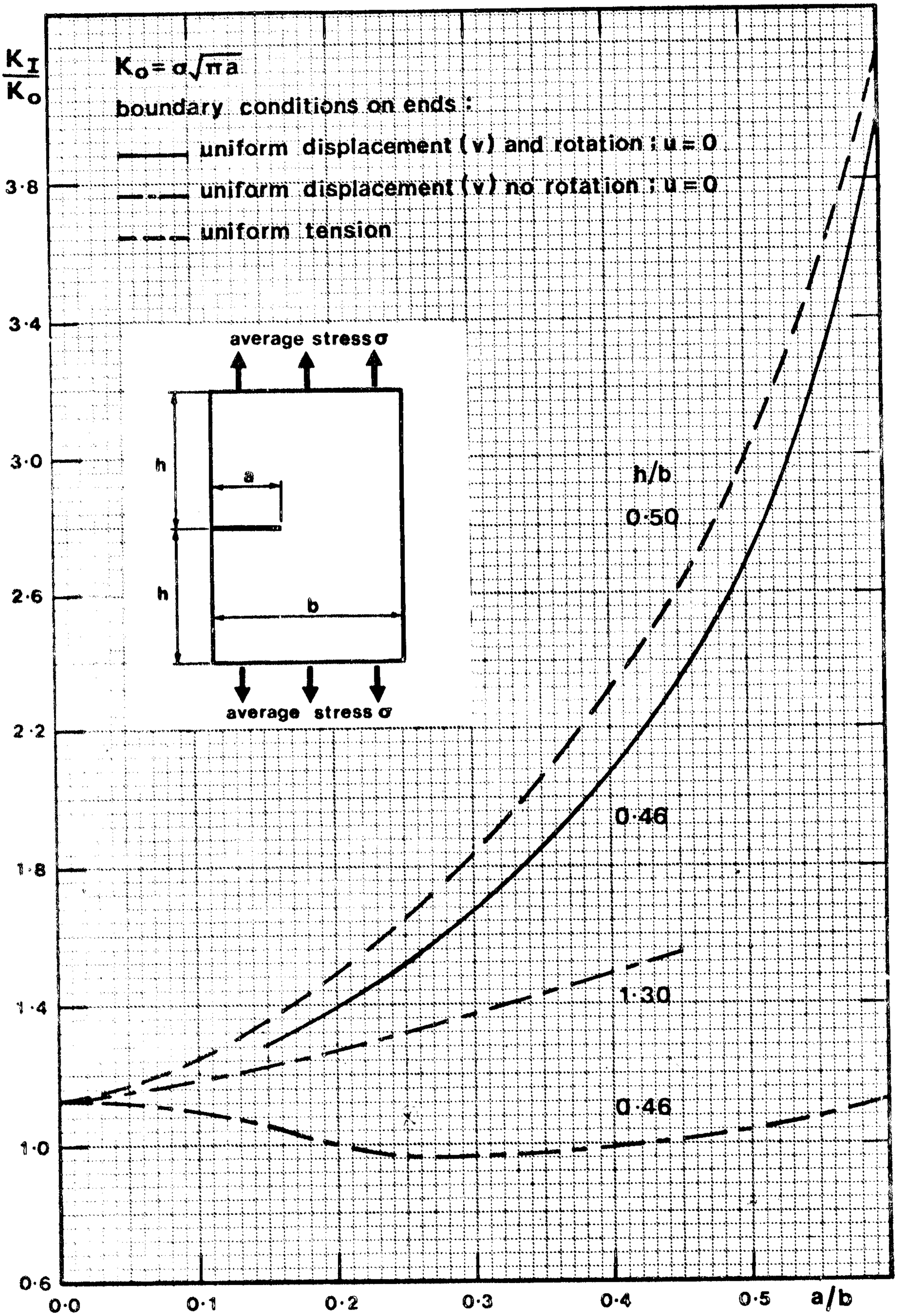


Fig.57 K_I for an edge crack in a rectangular sheet subjected to a uniform normal displacement

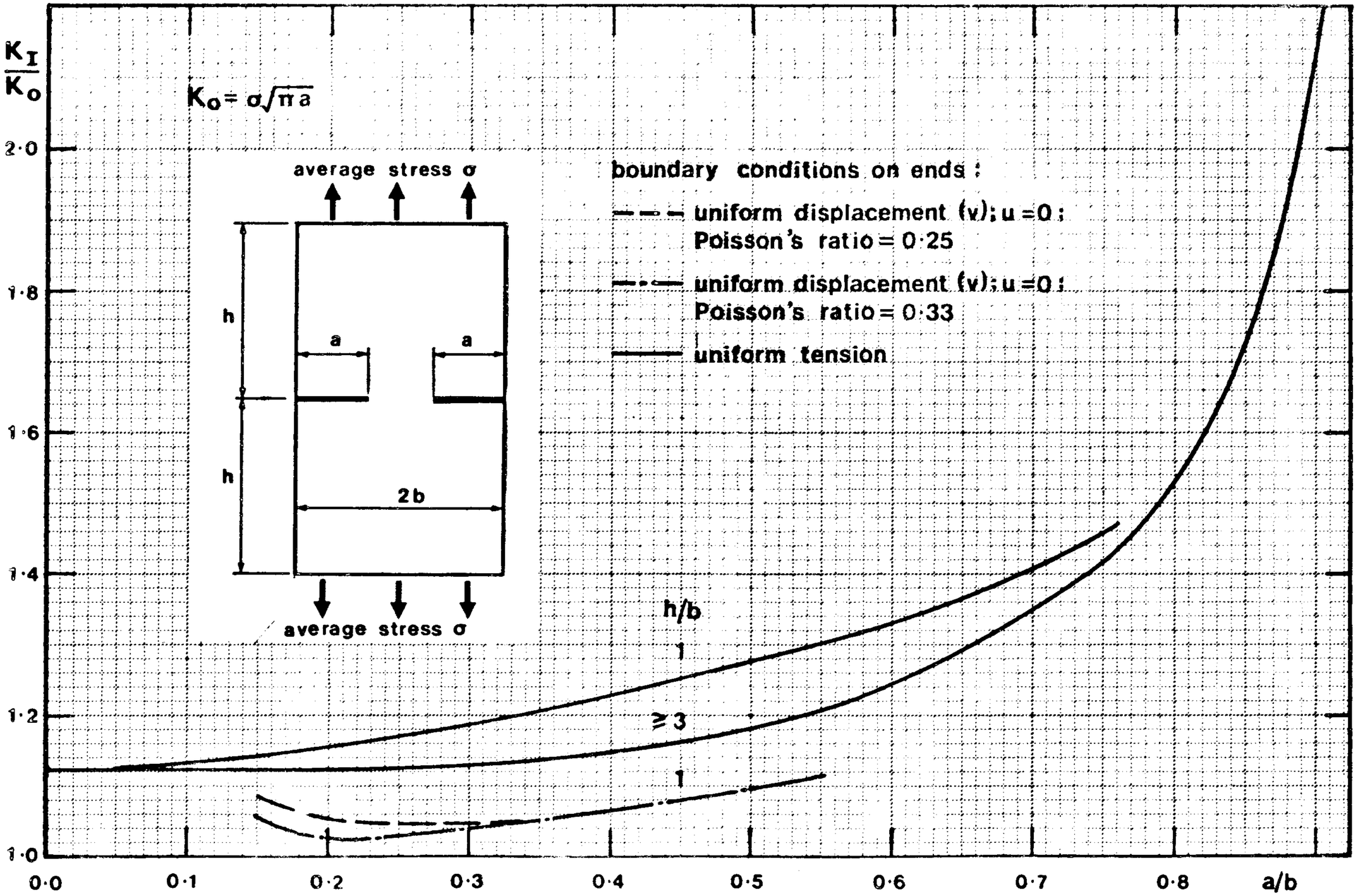


Fig.72 K_I for two edge cracks in a rectangular sheet subjected to a uniform uniaxial tensile stress or a uniform normal displacement

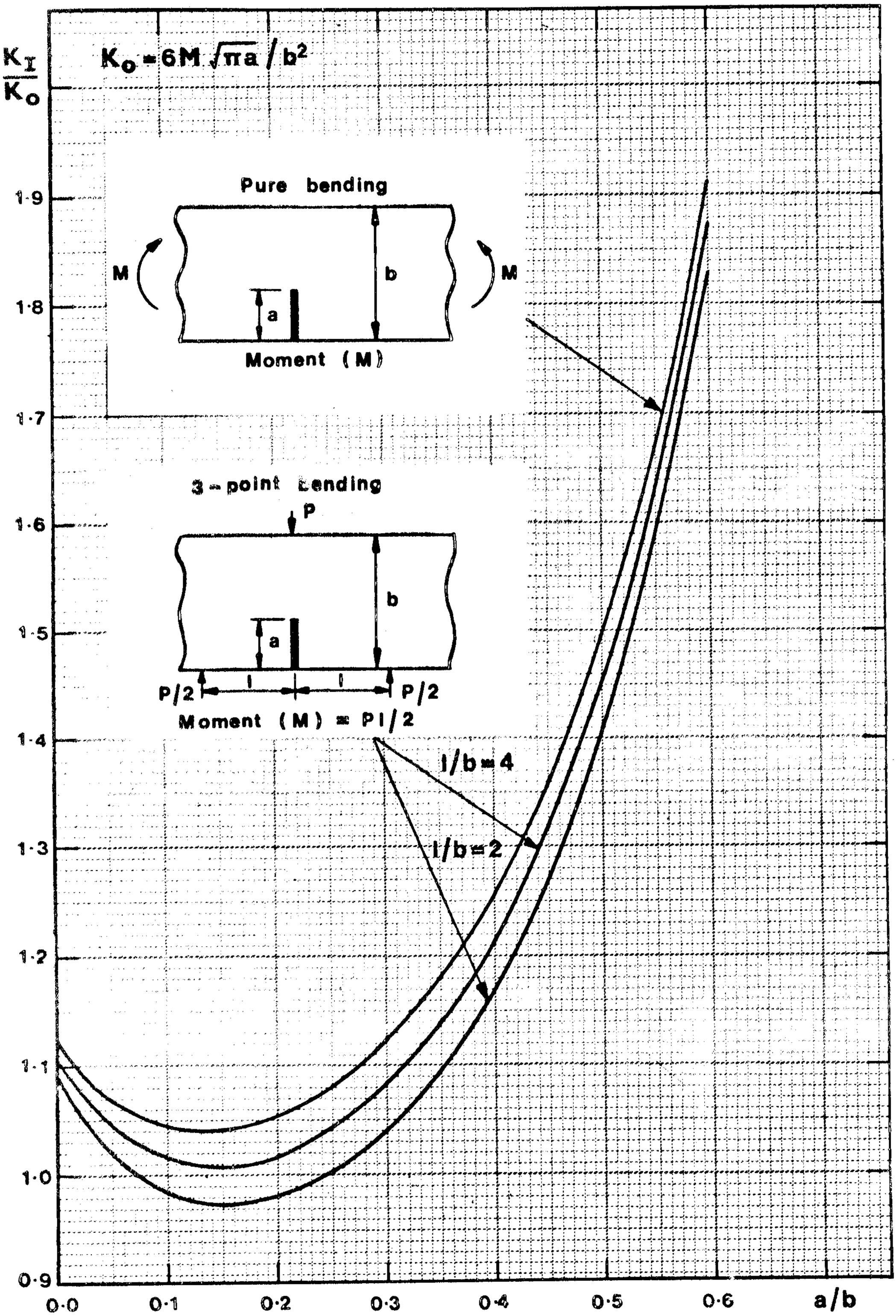


Fig.56 K_I for an edge crack in a finite width sheet subjected to pure bending or three point bending

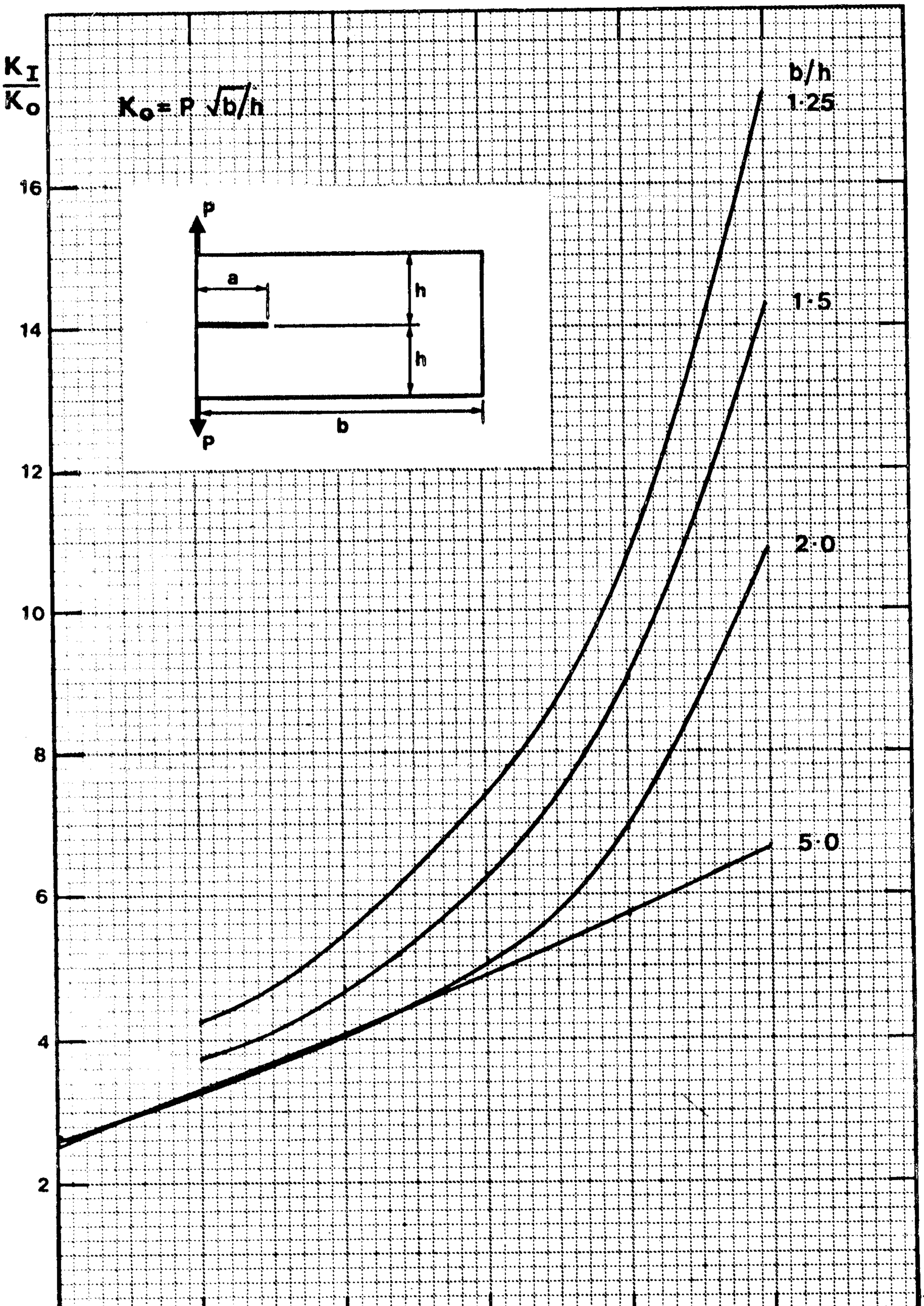


Fig.64 K_1 for an edge crack in a rectangular sheet subjected to splitting forces

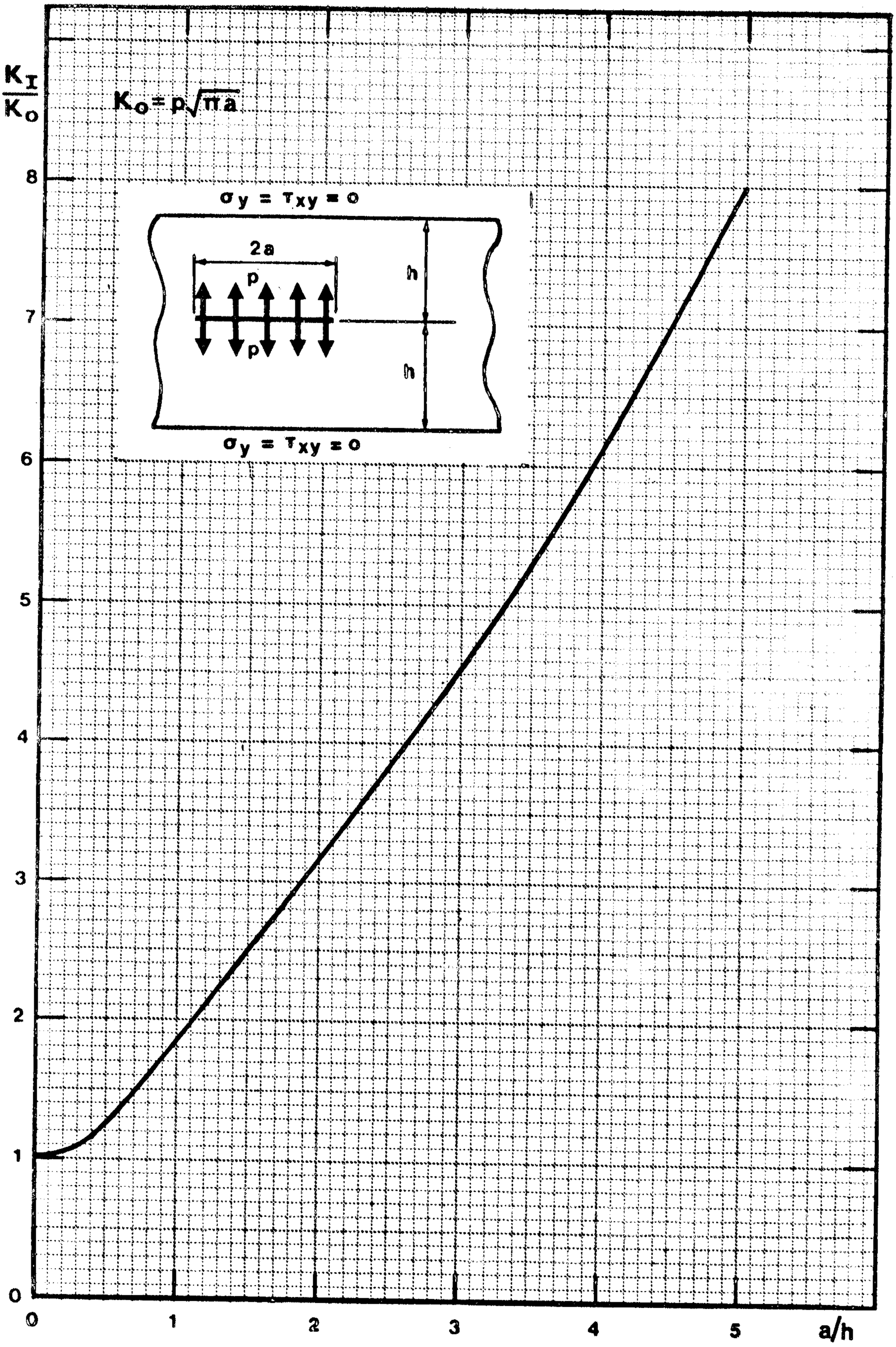


Fig.7 K_I for a crack subjected to a uniform internal pressure in a finite height sheet

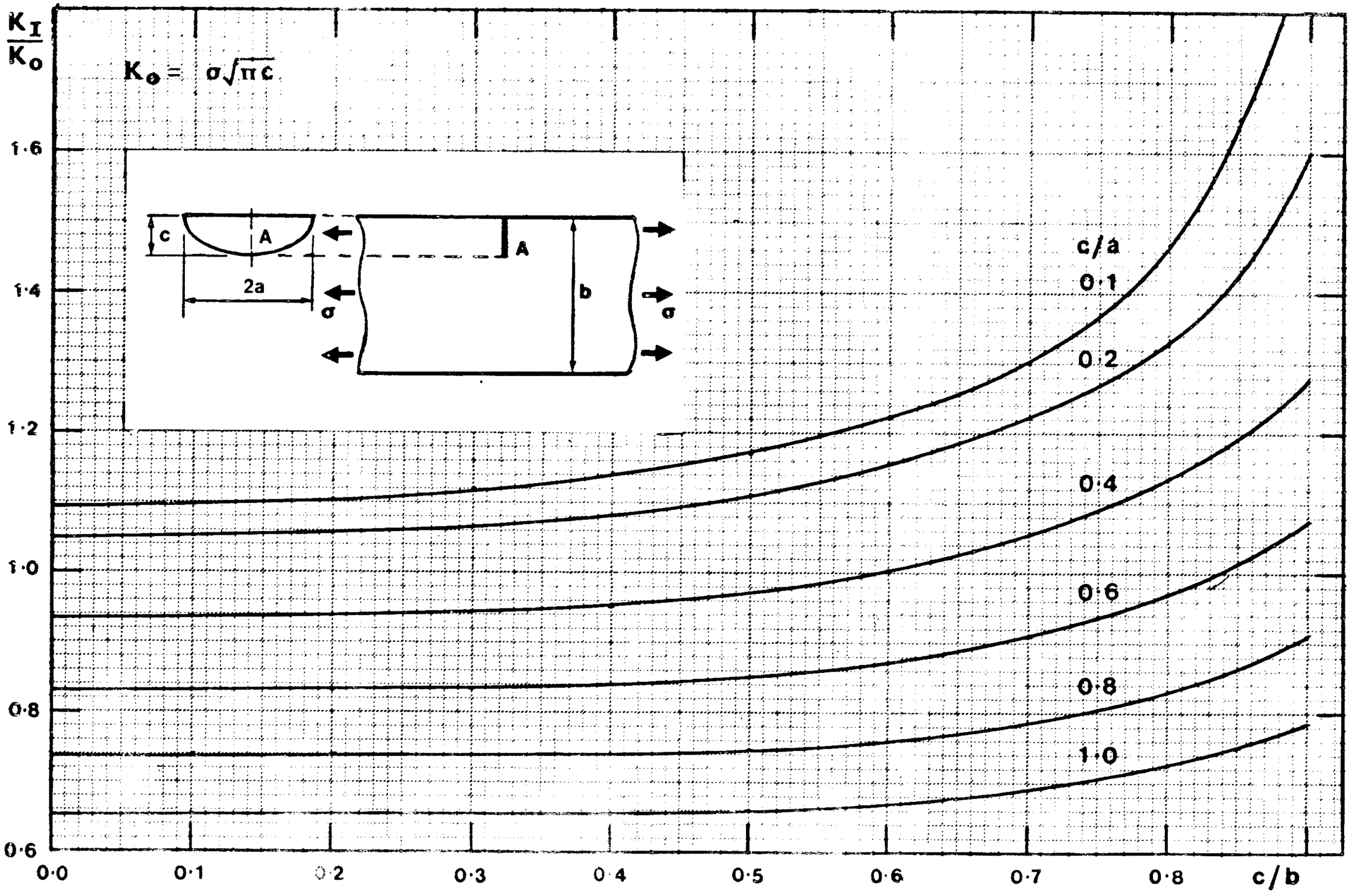


Fig.186 K_I for point A on a semi-elliptical edge crack in a slab subjected to a uniform uniaxial tensile stress

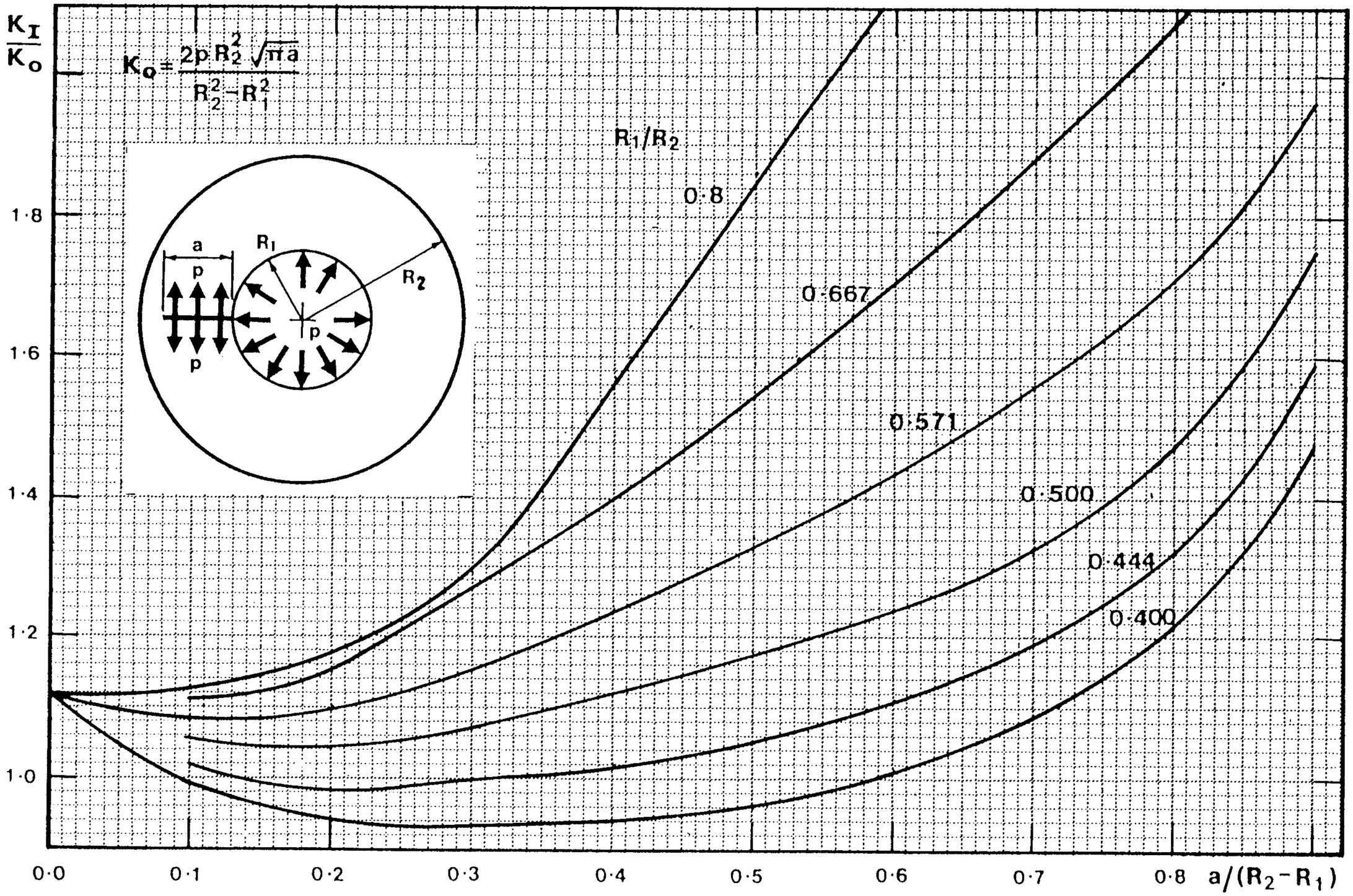
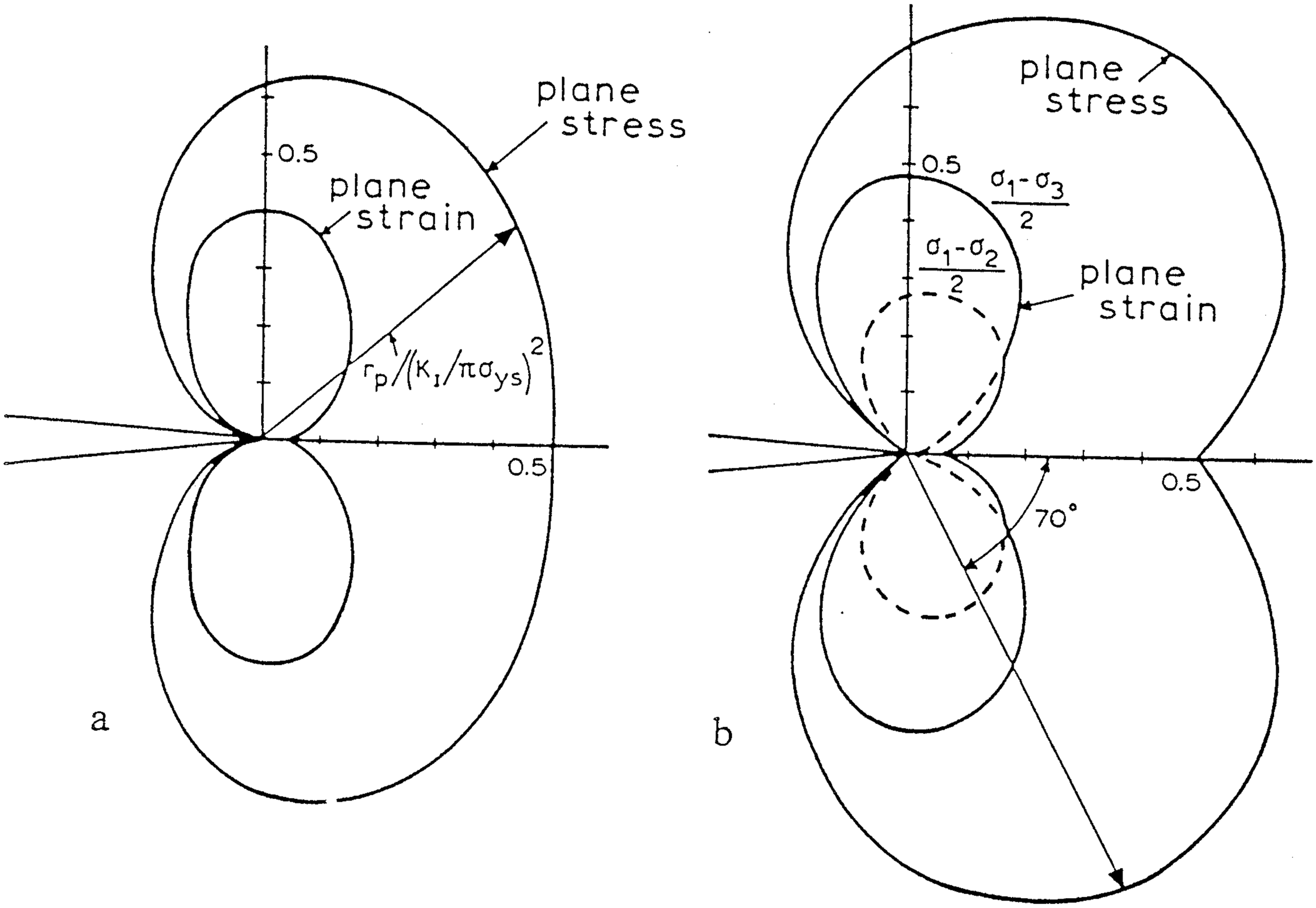


Fig.160 K_I for a pressurised internal radial edge crack in a tube subjected to a uniform internal pressure

crack tip plastic zone



Plastic zone shapes according to Von Mises and Tresca yield criteria
a. Von Mises criterion; b. Tresca criterion

Von Mises

$$\text{Plane strain: } r_p(\theta) = \frac{K^2}{4\pi\sigma_{ys}^2}\left[\tfrac{3}{2}\sin^2\theta + (1-2\nu)^2(1+\cos\theta)\right]$$

$$\text{Plane stress: } r_p(\theta) = \frac{K^2}{4\pi\sigma_{ys}^2}\left[1+\tfrac{3}{2}\sin^2\theta+\cos\theta\right].$$

Tresca

$$\text{Plane stress: } r_p = \frac{K^2}{2\pi\sigma_{ys}^2}\left[\cos\frac{\theta}{2}\left(1+\sin\frac{\theta}{2}\right)\right]^2$$

Plane strain: the larger of

$$r_p = \frac{K^2}{2\pi\sigma_{ys}^2}\cos^2\frac{\theta}{2}\left[1-2\nu+\sin\frac{\theta}{2}\right]^2 \text{ and } r_p = \frac{K^2}{2\pi\sigma_{ys}^2}\cos^2\frac{\theta}{2}.$$

The crack tip plastic zone

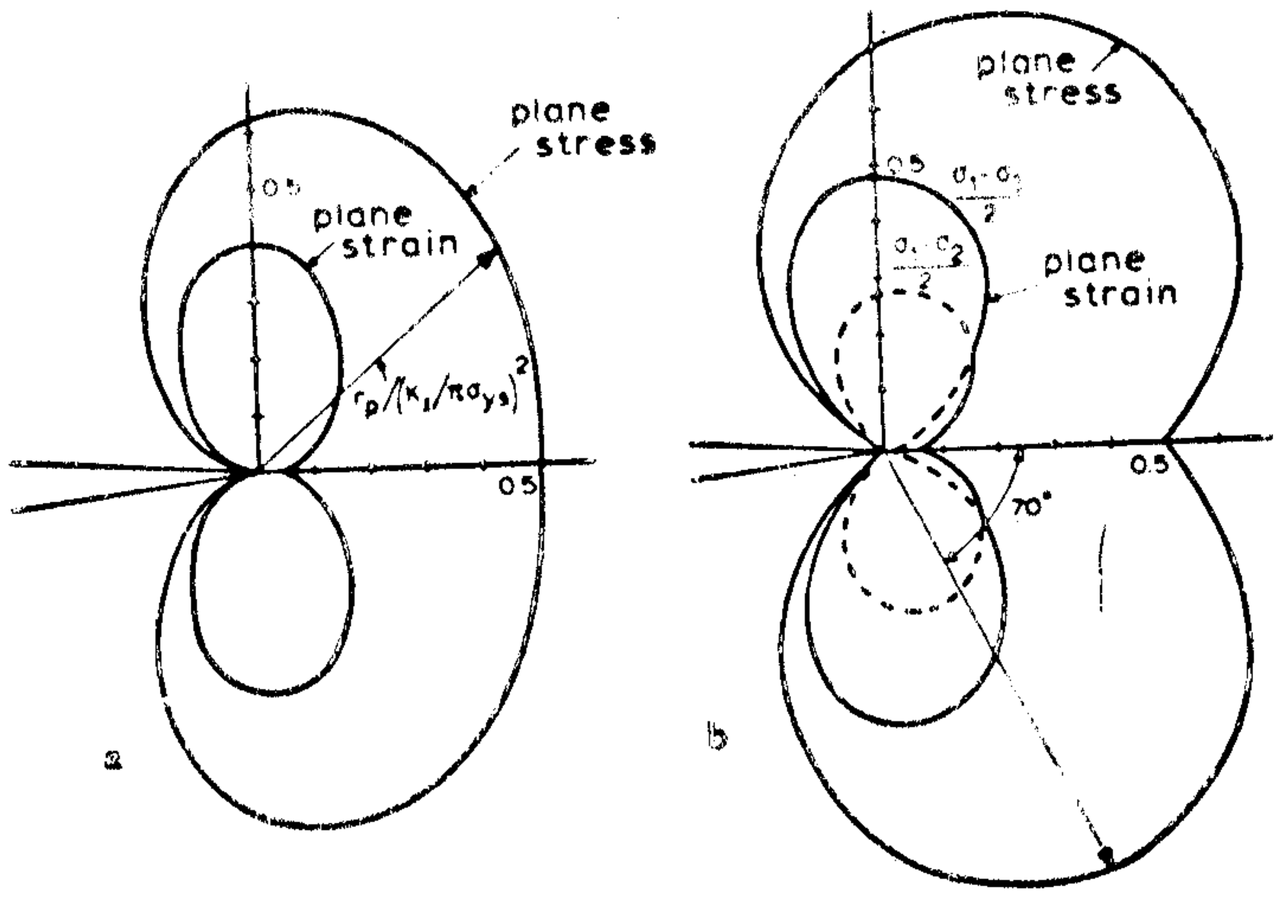


Figure 4.5. Plastic zone shapes according to Von Mises and Tresca yield criteria
a. Von Mises criterion; b. Tresca criterion

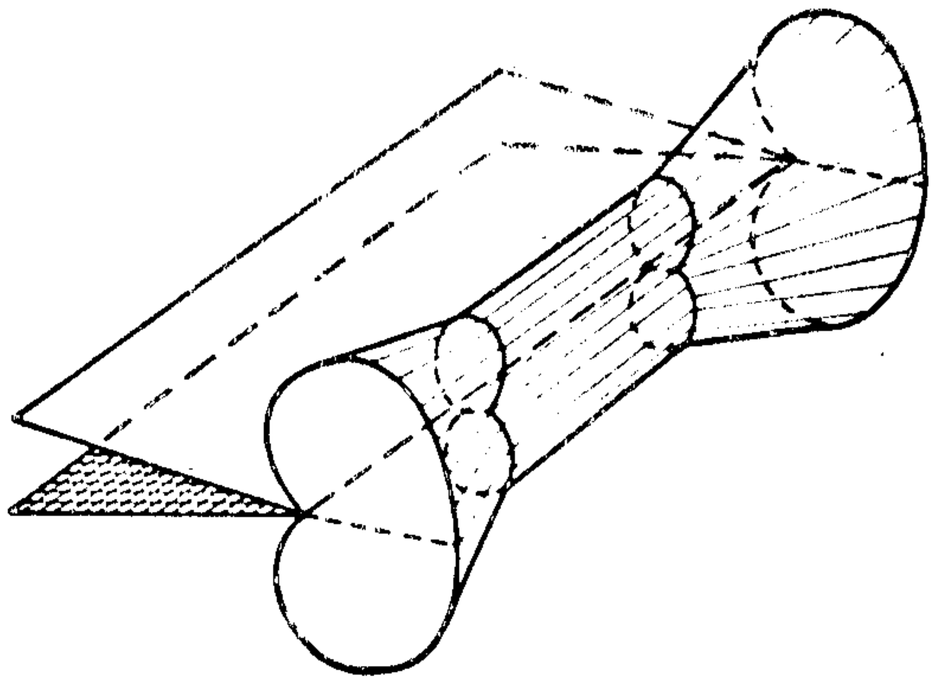


Figure 4.10. Three-dimensional plastic zone

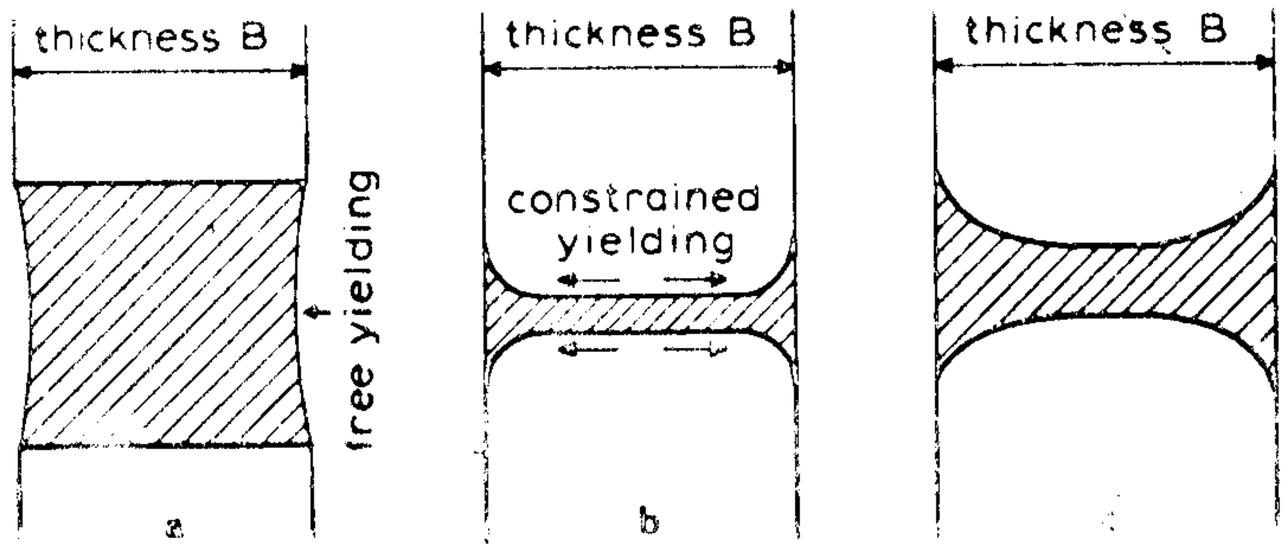
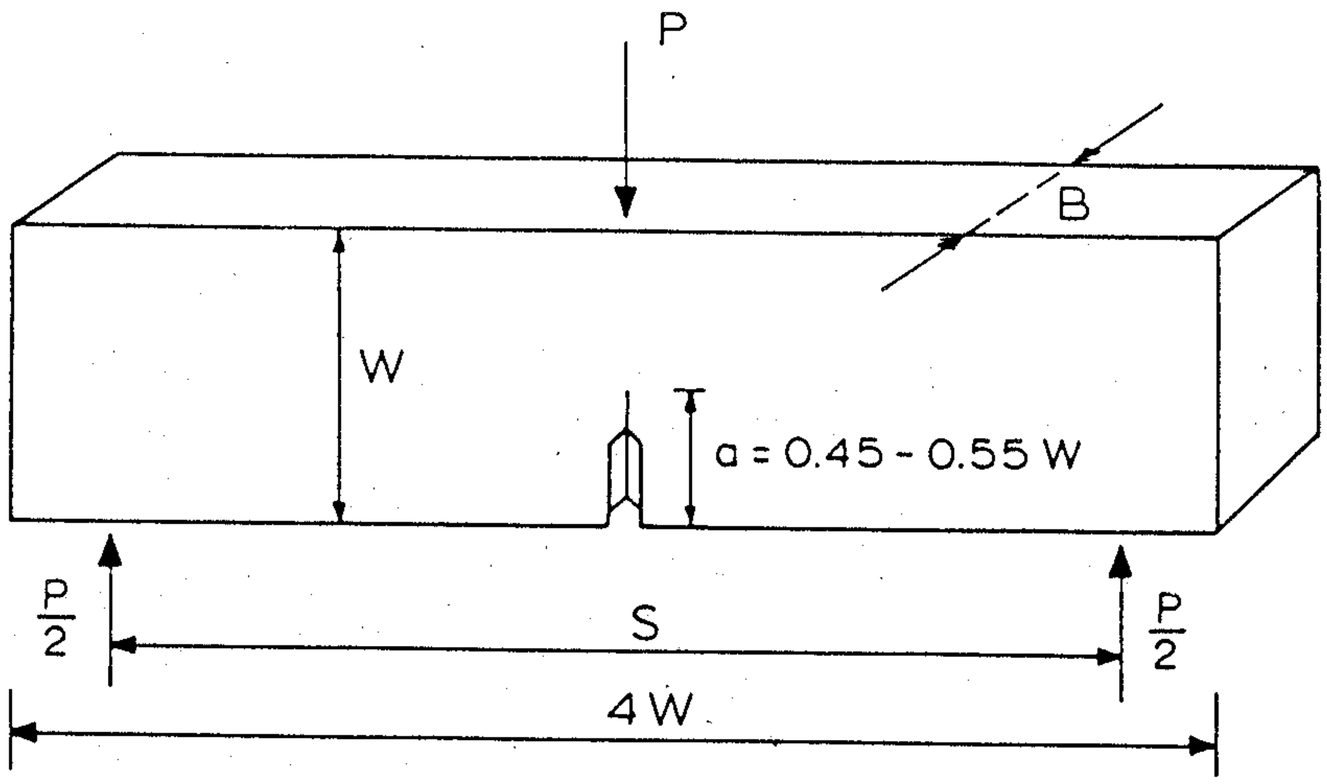


Figure 4.11. Plastic zone size and state of stress
a. Plastic zone size in the order of the plate thickness; b. Small plastic zone; c. Intermediate size

a



b

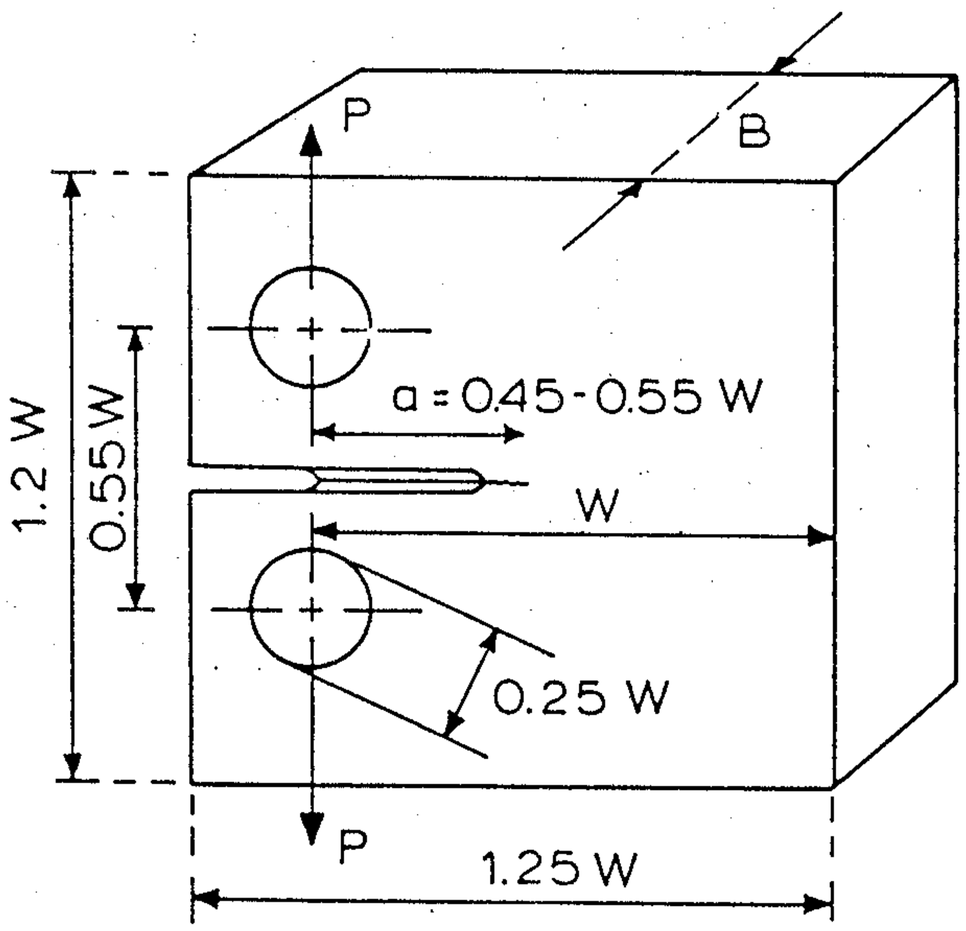


Figure 7.1. Standard specimens
a. Bend specimen; b. Compact tension specimen

bend specimen

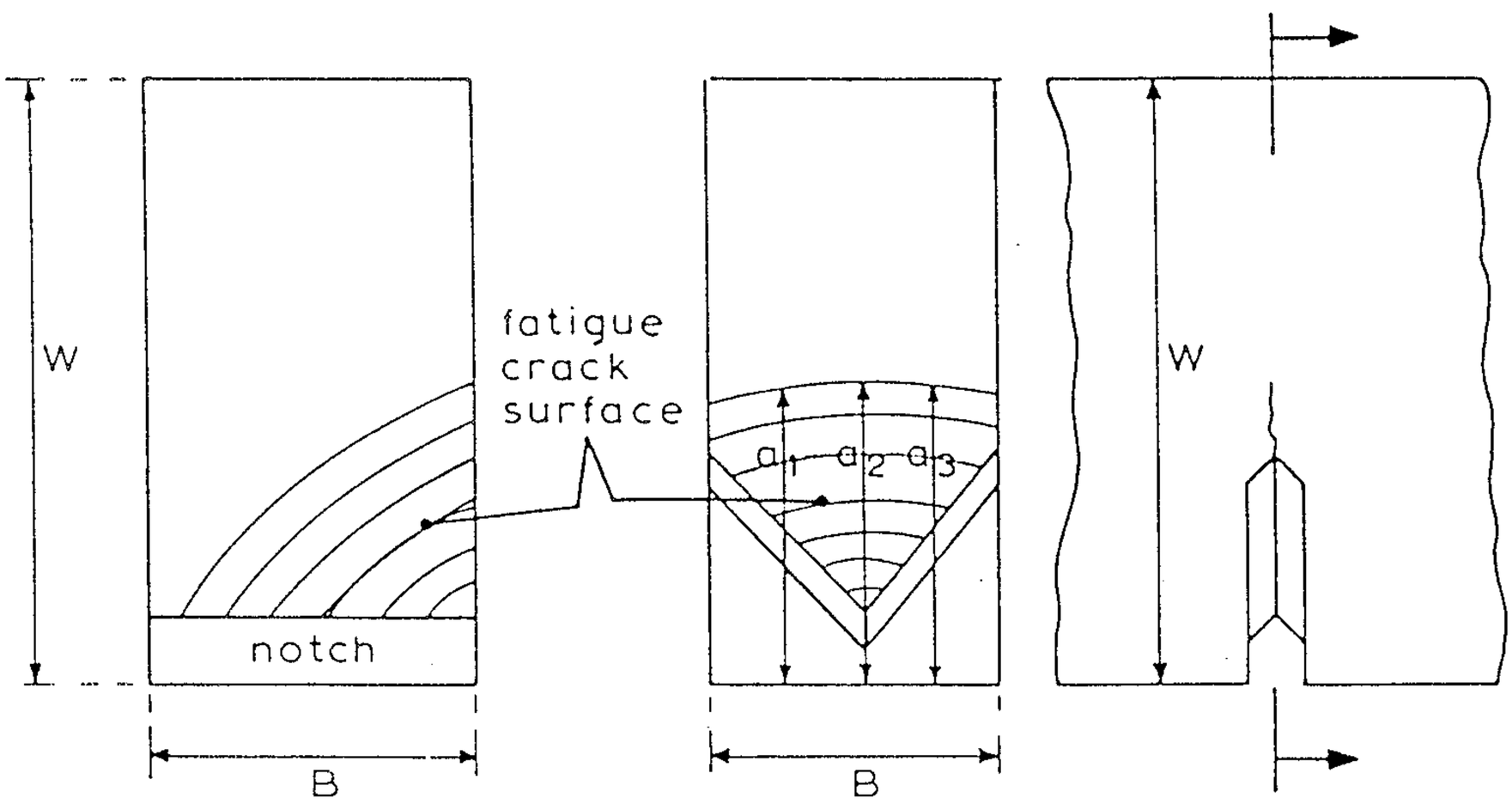
$$K = \frac{PS}{BW^{\frac{3}{2}}} \frac{3\left(\frac{a}{W}\right)^{\frac{1}{2}}\left[1.99 - \frac{a}{W}\left(1 - \frac{a}{W}\right)\left(2.15 - 3.93\frac{a}{W} + 2.7\frac{a^2}{W^2}\right)\right]}{2\left(1+2\frac{a}{W}\right)\left(1 - \frac{a}{W}\right)^{\frac{3}{2}}} \qquad (7.3)$$

compact tension specimen

$$K = \frac{P}{BW^{\frac{1}{2}}} \times \frac{\left(2 + \frac{a}{W}\right)\left[0.886 + 4.64\frac{a}{W} - 13.32\left(\frac{a}{W}\right)^2 + 14.72\left(\frac{a}{W}\right)^3 - 5.6\left(\frac{a}{W}\right)^4\right]}{\left(1 - \frac{a}{W}\right)^{\frac{3}{2}}} . \qquad (7.4)$$

* Eq (7.3) is accurate within 0.5 per cent over the entire range of a/W. Eq (7.4) is also accurate within 0.5 per cent, but only in the range $0.2 < a/W < 1$.

a



b

Figure 7.2. Starter notch
a. Normal edge notch; b. Chevron notch

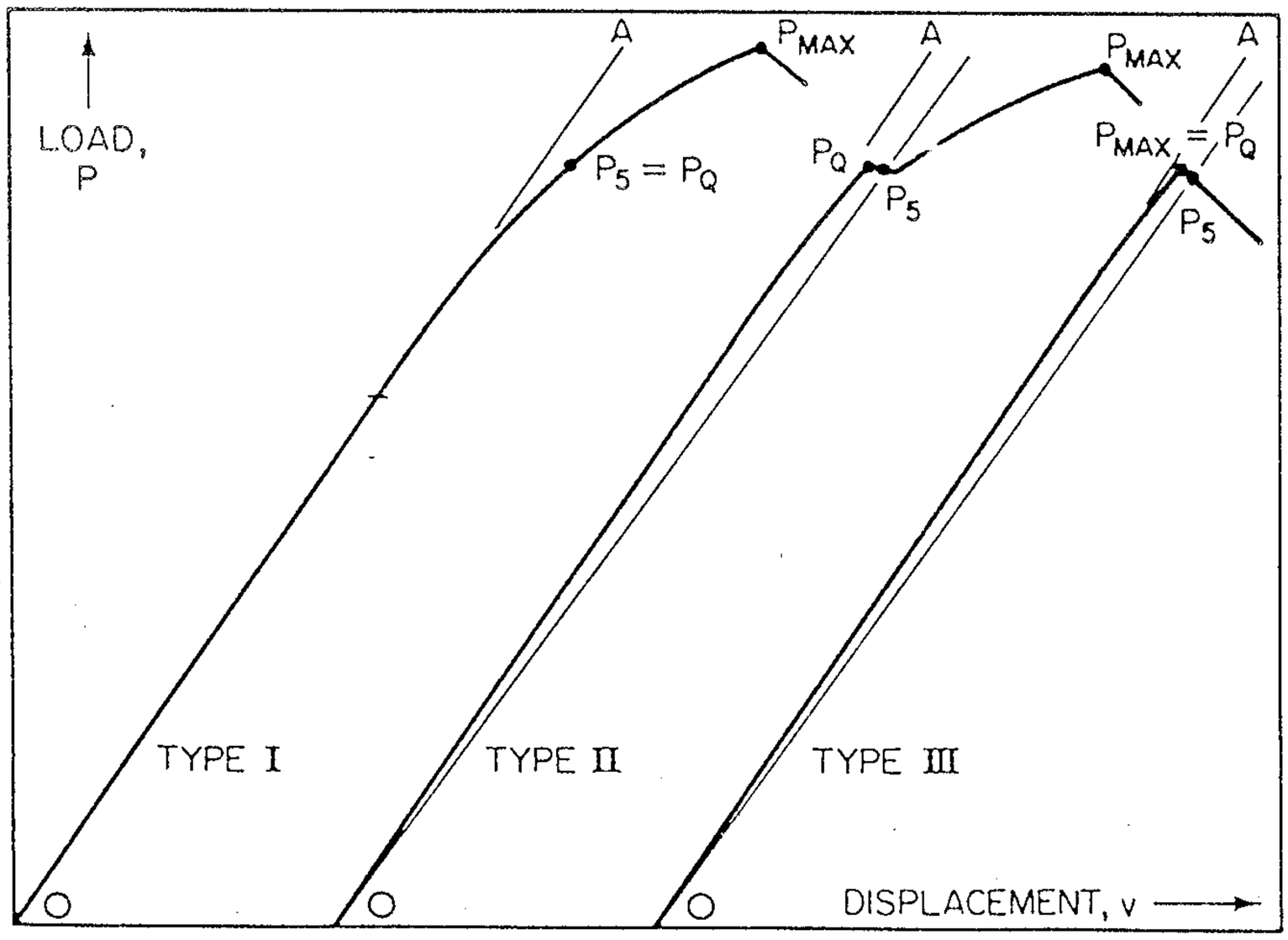


FIG. 3.21. Types of load displacement curves illustrating procedure for determination of K_{Ic}.

Typical K_{Ic} data at room temperature

ערכים מייצגים של K_{Ic} בטמפרטורת החדר

Material	Condition	σ_{ys}		K_{Ic}		Minimum thickness B	
		kg/mm²	ksi	kg/mm²	ksi$\sqrt{in}$	mm	inches
Steel							
Maraging steel							
300	900°F 3 hrs	200	285	182	52	2.1	0.09
300	850°F 3 hrs	170	242	300	85	7.8	0.31
250	900°F 3 hrs	181	259	238	68	4.3	0.18
D 6 AC steel	heat treated	152	217	210	60	4.8	0.20
	heat treated	150	214	311	89	10.7	0.44
	Forging	150	214	178-280	51-80		
4340 steel	hardened	185	265	150	43	1.7	0.07
A 533 B	reactor steel	35	50	≈ 630	≈180	810	33
Carbon steel	low strength	24	35	> 700	>200	2150	82
Titanium							
6Al - 4V	(α+β)STA	112	160	122	35	3	0.12
13V - 11Cr - 3Al	STA	115	164	89	25	1.5	0.07
6Al - 2Sn - 4Zr - 6Mo	(α+β)STA	120	171	85	24	1.3	0.05
6Al - 6V - 2Sn	(α+β)STA	110	157	120	34	3.0	0.12
4Al - 4Mo - 2Sn - 0.5Si	(α+β)STA	96	137	224	64	13.6	0.55
Aluminium							
7075	T651	55	79	94	27	7.3	0.30
7079	T651	47	68	105	30	12.5	0.49
6061	T651	32	46	106	30	27.4	1.06
DTD 5024	Forged (long.)	50	72	126	36	15.9	0.65
	Short transverse	49	70	53	15	3.0	0.12
2014	T4	46	65	90	26	9.6	0.40
2024	T3	40	57	110	31	19.0	0.75

FATIGUE

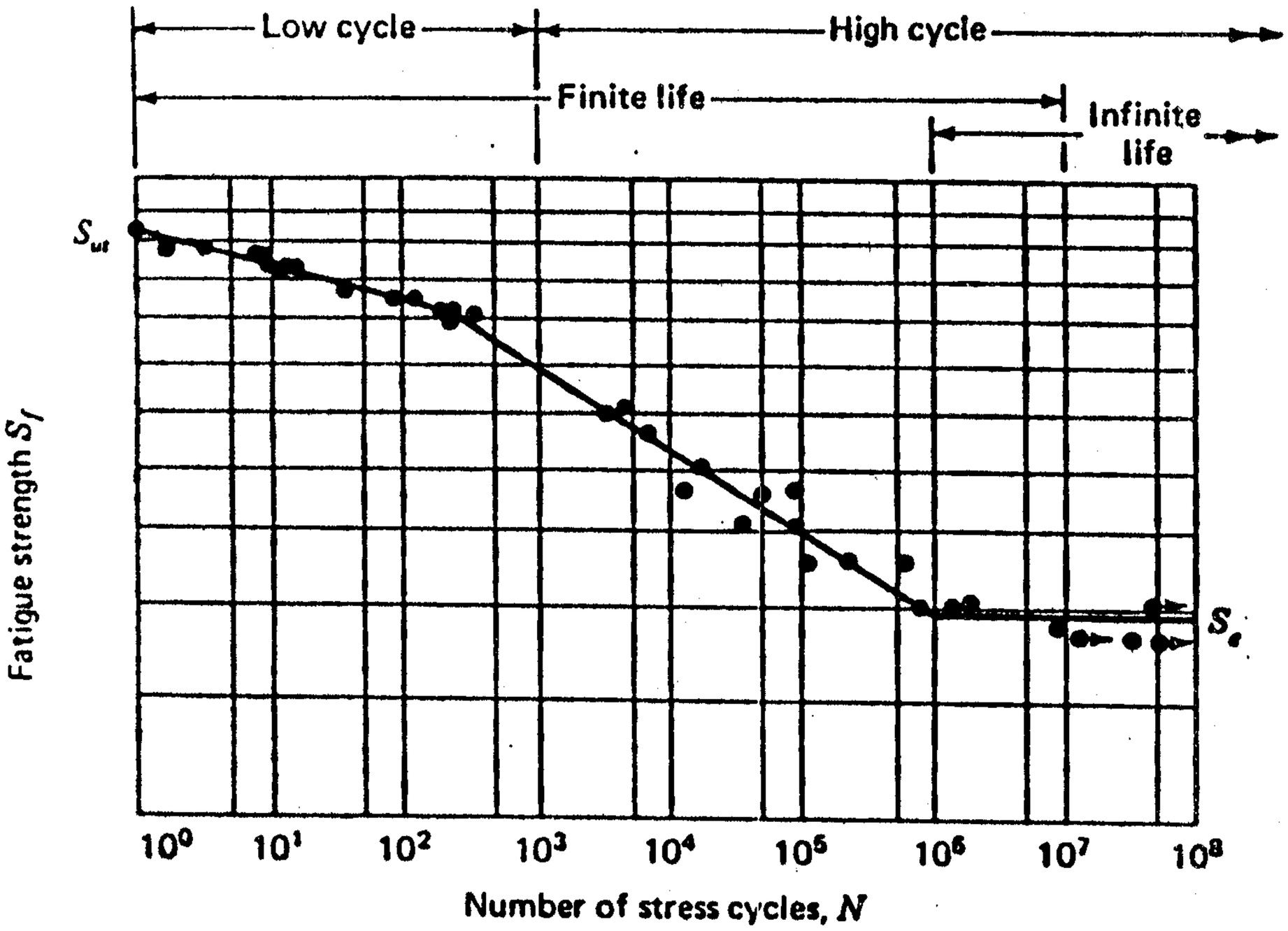


FIGURE 7-3 An *S-N* diagram plotted from the results of completely reversed axial fatigue tests. Material: chromium-molybdenum steel, normalized; $S_{ut} = 800$ MPa; maximum $S_{ut} = 860$ MPa; $S_e = 338$ MPa. (*Data from NACA Technical Note 3866, December 1966.*)

CUMULATIVE FATIGUE DAMAGE

Palmgren-Miner cycle-ratio summation theory*

$$\sum \frac{n_i}{N_i} = 1$$

---

* A. Palmgren «Die Lebensdauer von Kugellagern», *ZVDI*, vol. 68, 1924, pp. 339-41; M. A. Miner, "Cumulative Damage in Fatigue," *J. Appl. Mech.*, vol. 12, *Trans. ASME*, Vol. 67, 1945, pp. A159–A164.

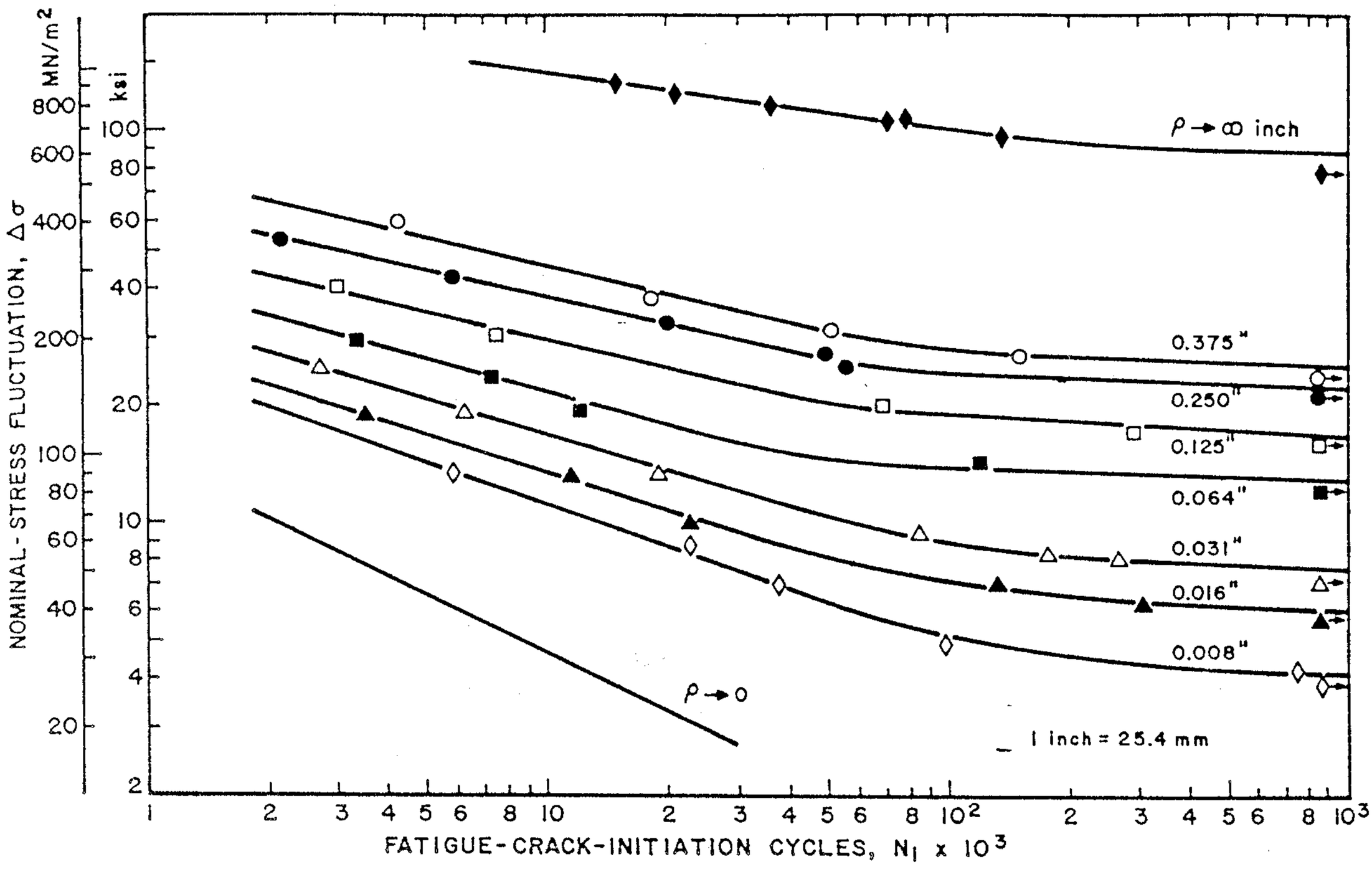


FIG. 7.6. Dependence of fatigue-crack initiation of HY-130 steel on nominal-stress fluctuations for various notch geometries.

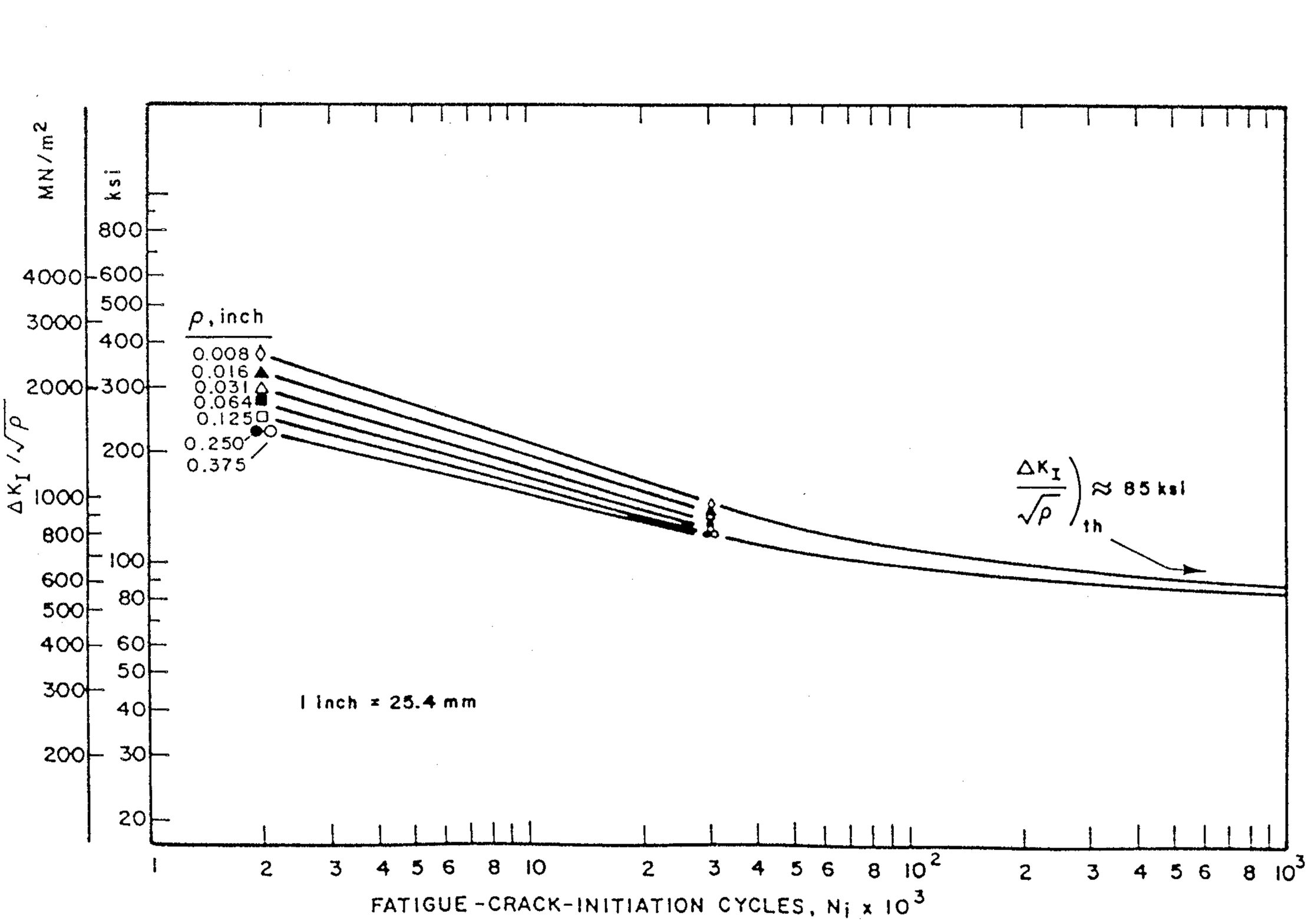


FIG. 7.7. Correlation of fatigue-crack-initiation life with the parameter $\Delta K_I/\sqrt{\rho}$ for HY-130 steel.

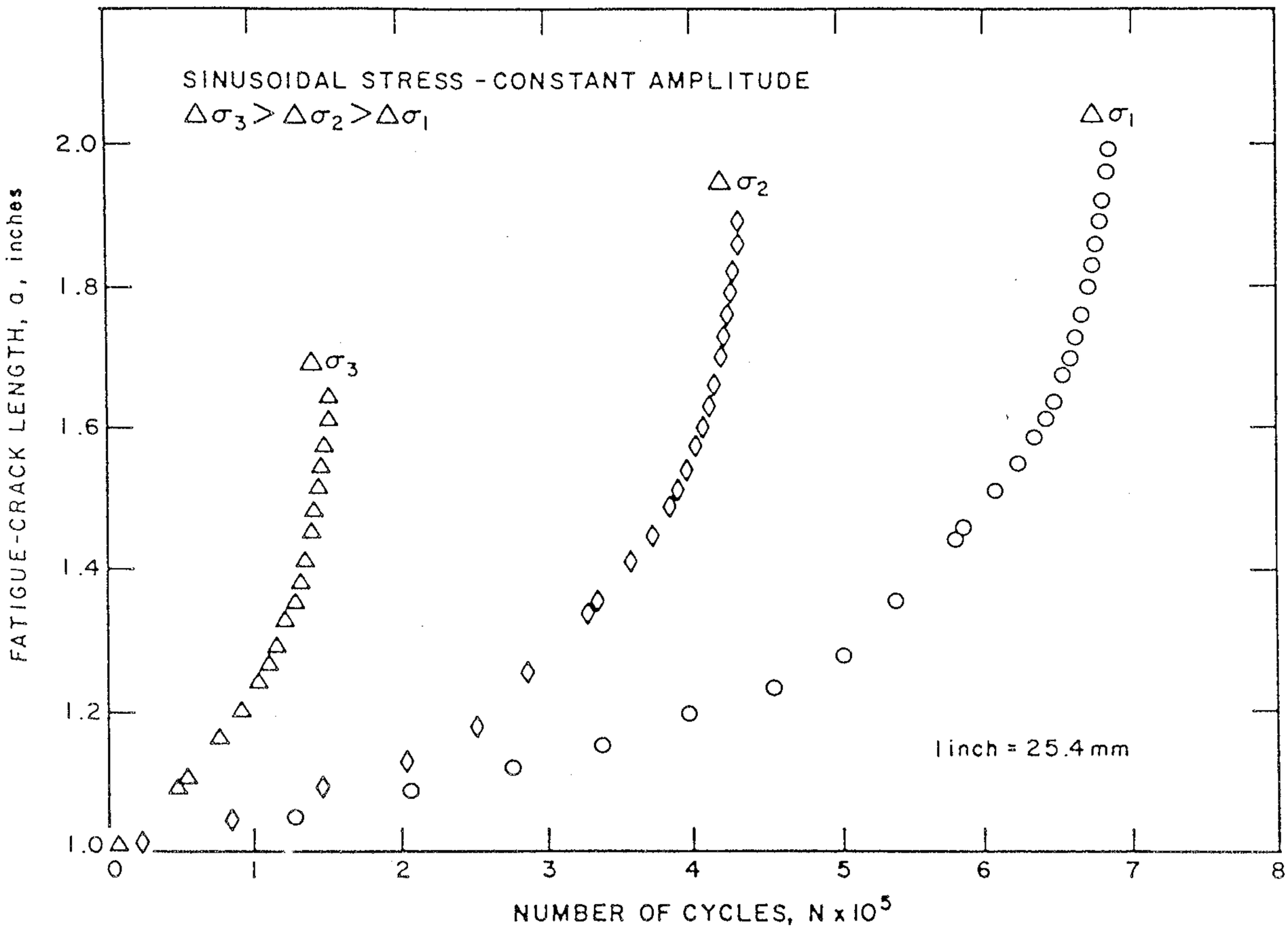


FIG. 8.2. Effect of cyclic-stress range on crack growth.

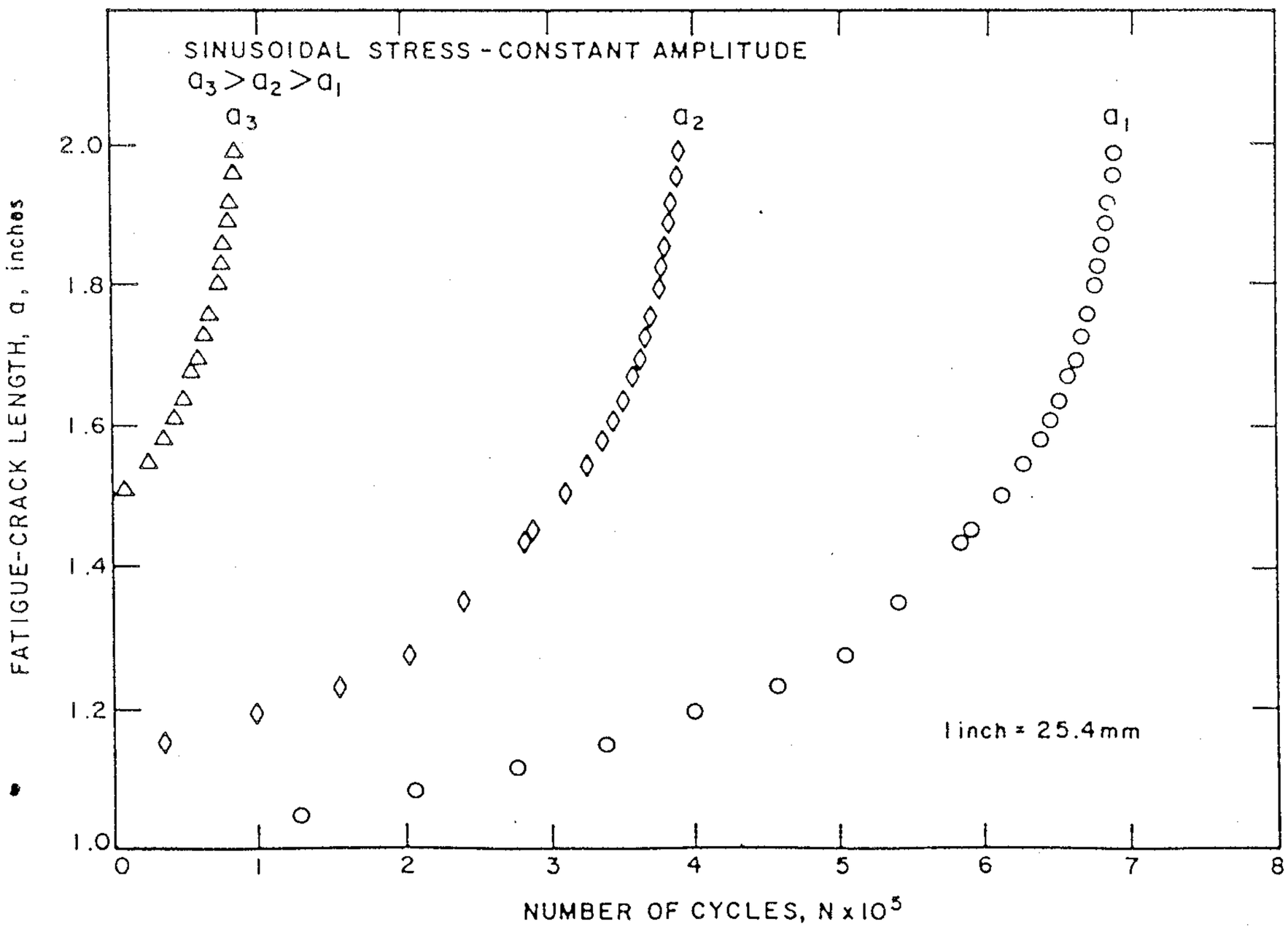


FIG. 8.3. Effect of initial crack length on crack growth.

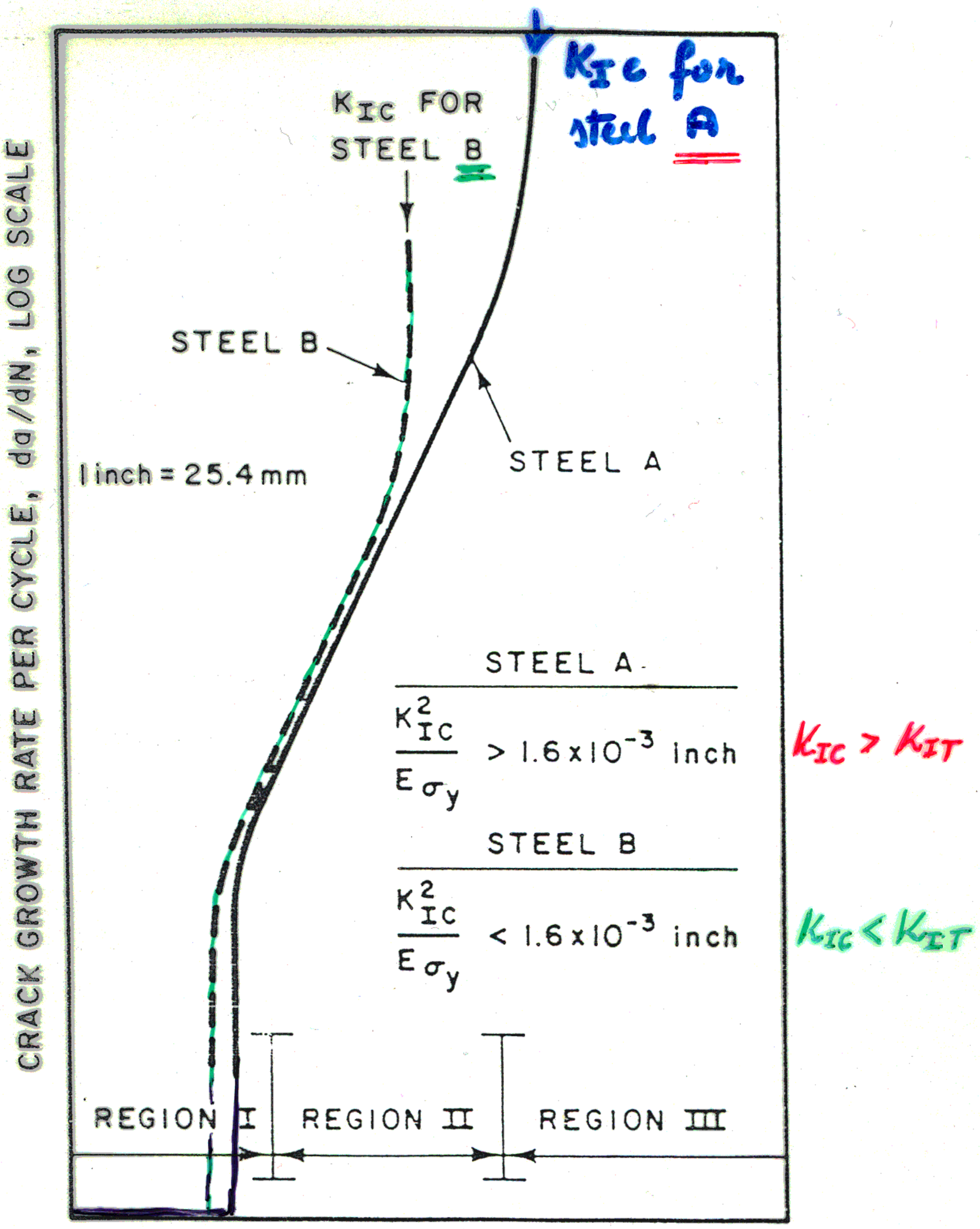


FIG. 8.4. Schematic representation of fatigue-crack growth in steel.

$$\delta_T = \frac{K_T^2}{E\sigma_{ys}} = 1.6 \times 10^{-3} \text{ in.} \quad (0.04 \text{ mm})$$

$K_T \equiv$ stress-intensity-factor-range value corresponding to onset of celeration in fatigue-crack-growth rates,

$E \equiv$ Young's modulus,

Martensitic Steels

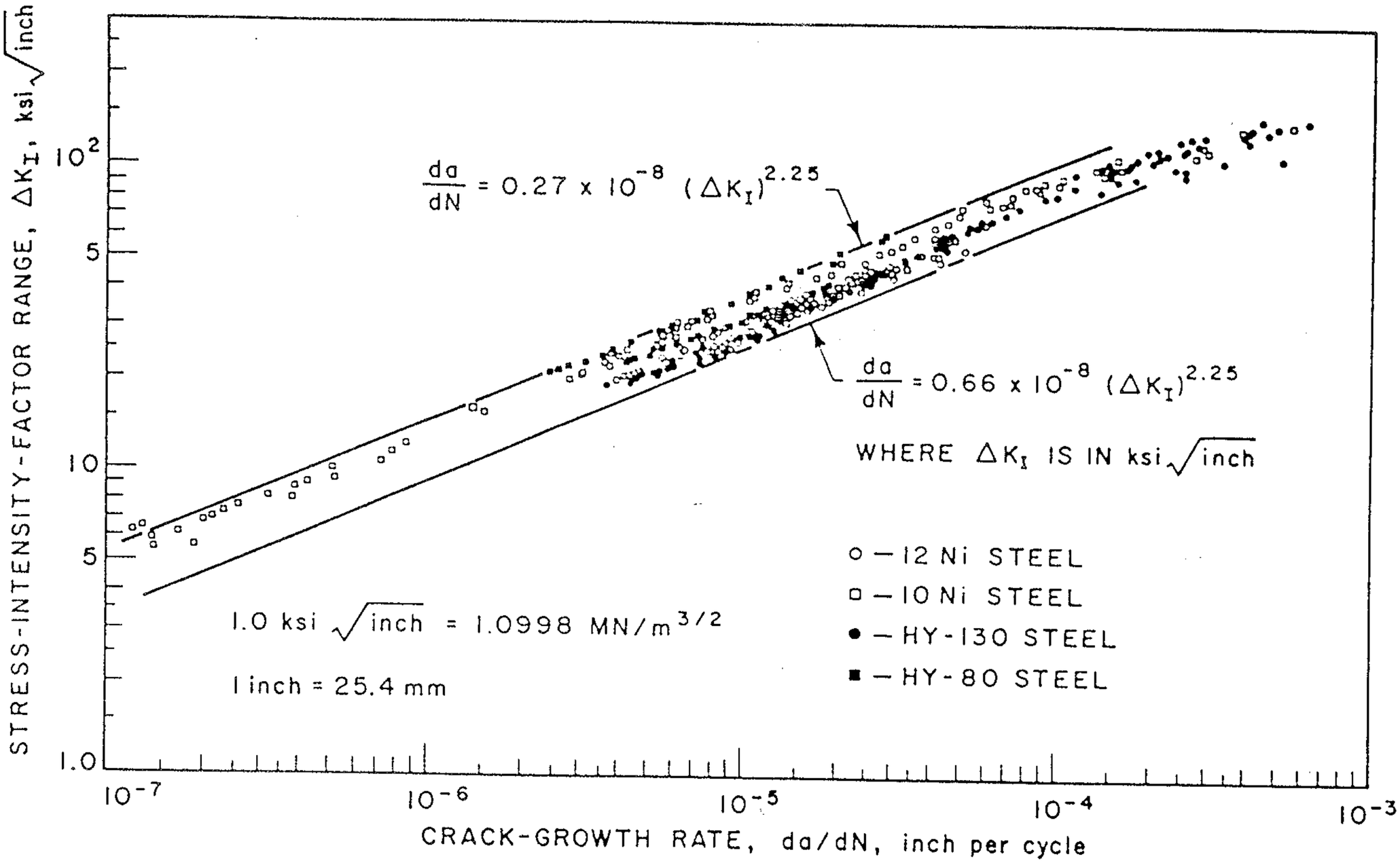
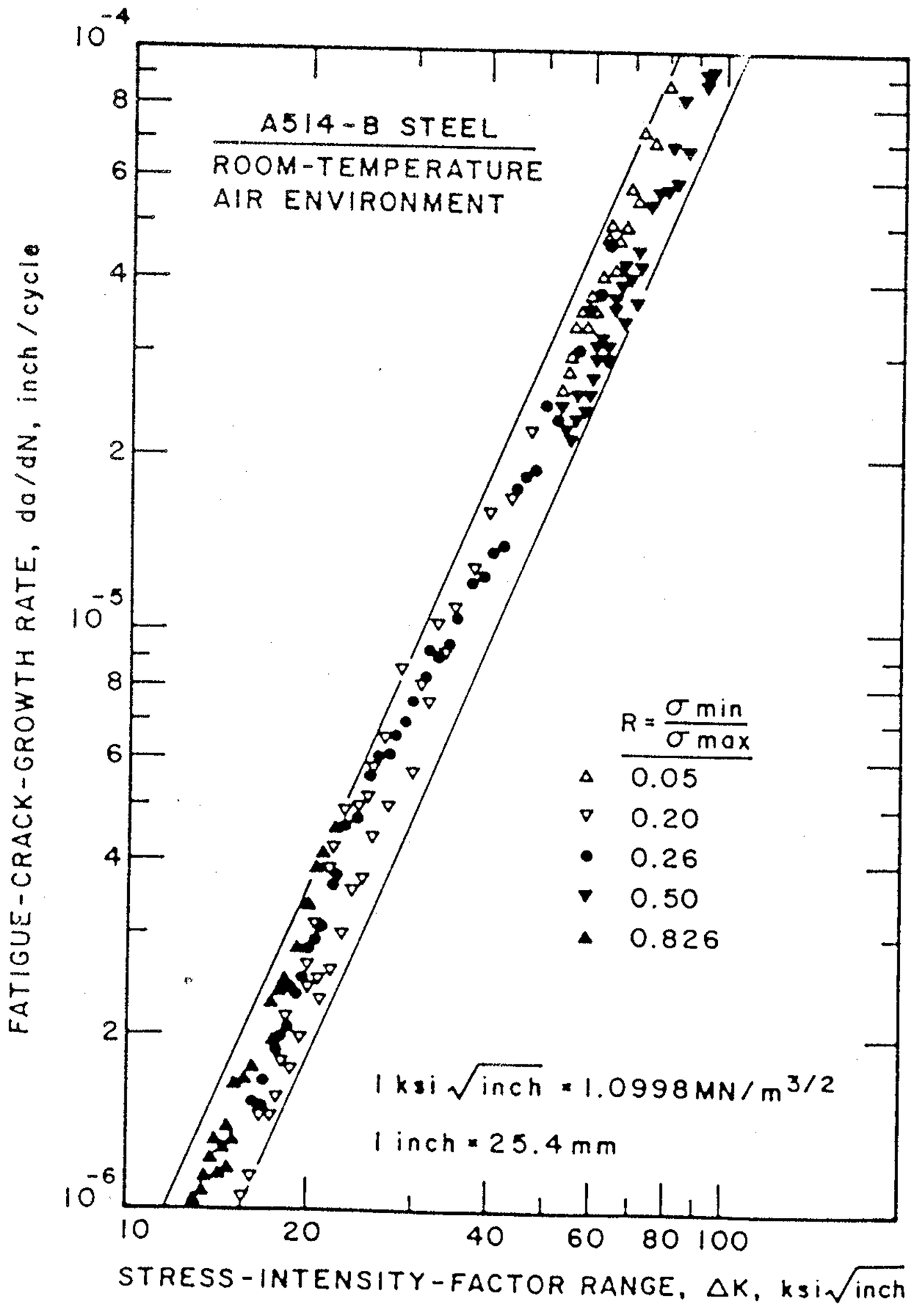


FIG. 8.5. Summary of fatigue-crack-propagation for martensitic steels.



$$\frac{da}{dN} = 0.66 \times 10^{-8}(\Delta K_I)^{2.25}$$

where: a = in.,
K_I = ksi$\sqrt{\text{in.}}$

FIG. 8.6. Crack-growth rate as a function of stress-intensity range for A514-B steel.

Ferrite-Pearlite Steels

$$\frac{da}{dN} = 3.6 \times 10^{-10}(\Delta K_I)^{3.0}$$

where a = in.,
ΔK_I = ksi$\sqrt{\text{in.}}$

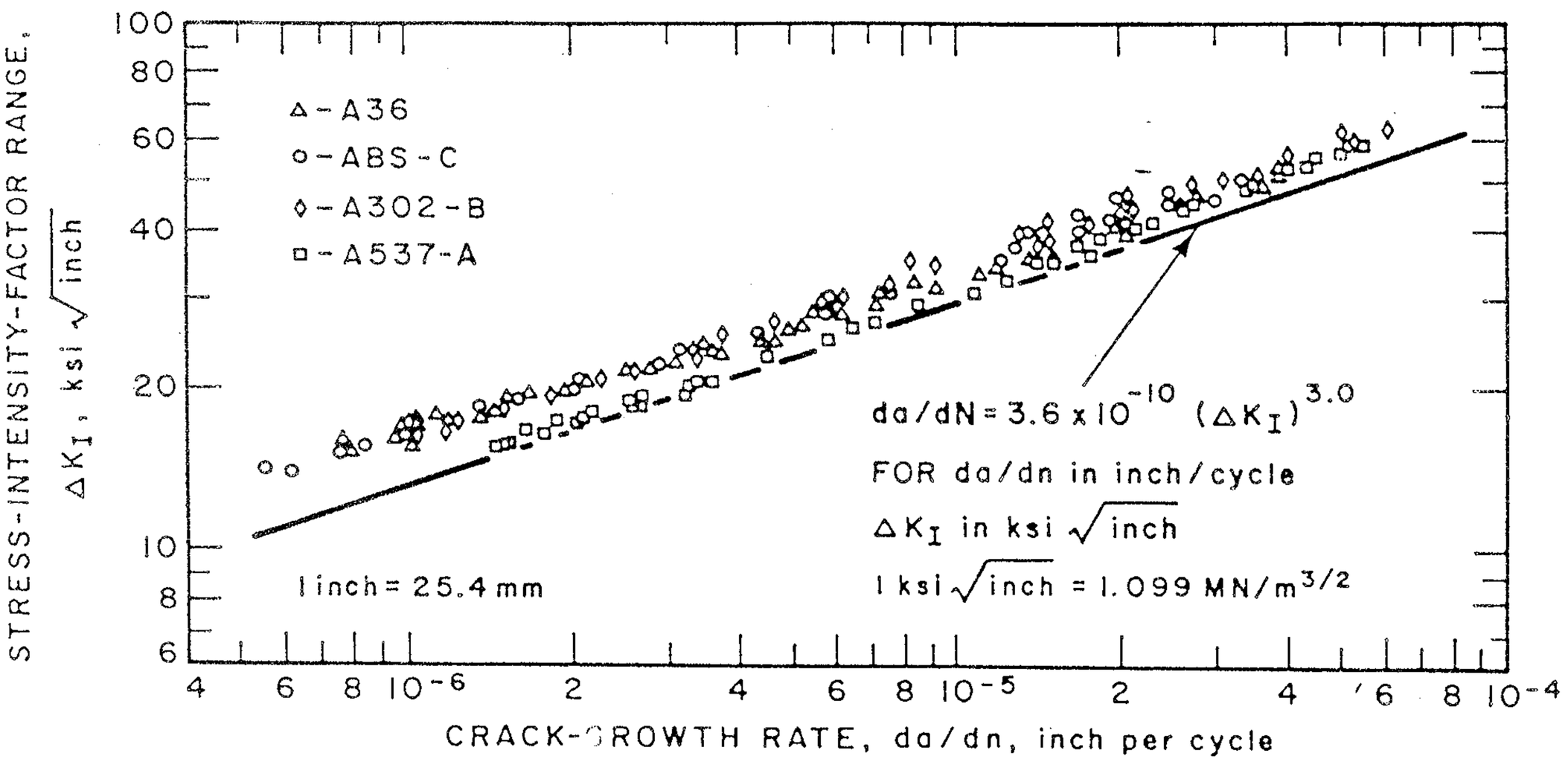


FIG. 8.8. Summary of fatigue-crack-growth data for ferrite-pearlite steels.

Austenitic Stainless Steels

$$\frac{da}{dN} = 3.0 \times 10^{-10}(\Delta K_I)^{3.25}$$

a = in.,
K_I = ksi$\sqrt{\text{in.}}$

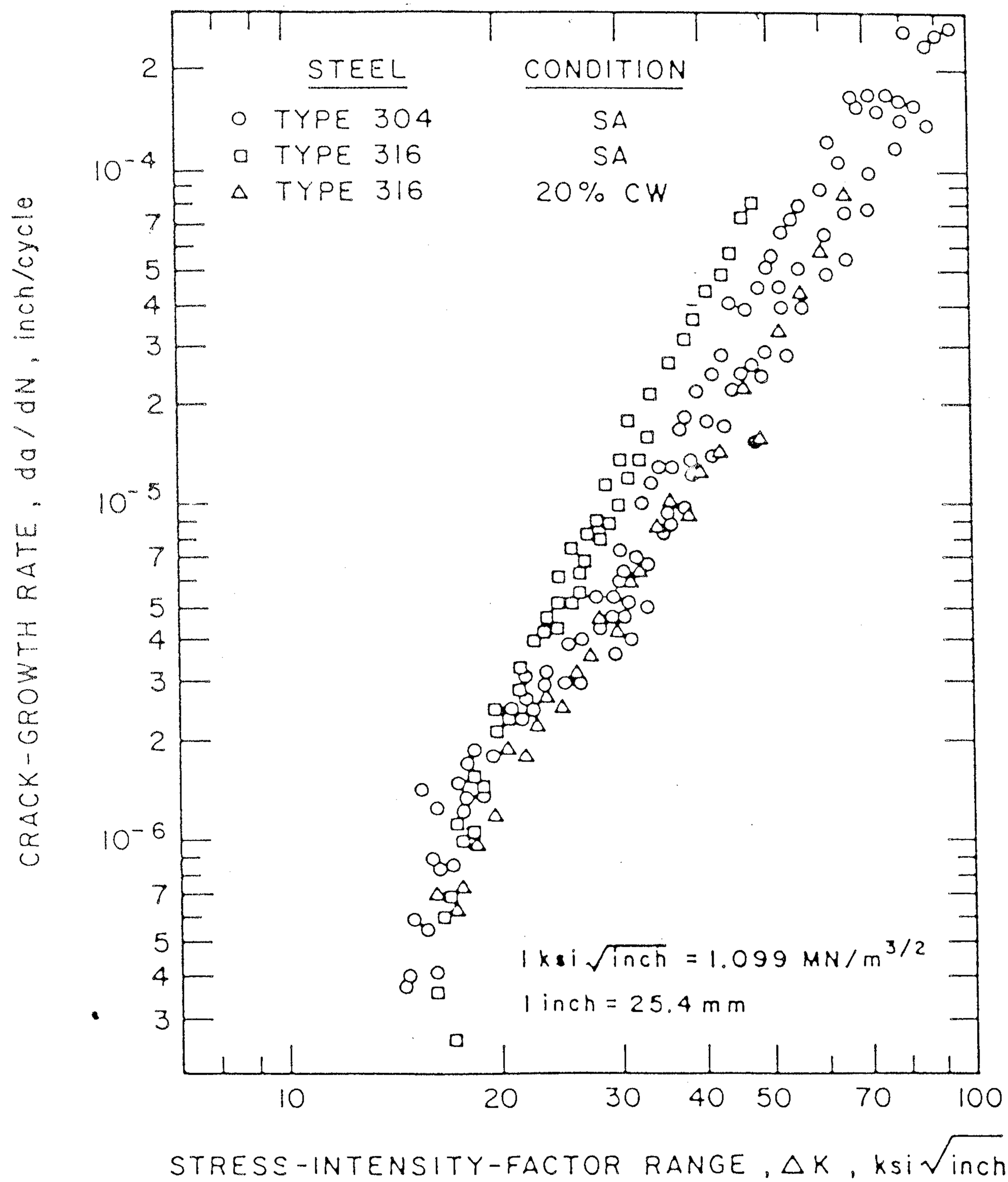


FIG. 8.9. Fatigue-crack-growth rate of solution-annealed type 304 and 316 stainless steels and 20 percent cold-worked type 316 stainless steel at 75°F.

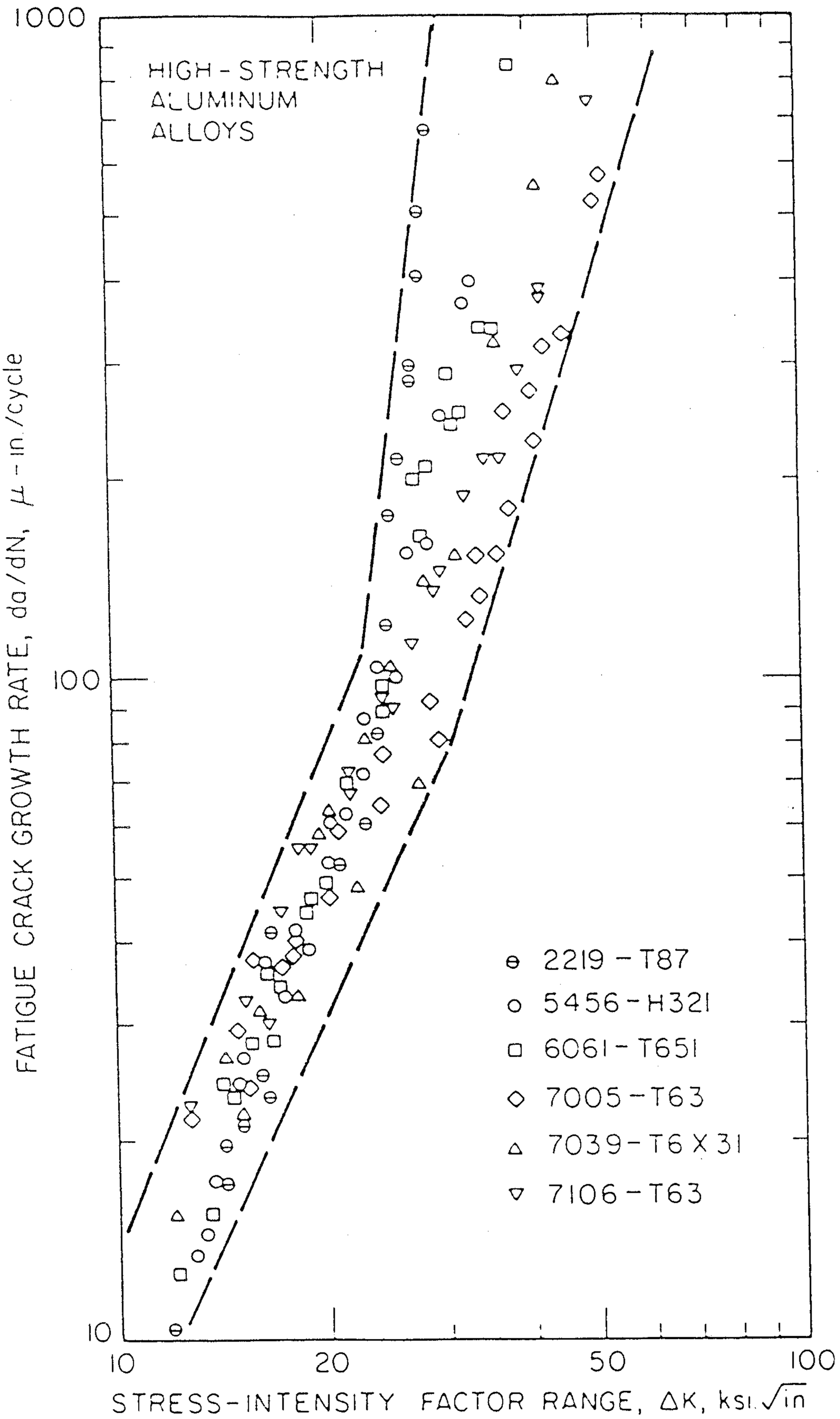


FIG. 8.13. Summary plot of *da/dN* versus ΔK for six aluminum alloys. The yield strengths of these alloys range from 34 to 55 ksi.

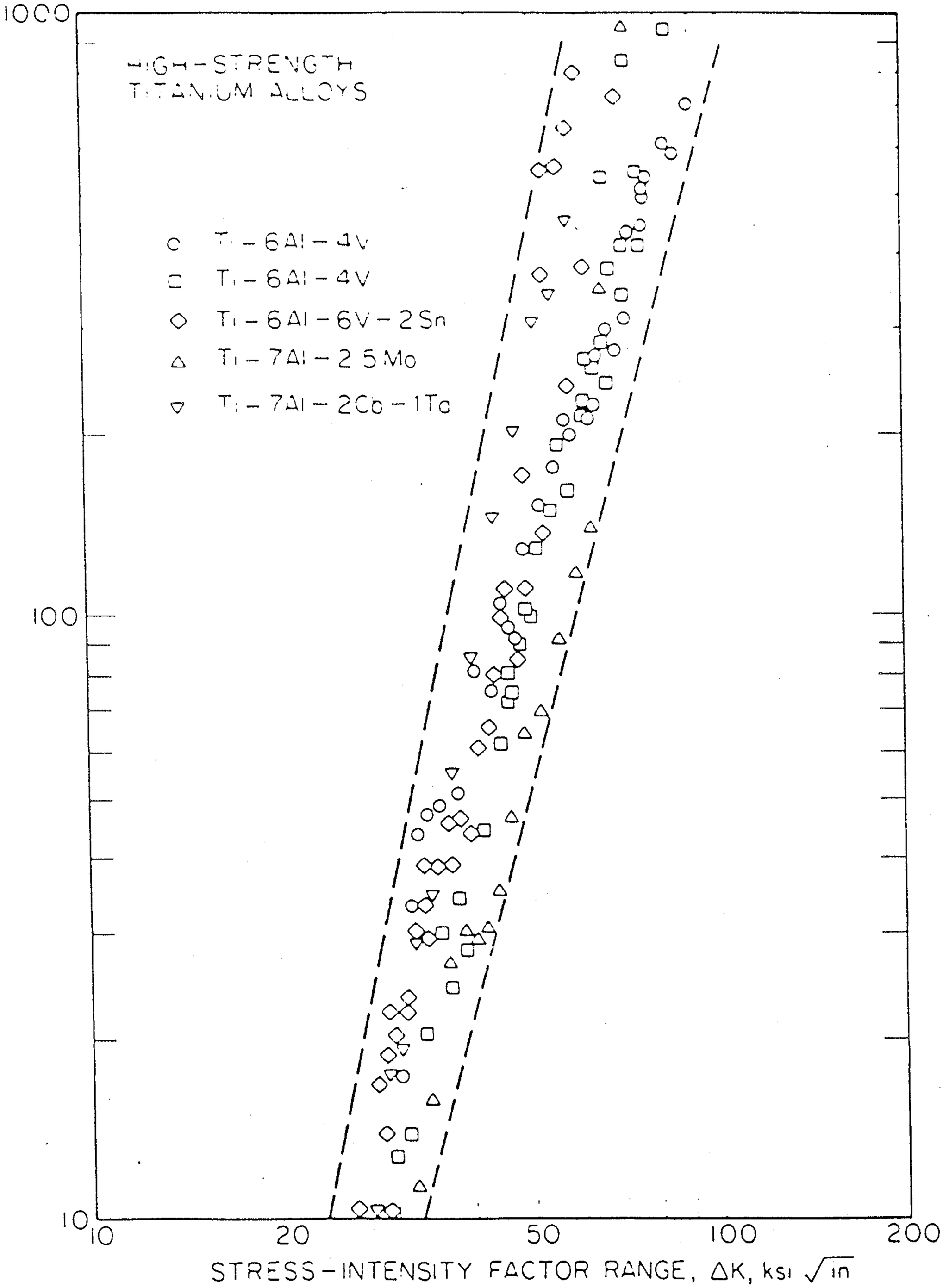


FIG. 8.14. Summary plot of da/dN versus ΔK data for five titanium alloys ranging in yield strength from 110 to 150 ksi.

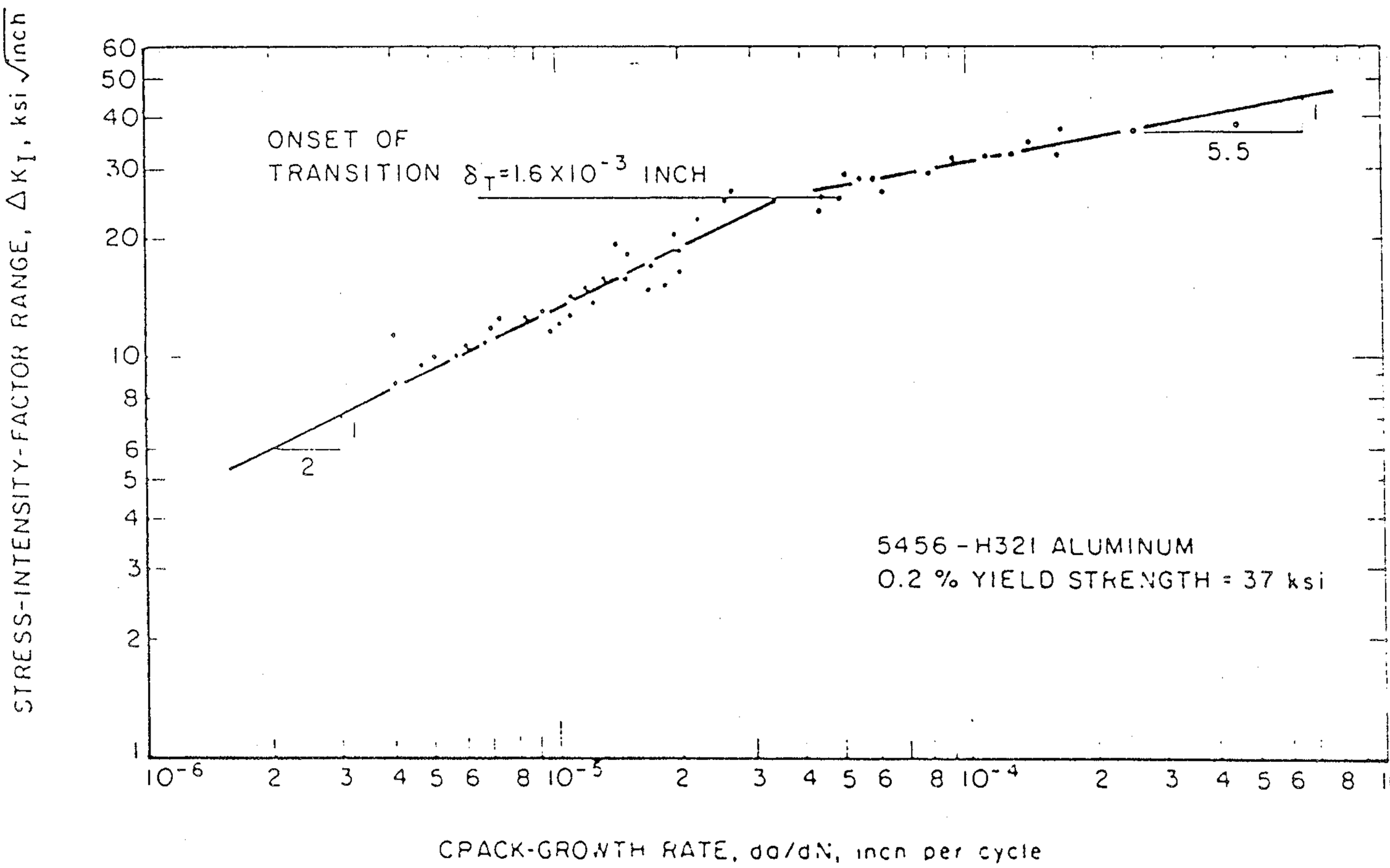


FIG. 8.15. Fatigue-crack-growth rate as a function of stress intensity for 5456-H321 aluminum.

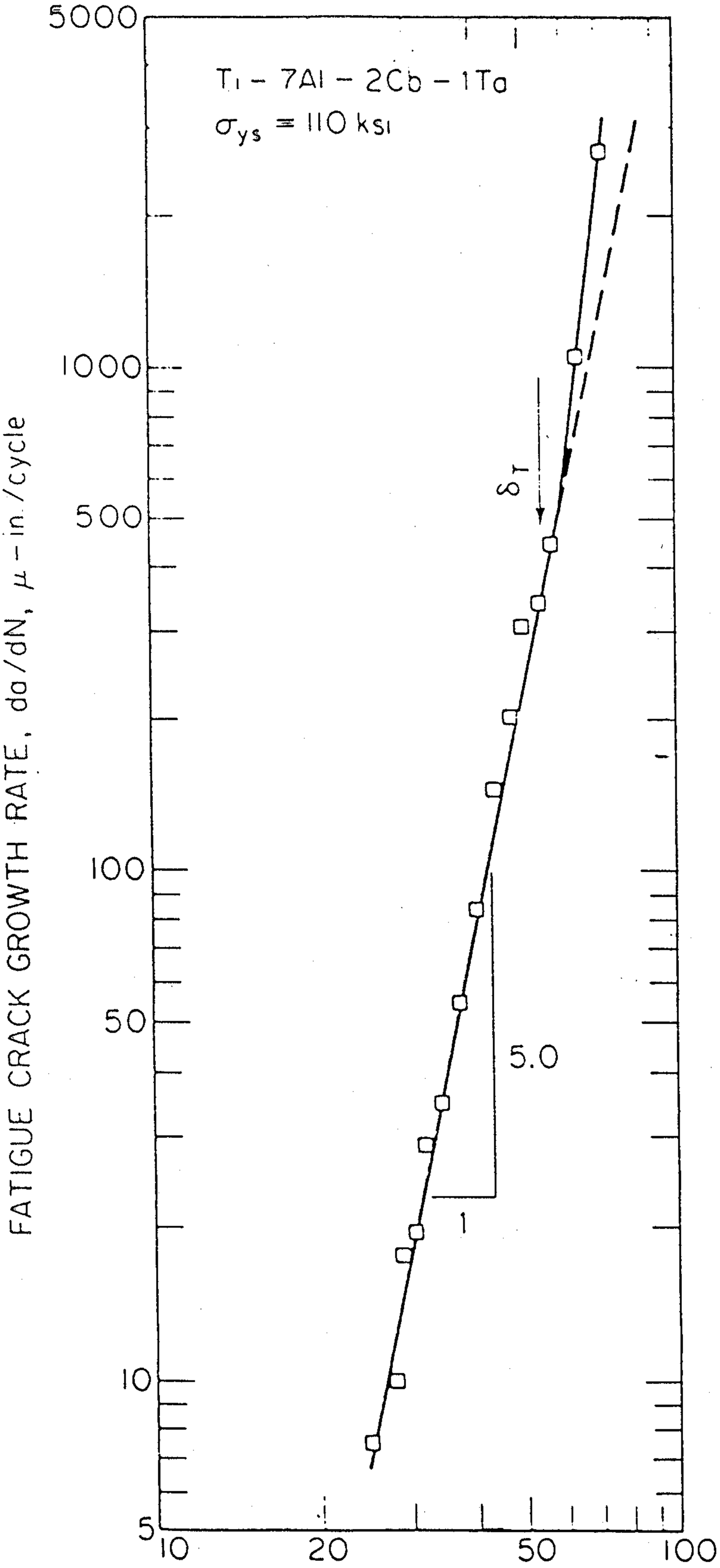


FIG. 8.16. Fatigue-crack-growth rate in a titanium alloy.

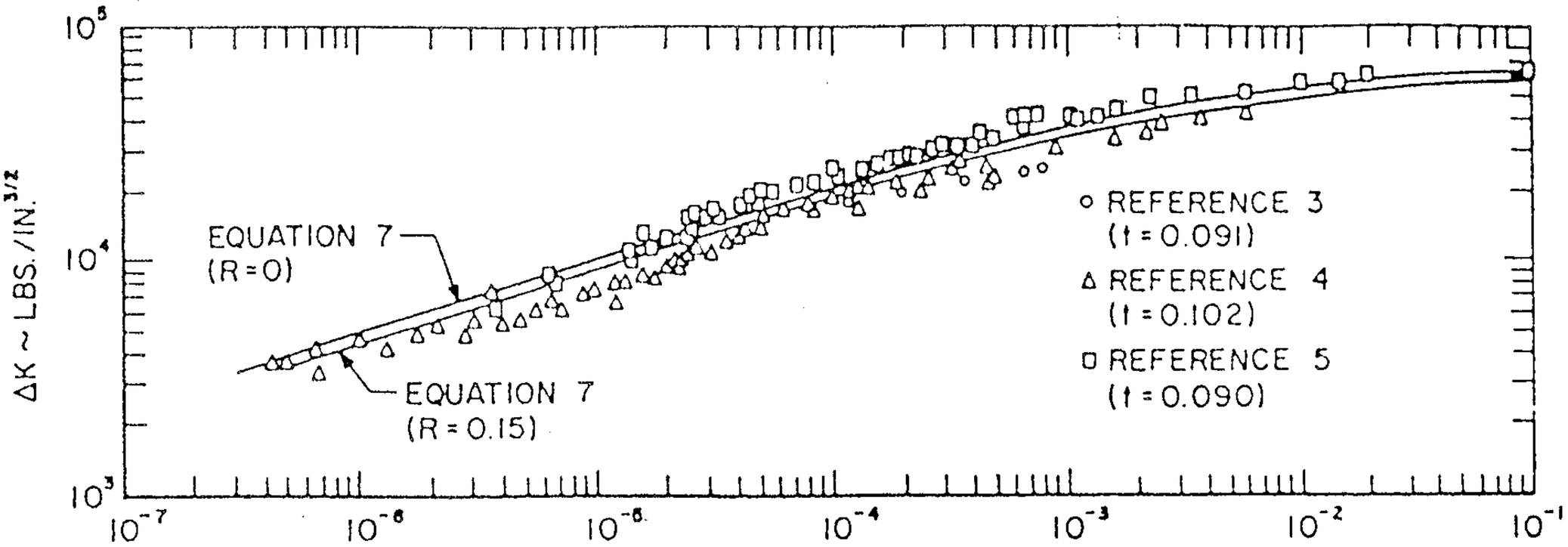


Fig. 1 Comparison of experimental and theoretical crack-propagation rates in 7075-T6 aluminum plate for $R = 0$ to $R = 0.15$

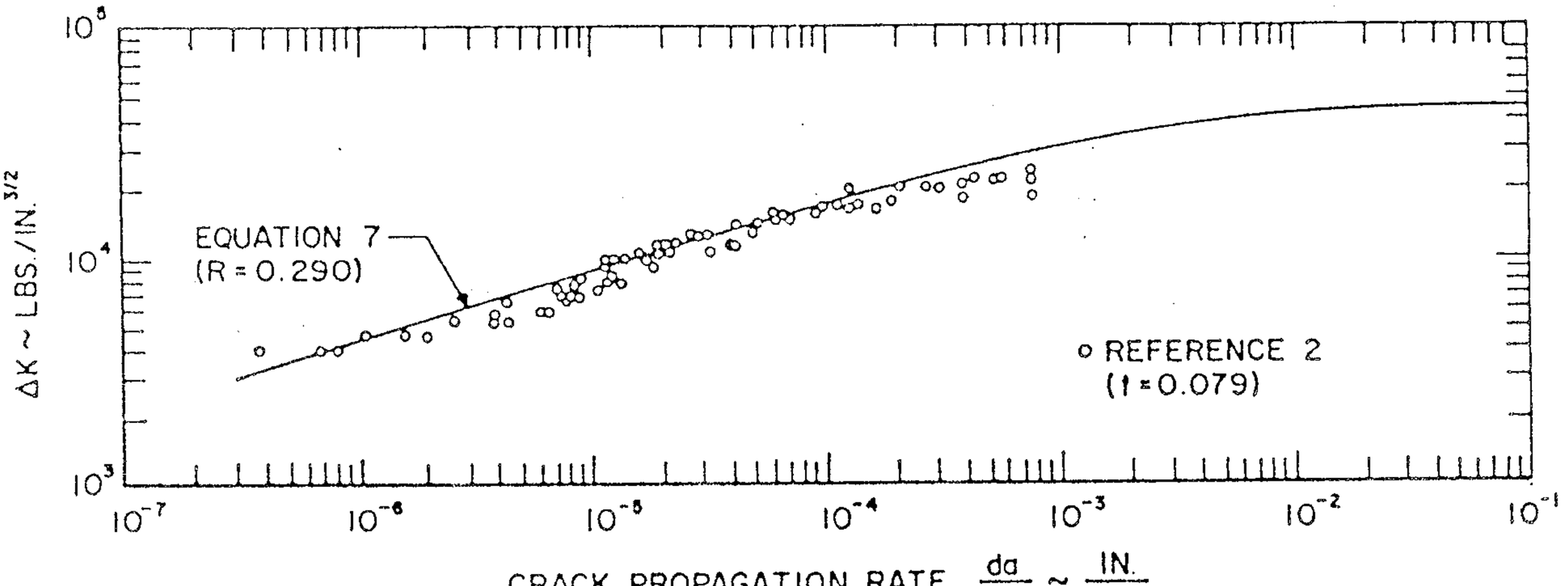


Fig. 2 Comparison of experimental and theoretical crack-propagation rates in 7075-T6 aluminum plate for $R = 0.285$ to $R = 0.297$

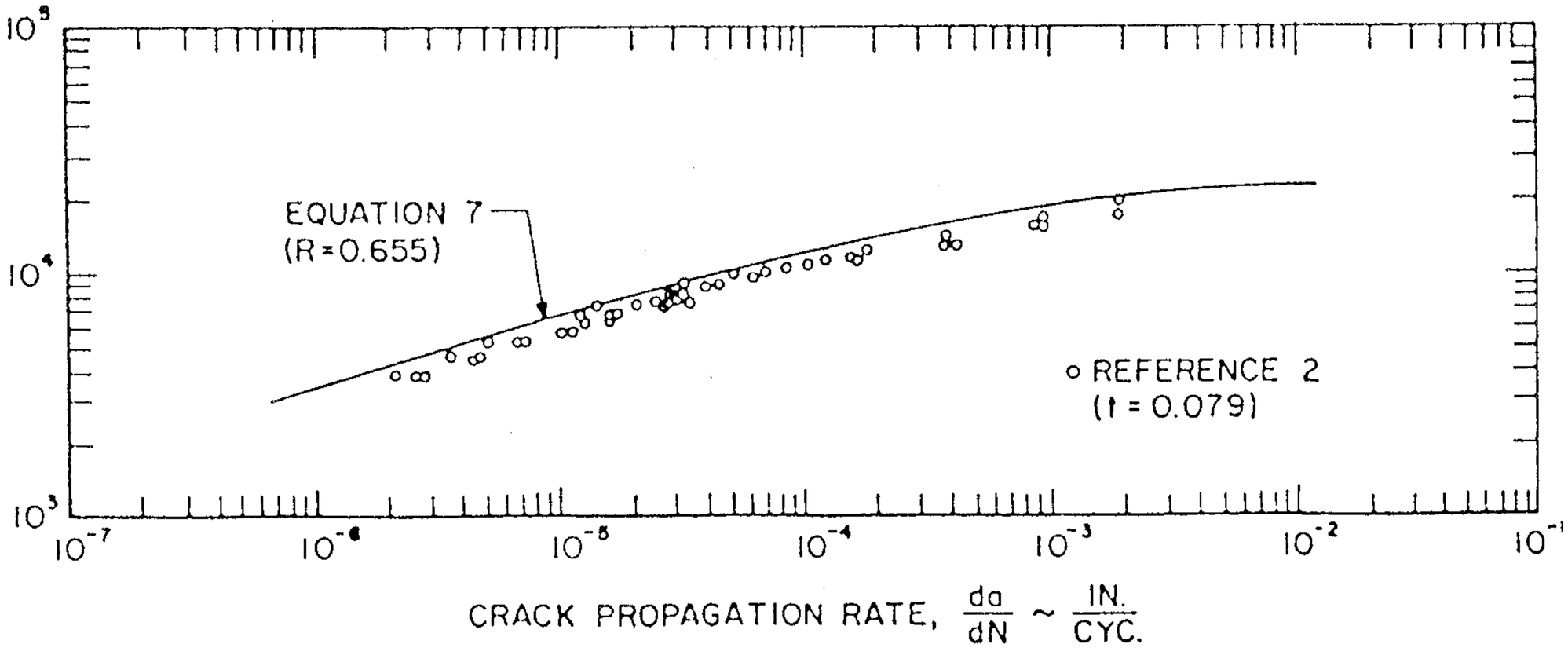


Fig. 3 Comparison of experimental and theoretical crack-propagation rates in 7075-T6 aluminum plate for $R = 0.655$

$$\frac{da}{dN} = \frac{C(\Delta K)^n}{(1 - R)K_c - \Delta K}$$

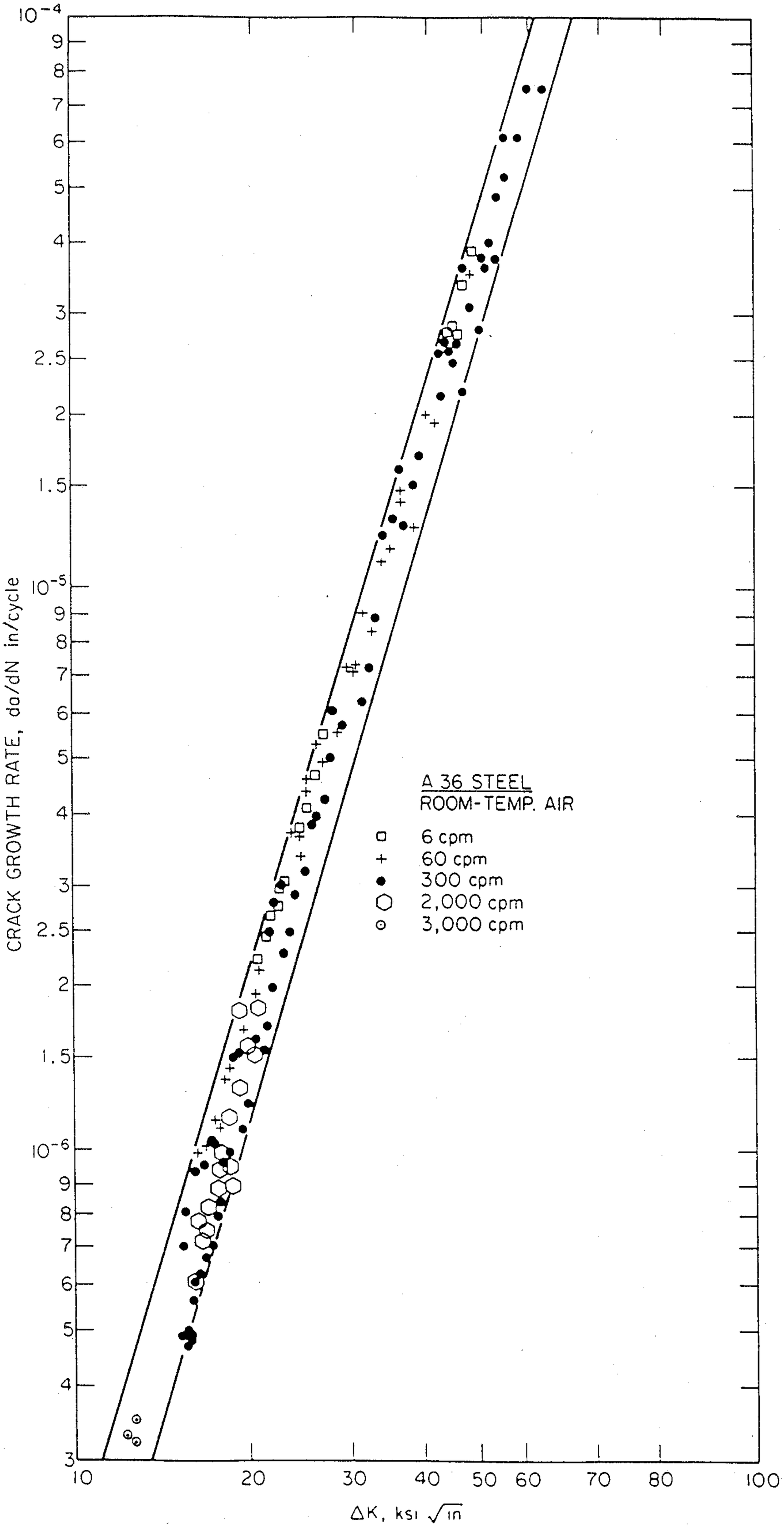


FIG. 8.19. Effect of cyclic frequency on crack growth rates in benign environment.

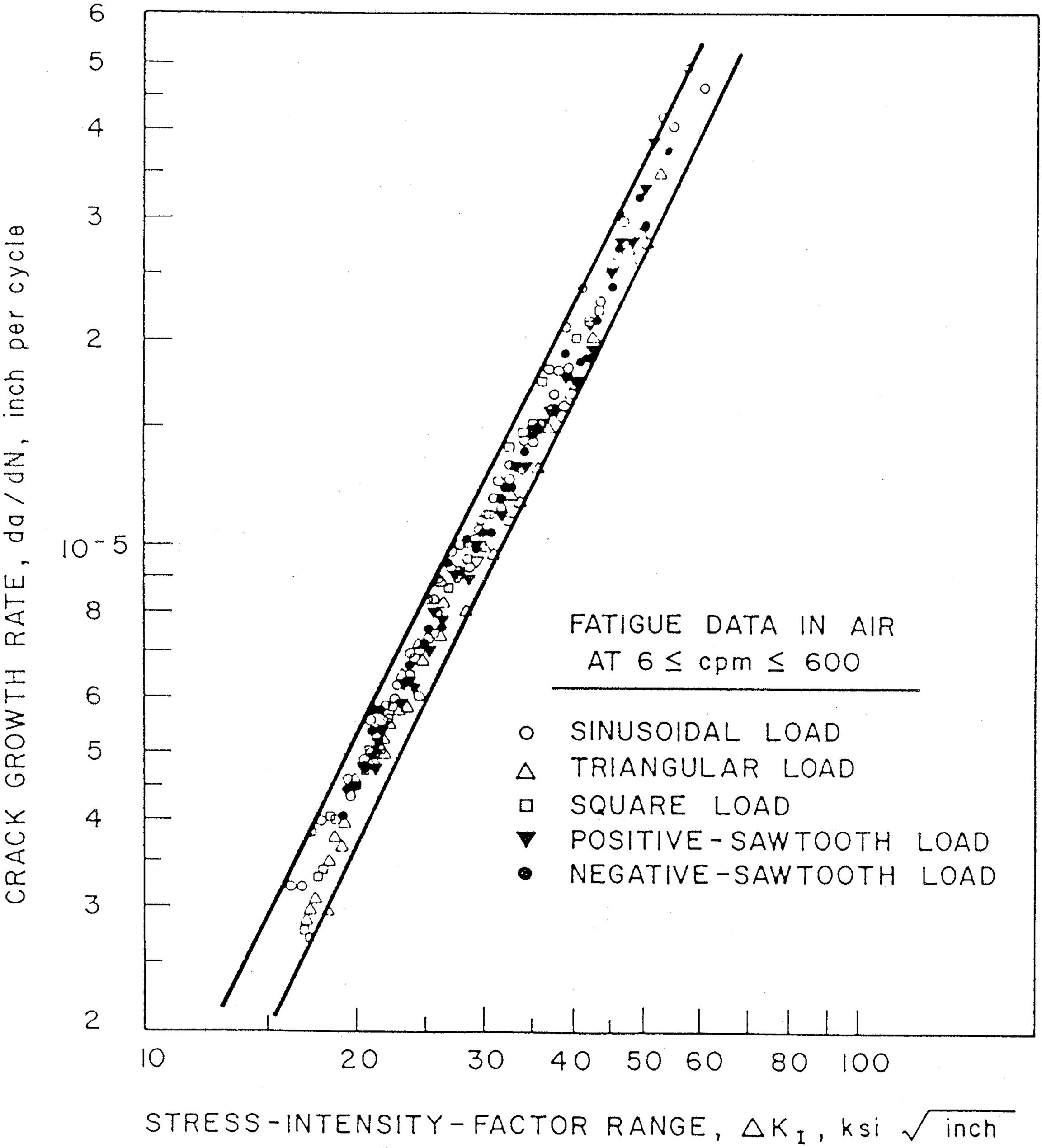


FIG. 8.20. Fatigue-crack-growth rates in 12Ni-5Cr-3Mo steel under various cyclic-stress fluctuations with different stress-time profiles.

FATIGUE - LIFE PREDICTION

The Basic Algorithm

a) Determine the initial crack size a_o by measuring it, or by estimating it based on the NDT resolution.

b) Determine the relation K_I (a) for the given structure and loading conditions.

c) Calculate K_r

d) Determine the crack critical size a_{cr} based on K_{IC} or K_r.

e) Determine experimentally or from handbook the appropriate fatigue-crack growth rate equation e.g.,:

$$\frac{da}{dN} = A_p (\Delta K_I)^{n_p}$$

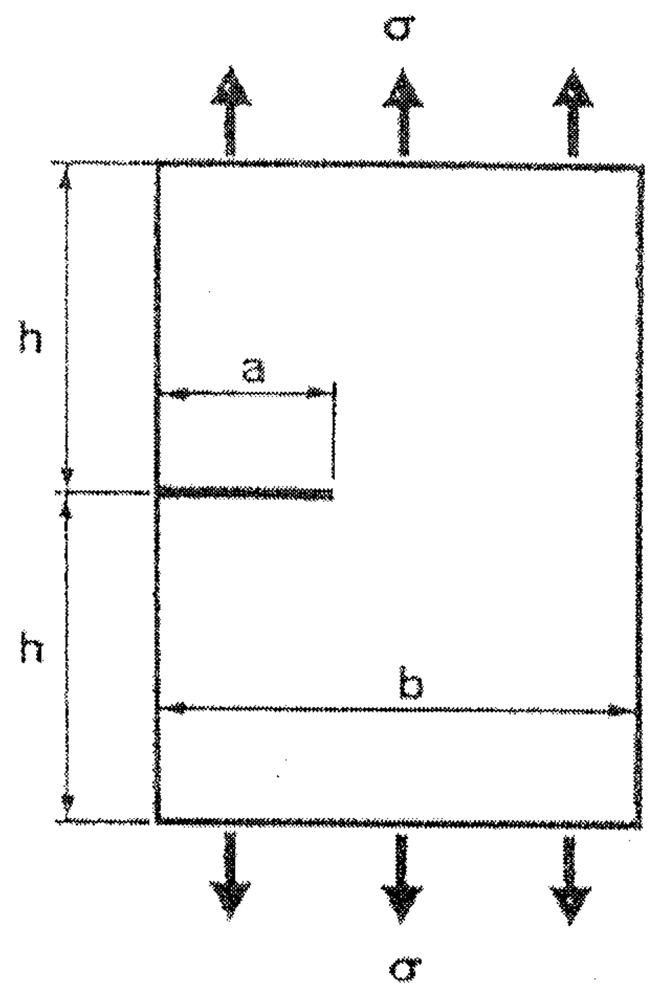
f) Determine ΔK_I from the prescribed loading

g) Integrate from a_o to a_{cr}

$$N_f = \int_{a_o}^{a_{cr}} \frac{da}{Ap(\Delta K_I)^{n_p}}$$

Example #4– Fatigue Life Evaluation

A plate, made of A514 steel, is cyclically loaded by a uniform tensile stress σ, as described in the figure below. In a routine inspection a small edge crack ($a_o/b << 1$) was found in the plate.



Data

$\sigma_y = 100\ ksi$

$K_{Ic} = 150\ ksi\sqrt{in}$

a_o=0.3”

σ_{max}=45 *ksi*

σ_{min}=25 *ksi*

$K_I = 1.12\sigma\sqrt{\pi a}$

(a) Evaluate the fatigue life of the plate.

(b) Suggest possible ways to increase the fatigue life of the plate to N=100,000 loading cycles.

Fatigue-Crack-Growth Calculations

$$\Delta N = \frac{\Delta a}{0.66 \times 10^{-8}\left[1.985(\Delta\sigma)\sqrt{a_{avg}}\right]^{2.25}} = \frac{\Delta a}{0.66 \times 10^{8}\left[39.7\sqrt{a_{avg}}\right]^{2.25}}$$

a_0 (in.)	a_f (in.)	a_{avg} (in.)	ΔK_I (ksi$\sqrt{\text{in.}}$)	ΔN (cycles)	ΣN (cycles)
0.3	0.4	0.35	23.5	12,477	12,477
0.4	0.5	0.45	26.7	9,404	21,881
0.5	0.6	0.55	29.4	7,504	29,385
0.6	0.7	0.65	32.0	6,218	35,603
0.7	0.8	0.75	34.4	5,293	40,896
0.8	0.9	0.85	36.6	4,598	45,494
0.9	1.0	0.95	38.7	4,057	49,551
1.0	1.1	1.05	40.7	3,625	53,176
1.1	1.2	1.15	42.6	3,273	56,419
1.2	1.3	1.25	44.4	2,980	54,429
1.3	1.4	1.35	46.1	2,732	62,161
1.4	1.5	1.45	47.8	2,521	64,682
1.5	1.6	1.55	49.4	2,339	67,021
1.6	1.7	1.65	51.0	2,180	69,201
1.7	1.8	1.75	52.5	2,041	71,242
1.8	1.9	1.85	54.0	1,917	73,159
1.9	2.0	1.95	55.4	1,807	74,966
2.0	2.1	2.05	56.8	1,708	76,674
2.1	2.2	2.15	58.2	1,619	78,293
2.2	2.3	2.25	59.6	1,538	79,831
2.3	2.4	2.35	60.9	1,464	81,295
2.4	2.5	2.45	62.1	1,396	82,691
2.5	2.6	2.55	63.4	1,336	84,027
2.6	2.7	2.65	64.6	1,280	85,307
2.7	2.8	2.75	65.8	1,227	86,534

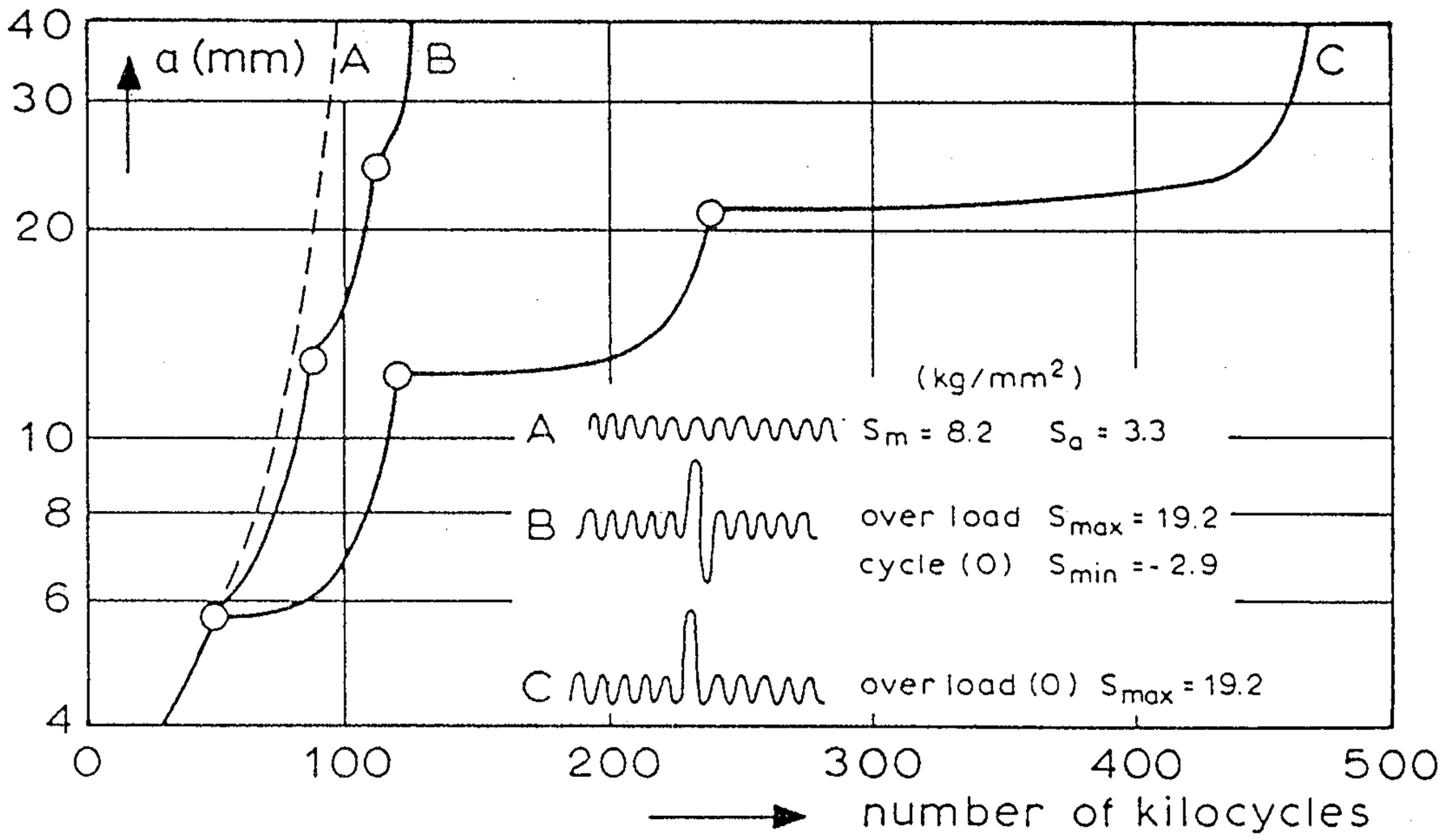


Figure 10.10. Retardation as a result of overloads [48] 2024-T3 Al-alloy

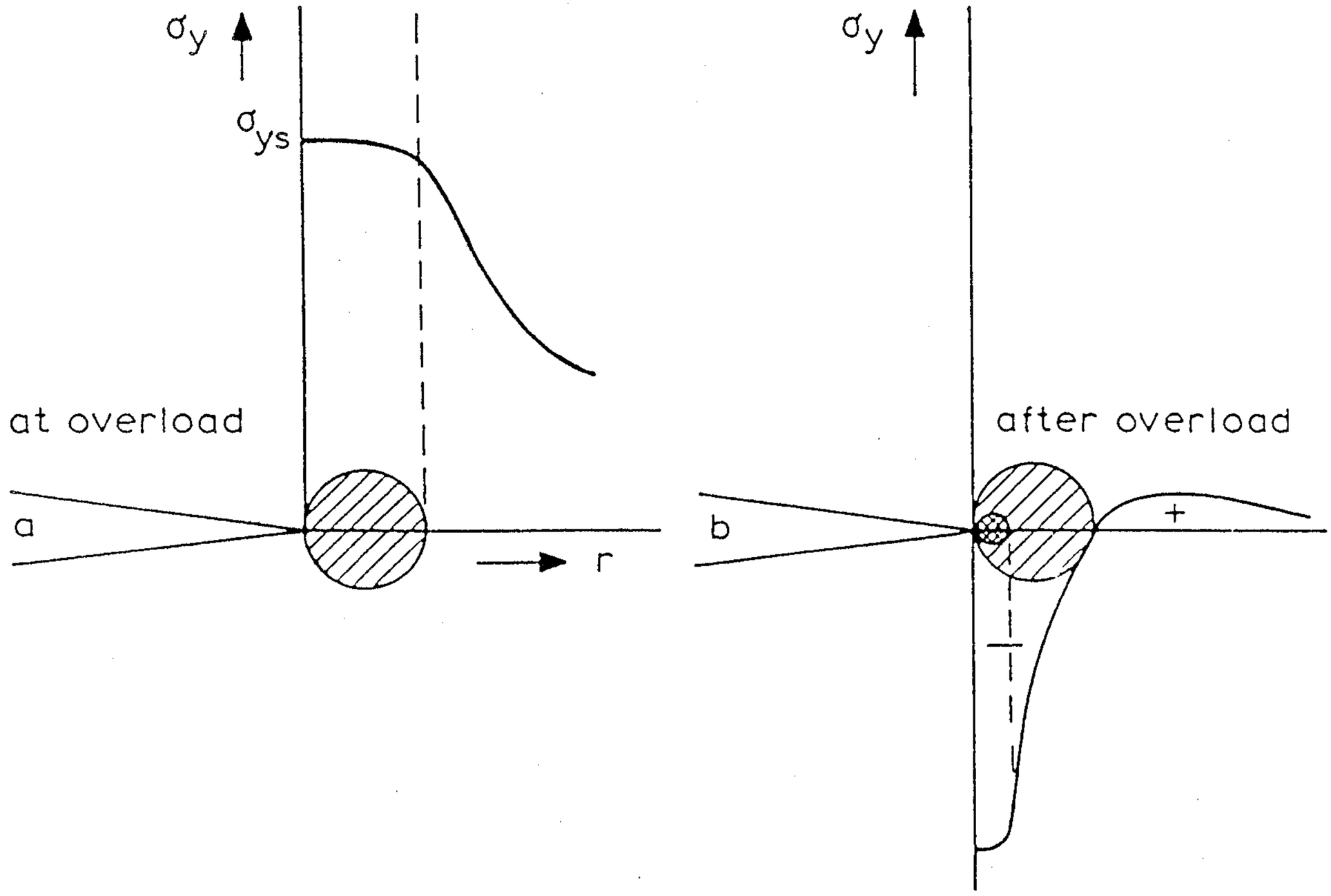


Figure 10.11. Residual compressive stresses at crack tip as a result of overload

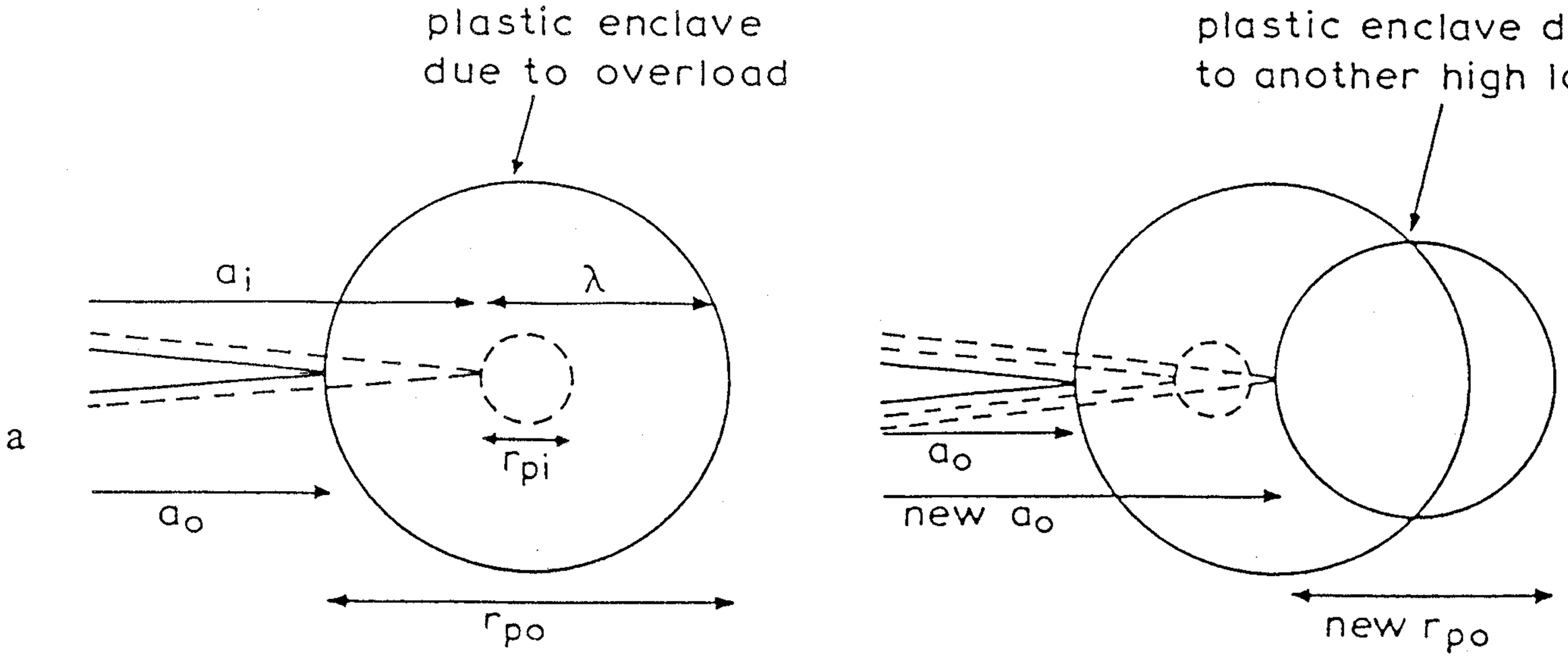


Figure 10.15. The model of Wheeler [61]
a. Situation after overload; b. Situation after second overload

$$\left(\frac{da}{dN}\right)_{\text{retarded}} = \phi\left(\frac{da}{dN}\right)_{\text{linear}} = \phi f(\Delta K)$$

$$\text{with } \phi = \left(\frac{r_{pi}}{a_o + r_{po} - a_i}\right)^m \text{ as long as } a_i + r_{pi} < a_o + r_{po}\,.$$

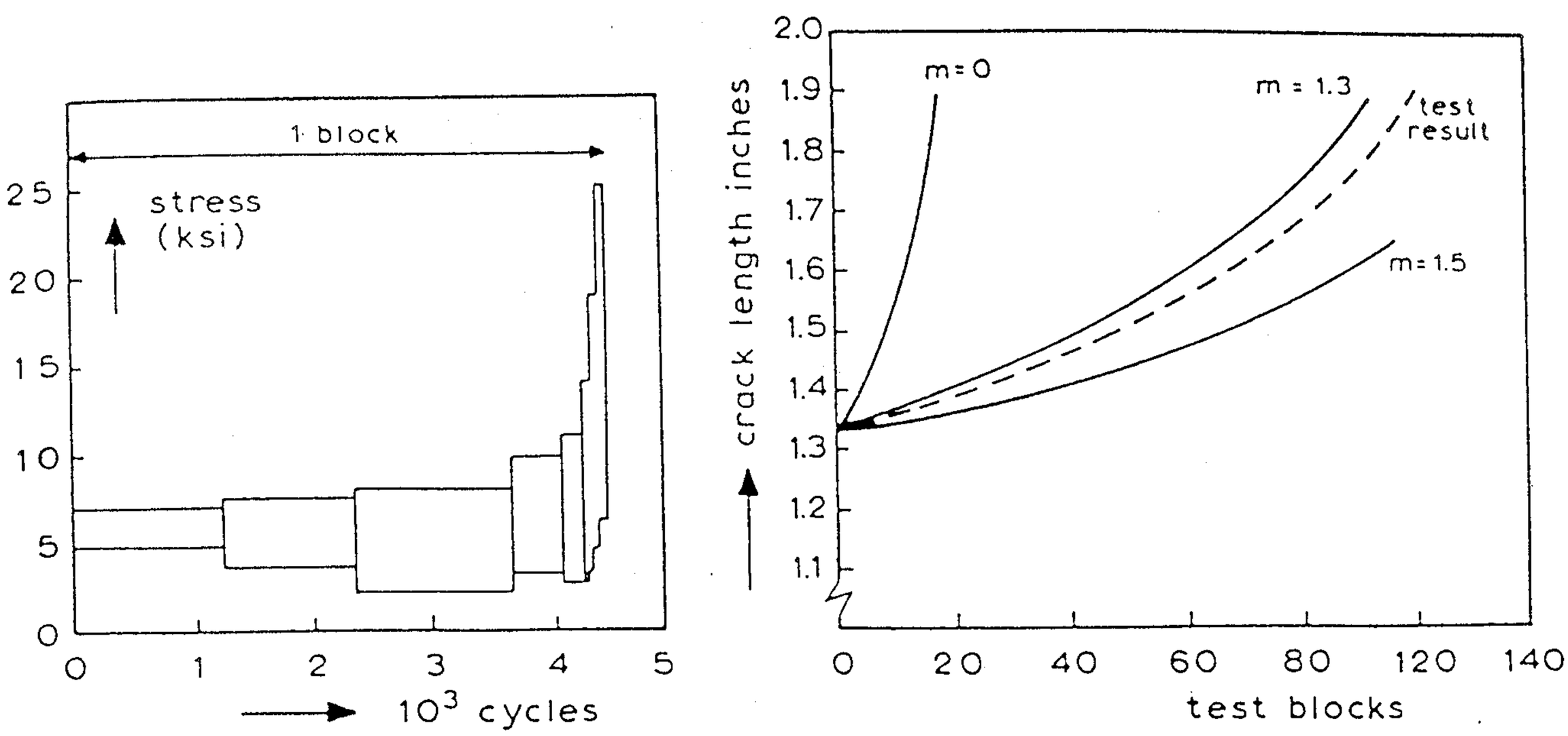
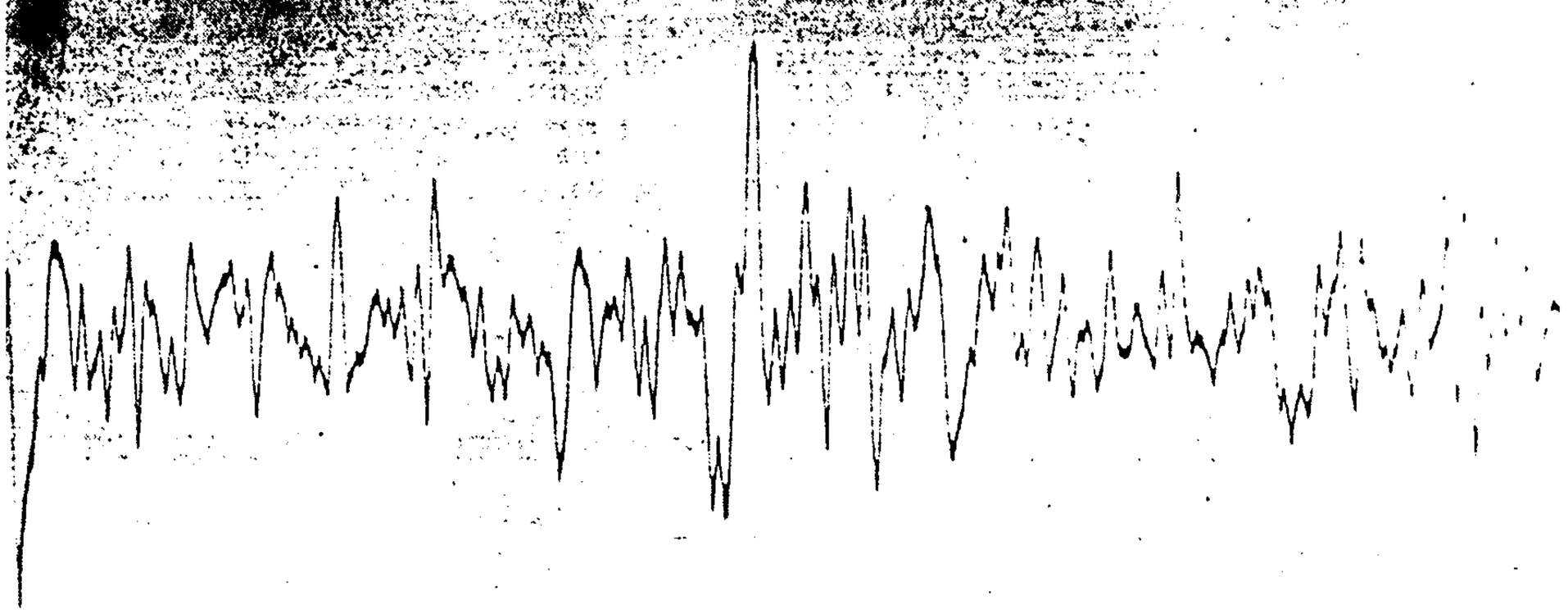


Figure 10.16. Prediction of crack growth made by Wheeler [61] (courtesy ASME)

a



b

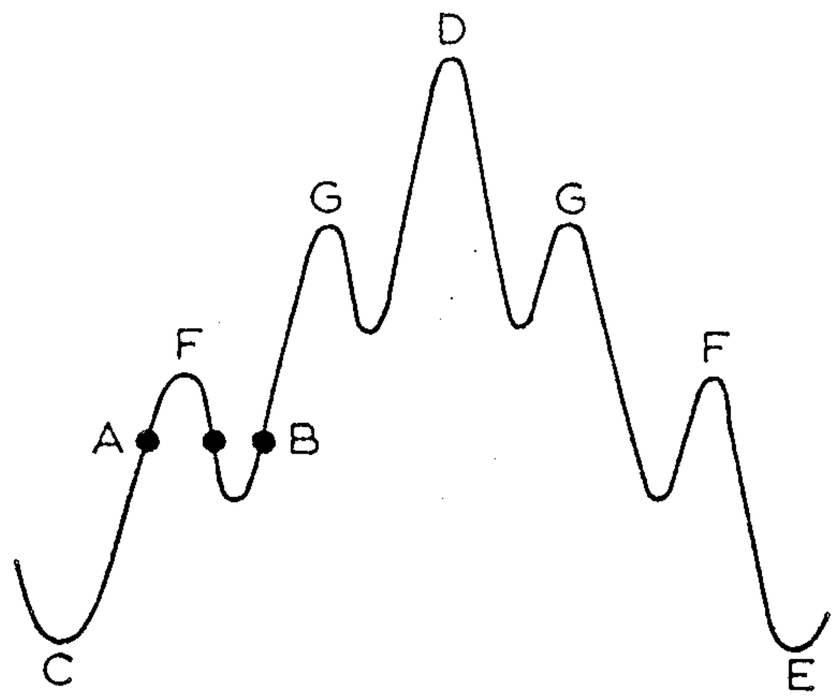
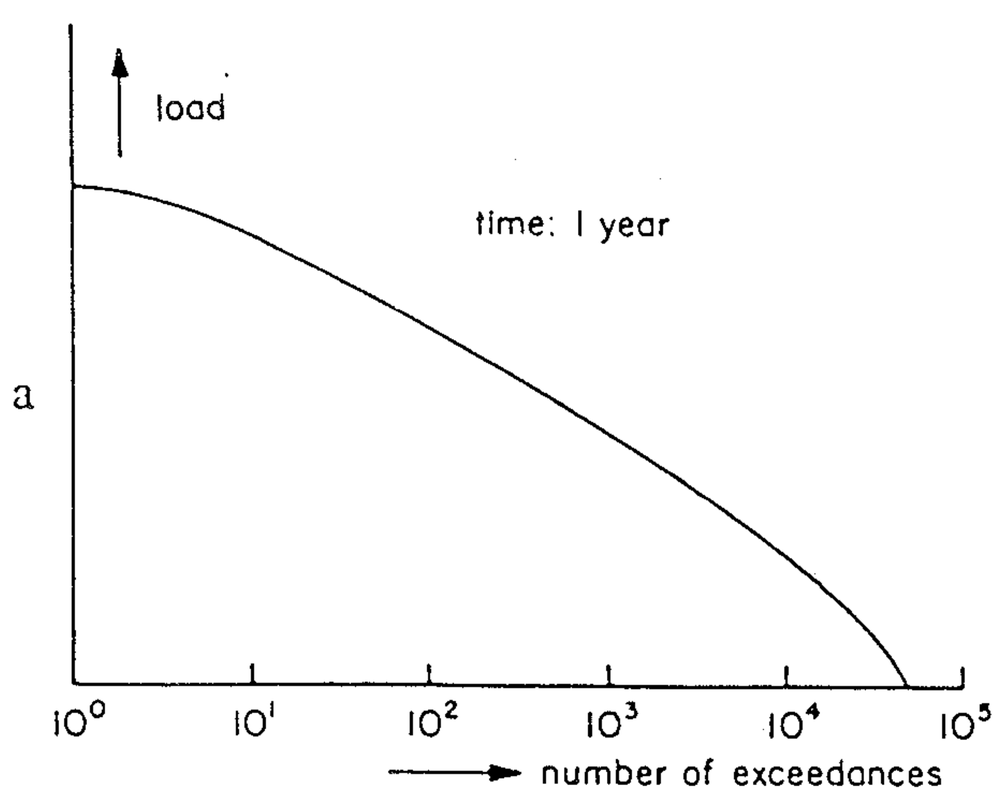
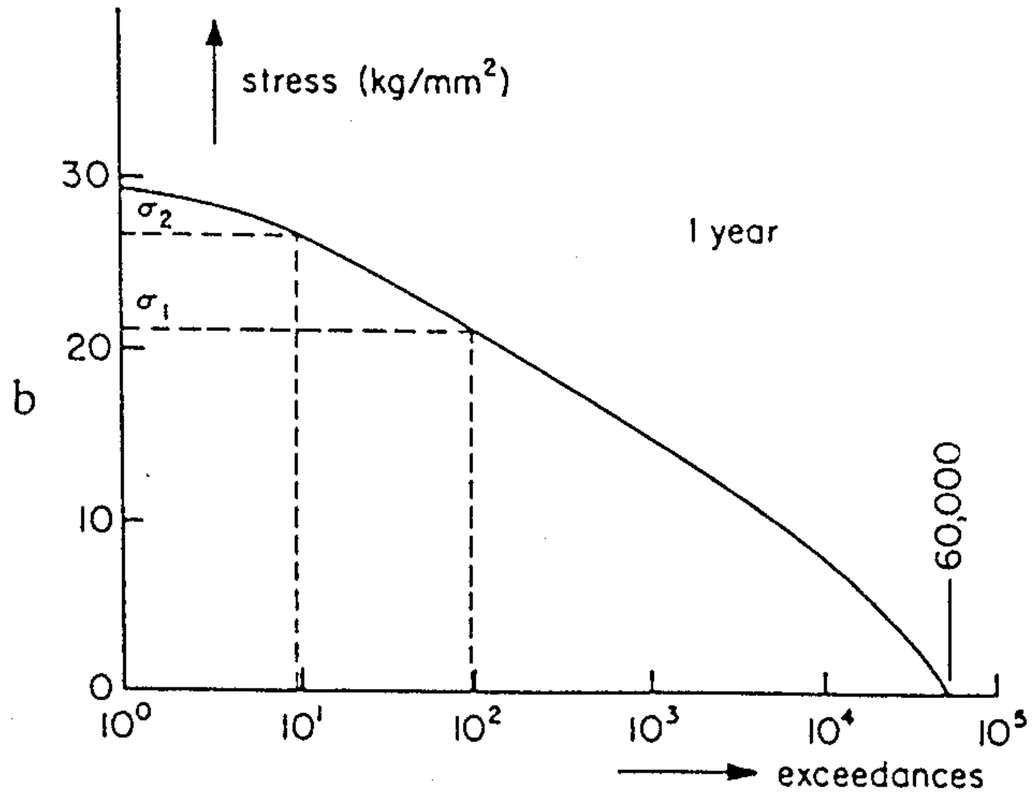


Figure 17.1. Analysis of load-time history
a. Measured load-time history of aircraft wing [2]; b. Two examples of counting procedures
Alternatives: 4 cycles AB plus one cycle CDE or 2 peaks to F, 2 peaks to G, 1 peak to D



a



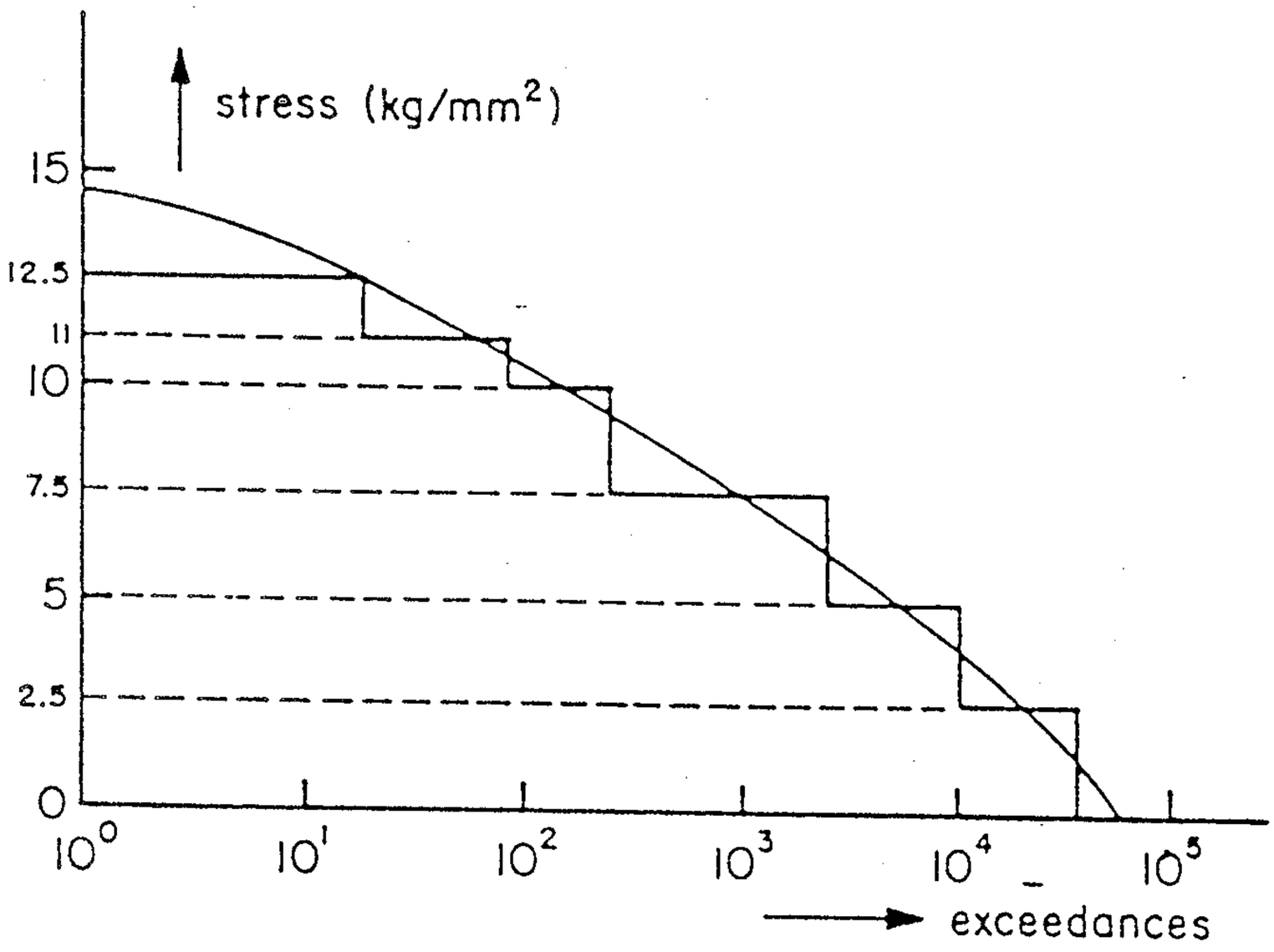
b

Figure 17.2. Assumed exceedance curve
a. Load exceedances; b. Stress exceedances

10.3

Approximation of the stress spectrum

a



b

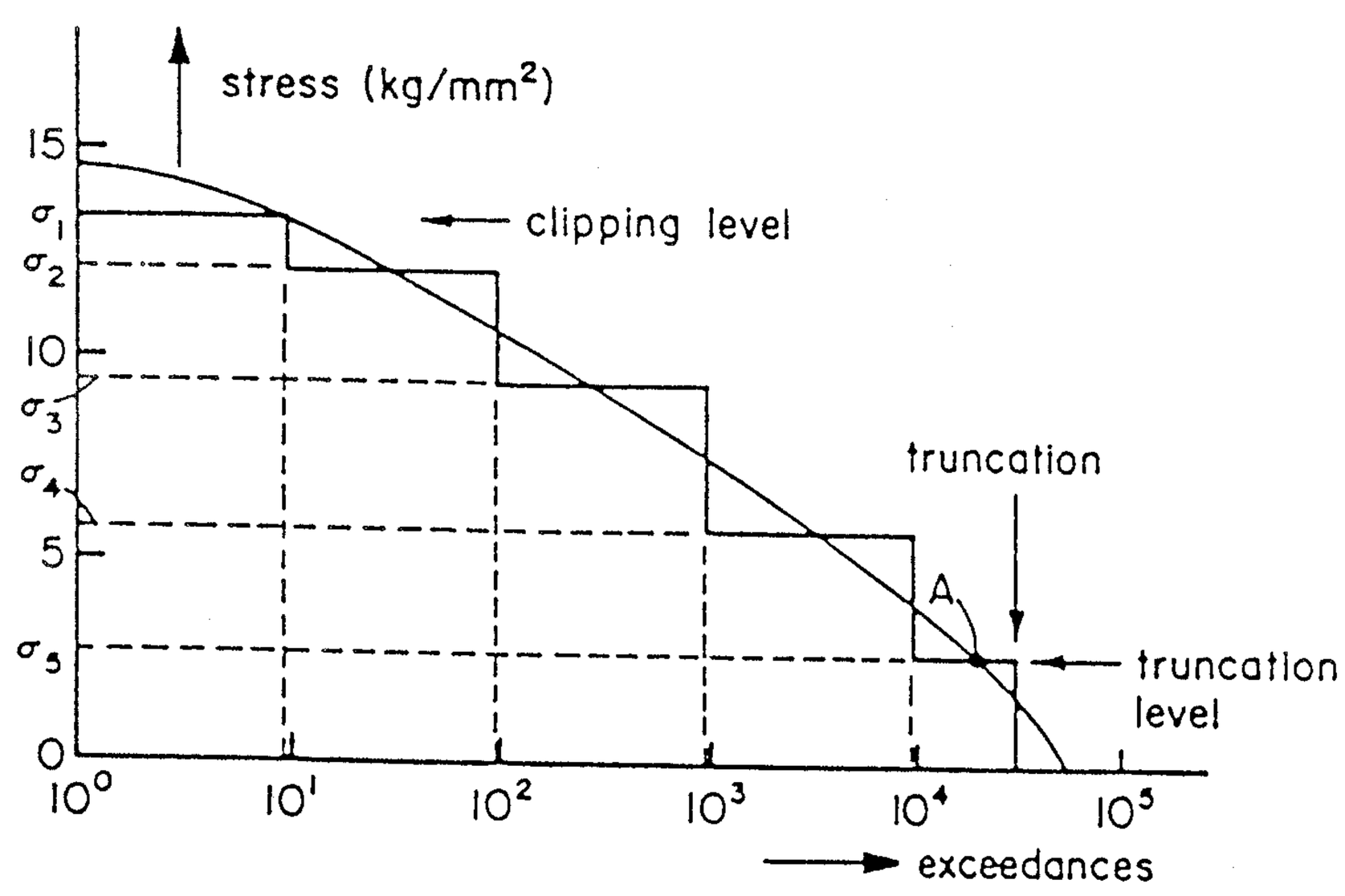


Figure 17.3. Stepwise approximation of exceedance curve
a. Discrete stress levels; b. Discrete exceedances

TABLE 17.1
Establishment of loads block

Stress Level, kg/mm²	Exceedances	Occurrences	Occurrences per day	Occurrences in one-tenth year
13.5	10	10	0.027	1
12	100	90	0.247	9
9	1,000	900	2.47	90
5.8	10,000	9,000	24.7	900
2.8	30,000	20,000	54.8	2000

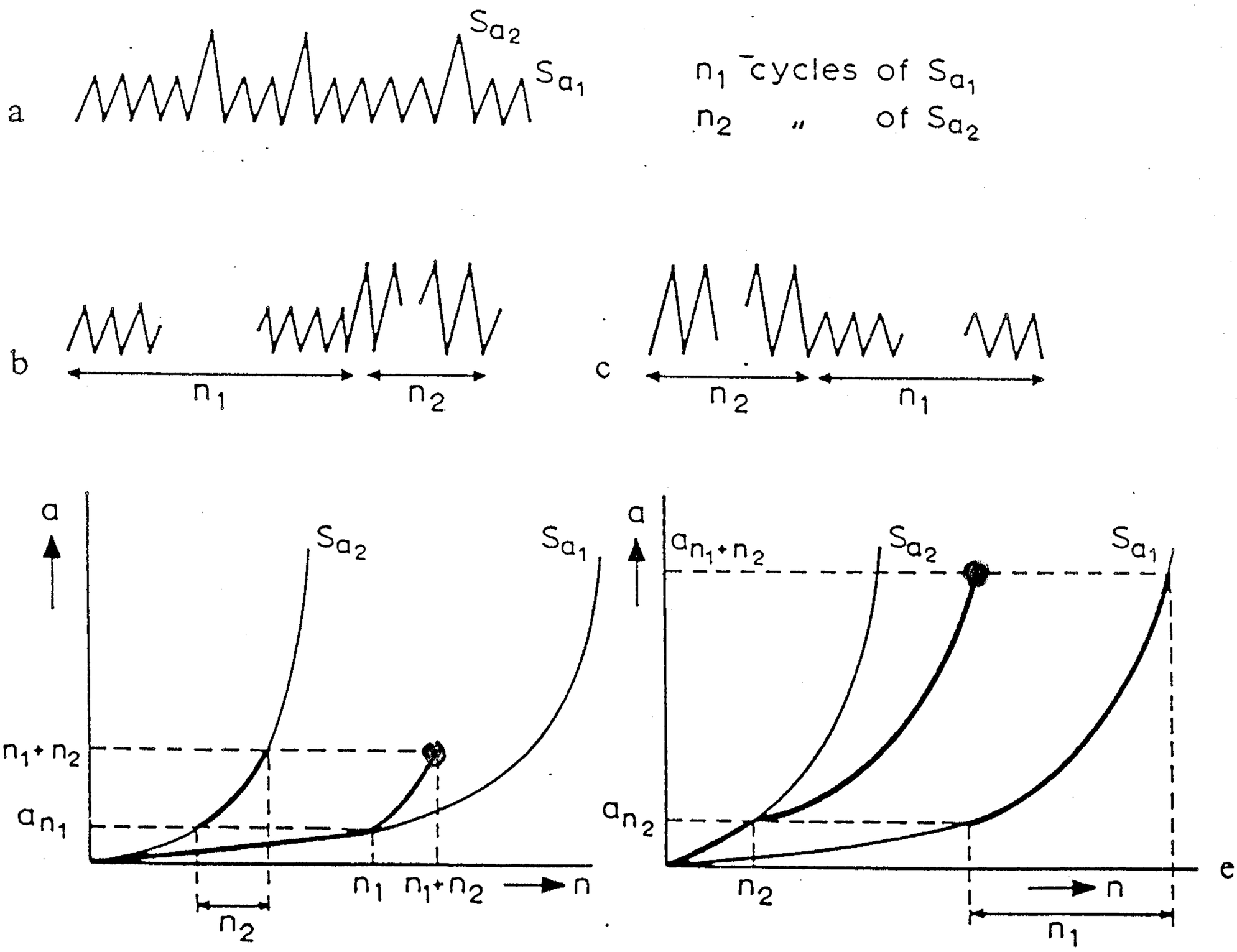


Figure 17.4. Effect of sequence on integration
a. Actual history; b. Simplification; c. Simplification; d. Result of b; e. Result of c

TABLE 17.2

Linear crack growth integration (no retardation)

		First block				Second block			
Stress level, (kg/mm^2)	Cycles in block	Crack size, (mm)	ΔK, $kg/mm^{\frac{3}{2}}$	da/dN, mm/cycles	Δa, (mm)	Crack size, (mm)	ΔK, ($kg/mm^{\frac{3}{2}}$)	da/dN mm/cycles	Δa, mm
13.5	1	5.0	53.5	2.45×10^{-3}	$\times 1$ $=0.00245$	5.1471	54.29	2.60×10^{-3}	0.0026
12	9	5.00245	47.57	1.54×10^{-3}	$\times 9$ $=0.01382$	5.1497	48.27	1.63×10^{-3}	0.0147
9	90	5.0163	35.73	4.89×10^{-4}	$\times 90$ $=0.0440$	5.1644	36.25	5.18×10^{-4}	0.0466
5.8	900	5.0603	23.13	8.58×10^{-5}	$\times 900$ $=0.0772$	5.2110	23.47	9.10×10^{-5}	0.0819
2.8	2000	5.1375	11.24	4.80×10^{-6}	$\times 2000$ $=0.0096$	5.2929	11.41	5.10×10^{-6}	0.0102
Alternative with fixed crack size per block									
13.5	1	5.0	53.5	2×10^{-3}	0.002	5.14	54.2	2.6×10^{-3}	0.0026
12	9	5.0	47.5	1.5×10^{-3}	0.0105	5.14	48.2	1.6×10^{-3}	0.0145
9	90	5.0	35.6	4.8×10^{-4}	0.0435	5.14	36.2	5.1×10^{-3}	0.0460
5.8	900	5.0	22.9	8.3×10^{-5}	0.0748	5.14	23.3	3.9×10^{-5}	0.0800
2.8	2000	5.0	11.1	4.5×10^{-6}	0.009	5.14	11.2	4.8×10^{-6}	0.0096
					$+\Delta a = 0.1398$				$+\Delta a = 0.1527$
					New $a = 5.1398$				New $a = 5.28$

TABLE 17.3

Crack-growth integration with retardation

Stress level, kg/mm^2	Cycles in block	Crack size a, mm	ΔK, kg/mm$^{\frac{3}{2}}$	da/dN linear, mm/cycle	r_p, mm	$a+r_p$	$a+r_{p0}$, mm	$a+r_{p0}-a_i$, mm	$\phi=\left(\frac{r_p}{a+r_{p0}-a_i}\right)^m$	da/dN retarded, mm/cycle	Δa, mm	New a, mm
						First block						
13.5	1	5.0	53.5	2.45×10^{-3}	0.061	5.061	5.061	0.061	1	2.45×10^{-3}	$\times1=0.00245$	5.00245
12	9	5.00245	47.57	1.54×10^{-3}	0.048	5.051	5.061	0.059	0.76	1.17×10^{-3}	$\times9=0.01053$	5.01298
9	90	5.01298	35.72	4.88×10^{-4}	0.027	5.040	5.061	0.048	0.47	2.29×10^{-4}	$\times90=0.02061$	5.03359
5.8	900	5.03359	23.06	8.48×10^{-5}	0.011	5.044	5.061	0.027	0.31	2.68×10^{-5}	$\times900=0.02366$	5.05725
2.8	2000	5.05725	11.16	4.65×10^{-6}	0.003	5.060	5.061	0.004	0.69	3.21×10^{-6}	$\times312=0.001$	5.05825
2.8	1688	5.05825	11.16	4.65×10^{-6}	0.003	5.061	5.061	0.003	1	4.65×10^{-6}	$\times1688=0.00785$	5.06610
						Second block						
13.5	1	5.066	53.9	2.5×10^{-3}	0.062	5.128	5.128	0.062	1	2.5×10^{-3}	$\times1=0.03$	5.069
12	9	5.069	47.9	1.6×10^{-3}	0.049	5.118	5.128	0.059	0.79	1.3×10^{-3}	$\times9=0.012$	5.081
9	90	5.081	36.0	5.0×10^{-4}	0.028	5.109	5.128	0.047	0.51	2.6×10^{-4}	$\times90=0.023$	5.104
5.8	900	5.104	23.2	8.7×10^{-5}	0.011	5.115	5.128	0.024	0.36	3.1×10^{-5}	$\times774=0.024$	5.128
5.8	126	5.128	23.3	8.8×10^{-5}	0.012	5.140	5.140	0.012	1	8.8×10^{-5}	$\times126=0.011$	5.139
2.8	2000	5.139	11.3	4.9×10^{-6}	0.003	5.142	5.142	0.003	1	4.9×10^{-6}	$\times2000=0.010$	5.149

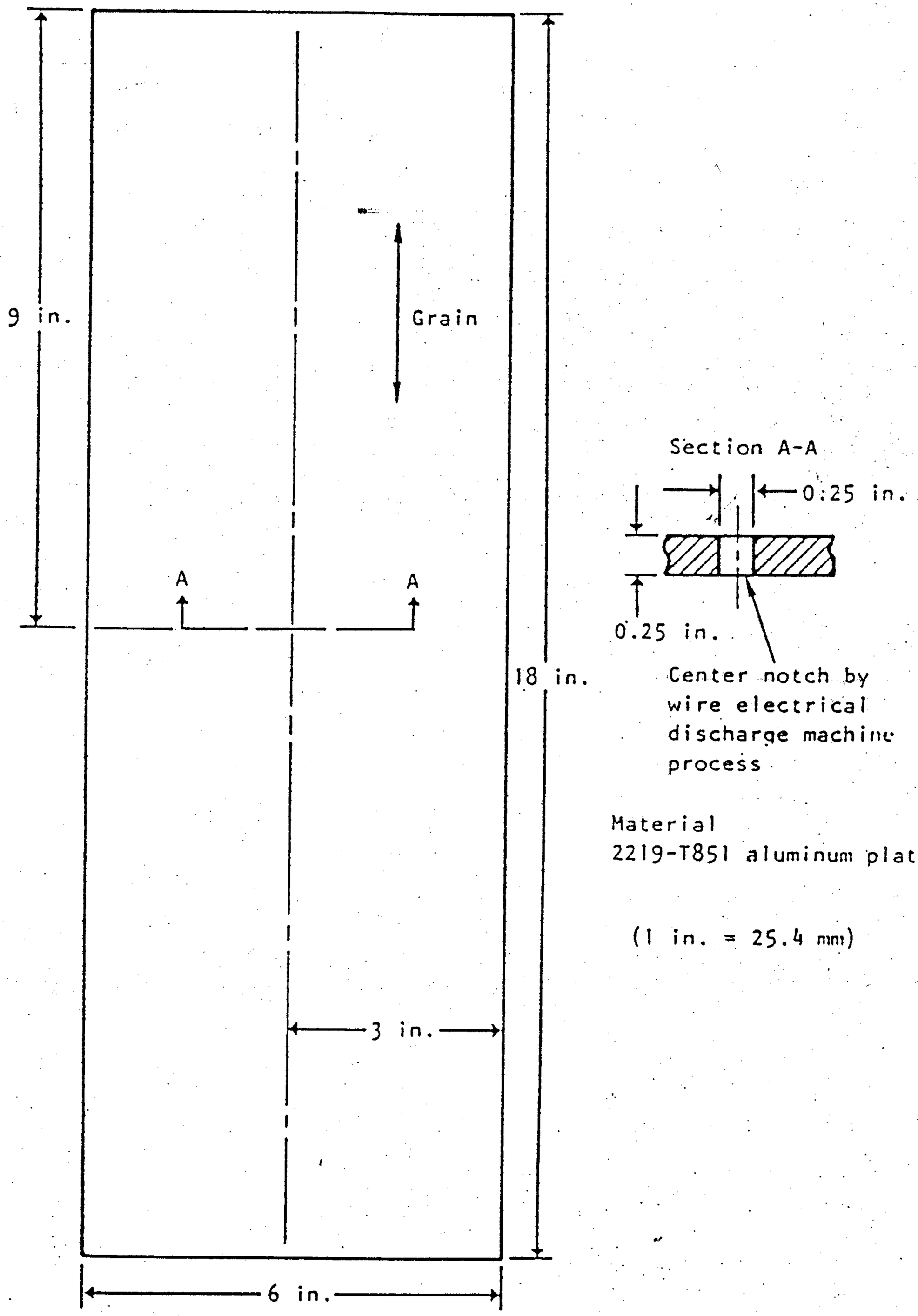


FIG. 2—*Test specimen configuration.*

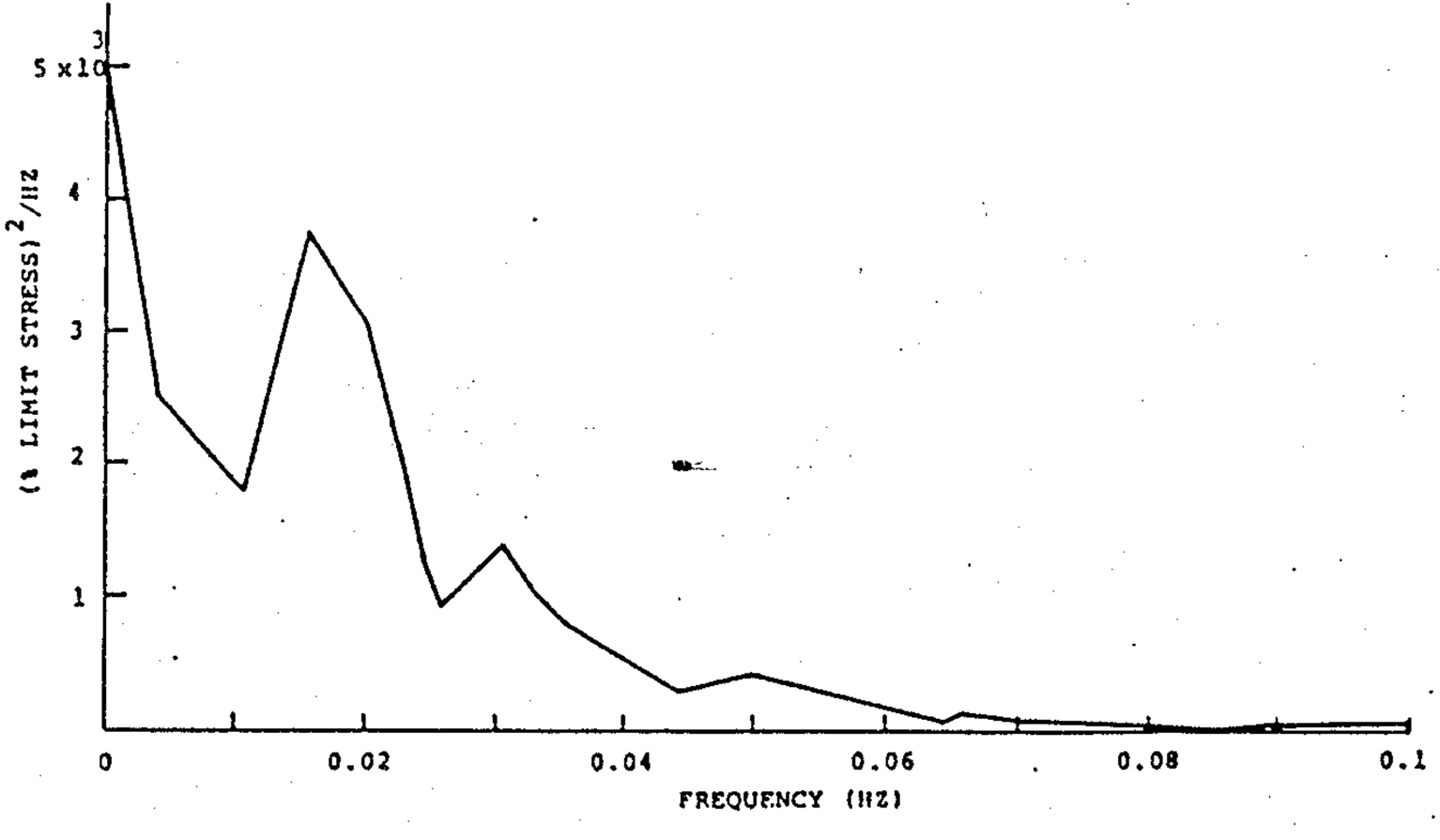


FIG. 4—*Power spectral density for a Fighter A-A mission.*

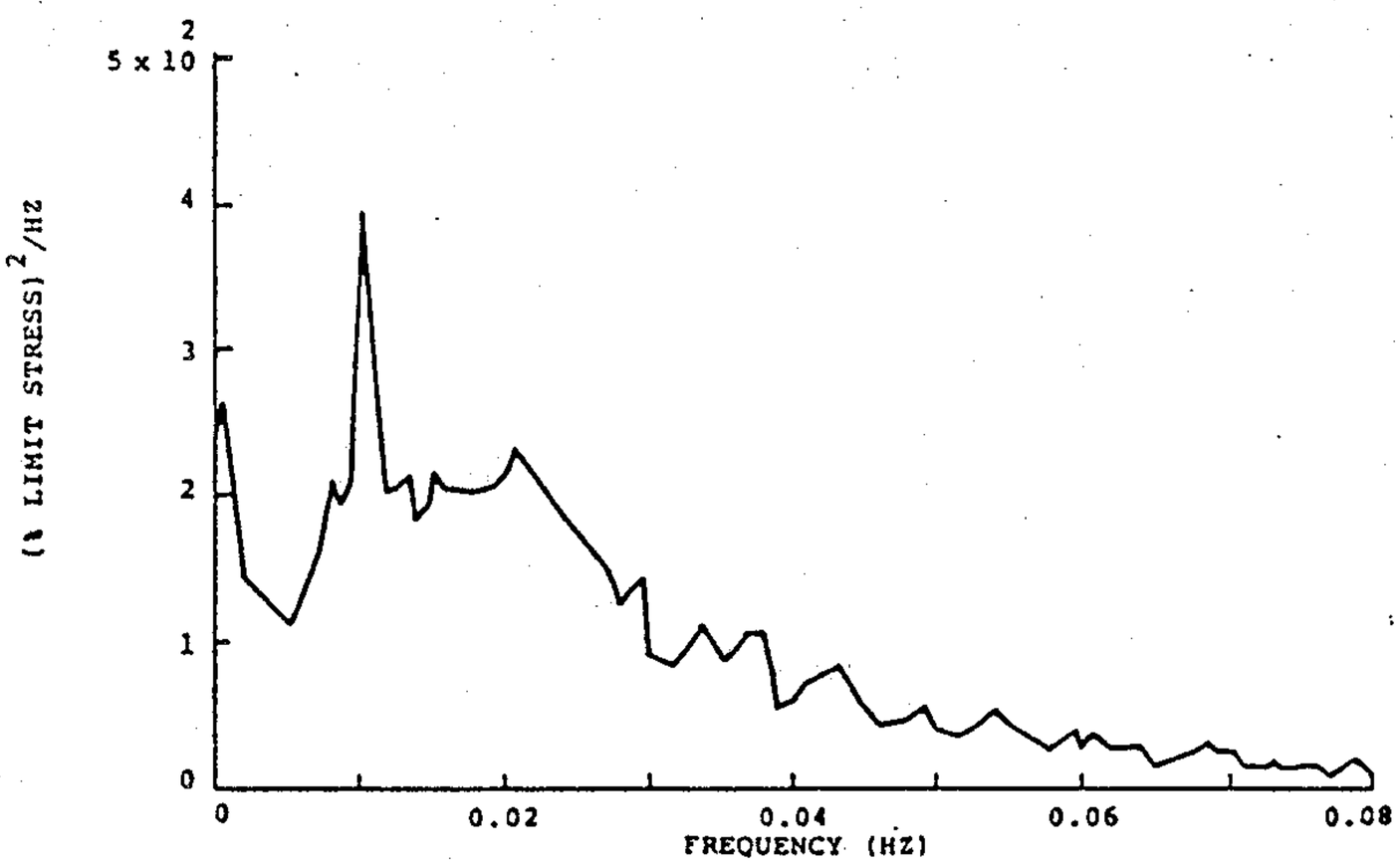


FIG. 5—*Power spectral density for a Fighter A-G mission.*

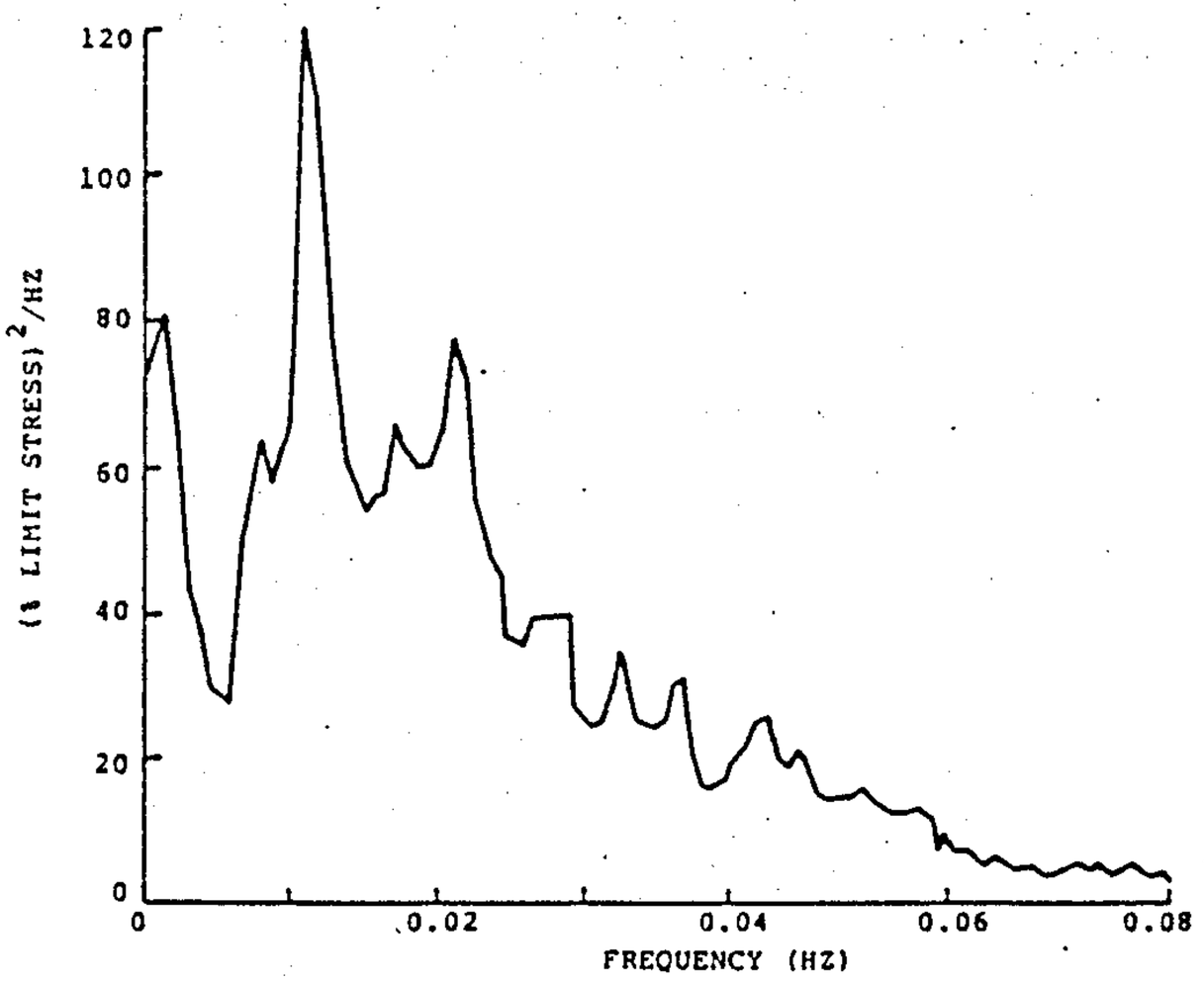


FIG. 6—*Power spectral density for a Fighter I-N mission.*

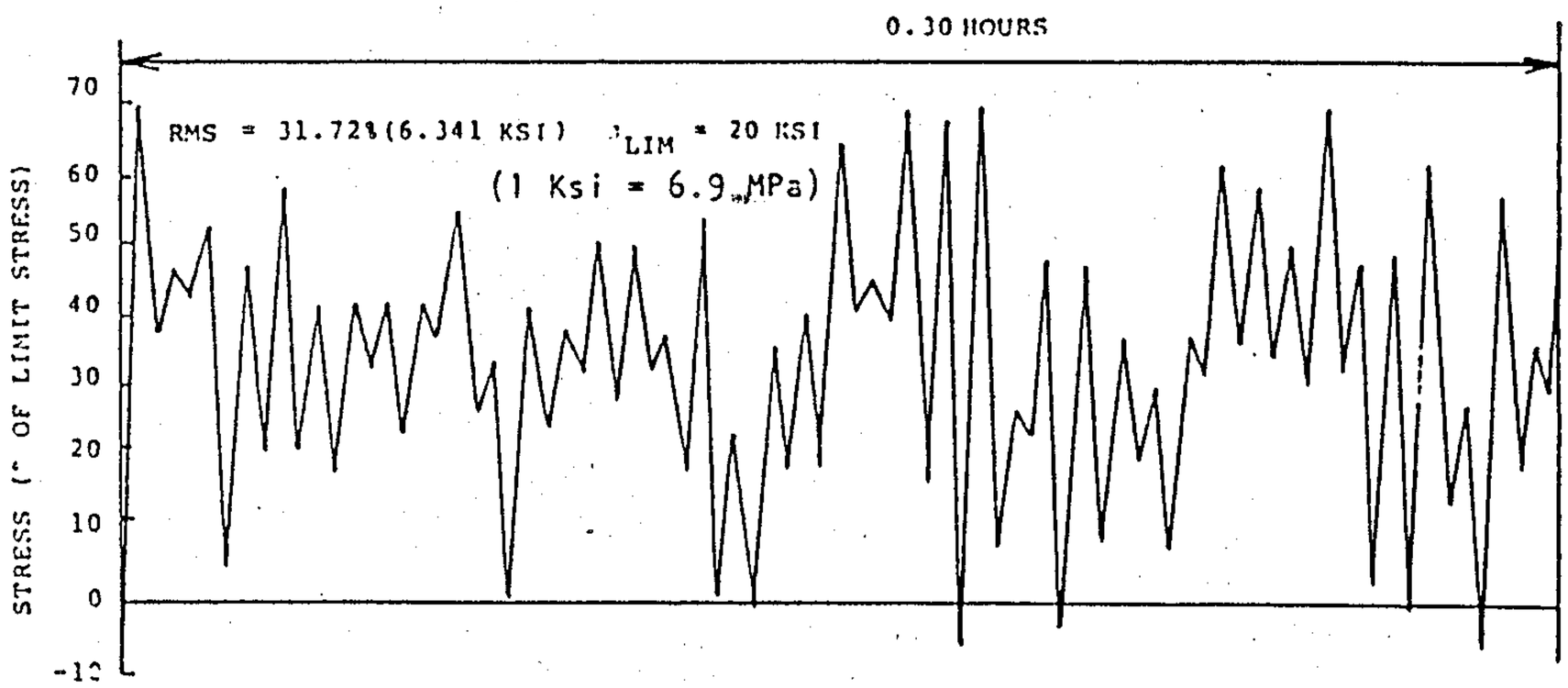


FIG. 7—*Sample load history for a Fighter A-A mission.*

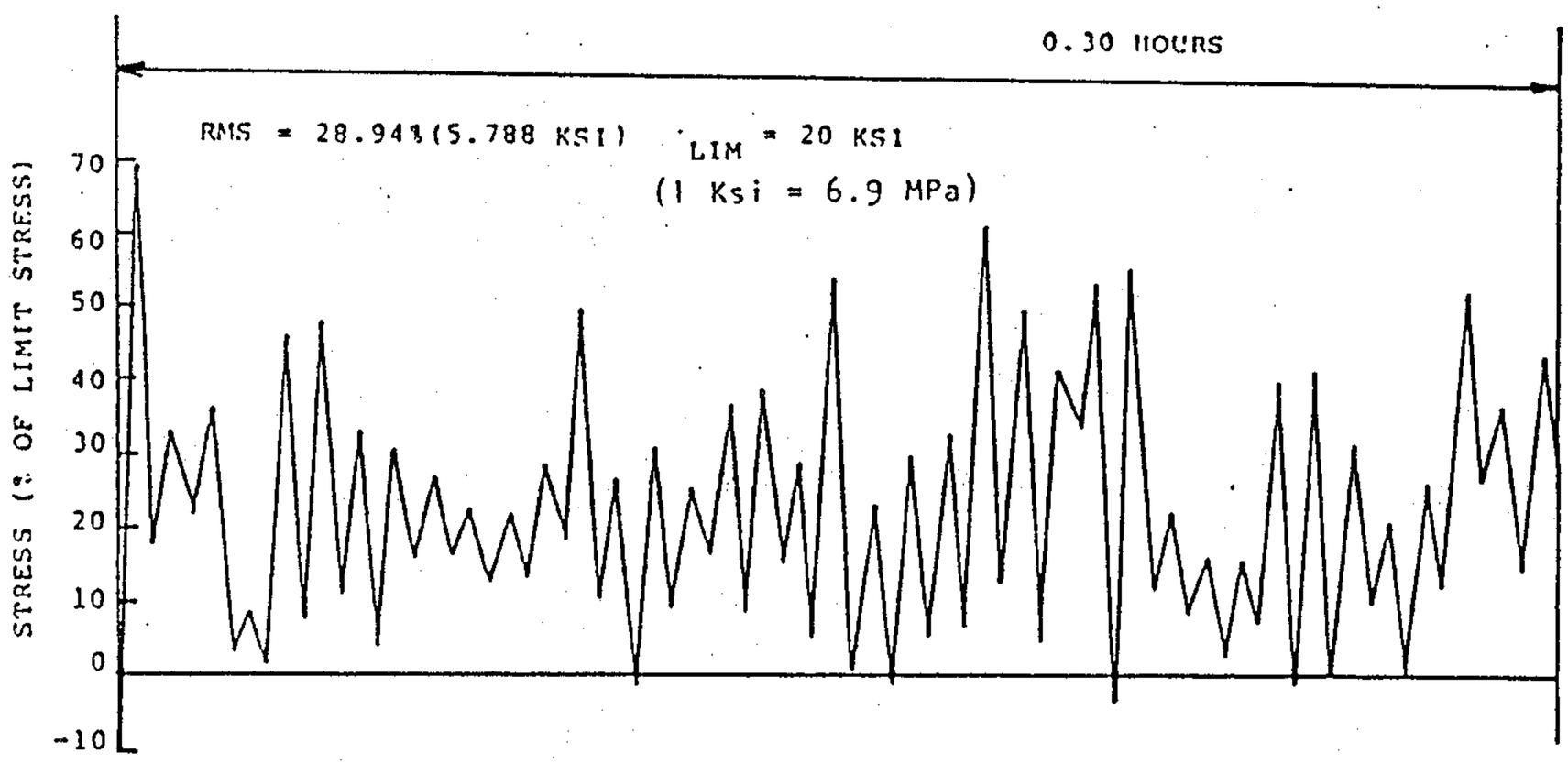


FIG. 8—*Sample load history for a Fighter A-G mission.*

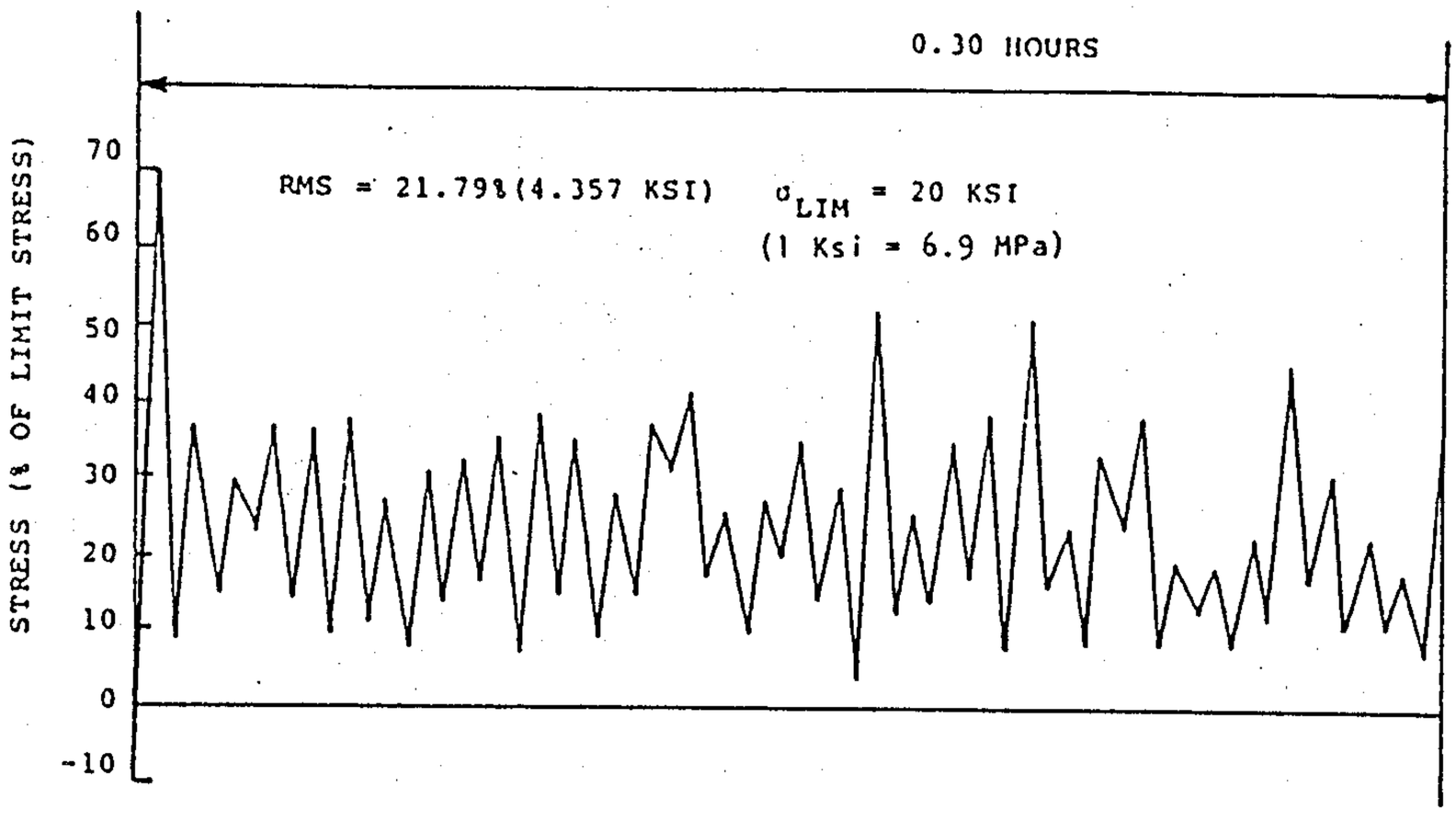


FIG. 9—*Sample load history for a Fighter I-N mission.*

TABLE 1—*Mission profile and stress data of a transport.*

Mission Type	Flight Segment	No. of Cycles	1.0 *g* Stress, ksi[a]	Ground Stress, ksi[a]
Assault	climb	65	10.783	...
	cruise	15	9.075	...
	gust	25	9.000	−6.4
	descent	45	10.622	...
Logistics	climb	10	9.339	...
	cruise	5	7.458	...
	gust	45	9.000	−11.5
	descent	10	10.272	...
Training	climb	40	6.559	...
	cruise	10	6.171	−8.9
	gust	45	9.000	...
	descent	20	8.648	...

[a]1 ksi = 6.9 MPa.

TABLE 2—*ASTM Task Group E24.06.01 random spectrum round-robin analysis summary.*

Test No.	Mission Type	Test Life, cycles; (c_i to c_f, in.[a])	Analytical Predictions, cycles; (N_{pred}/N_{test})					
			JC(1)	CMH	JN	WSJ	JR	JC(2)
M-81	Fighter (A-A)[b]	115 700	140 720	246 000	115 800	137 000	213 110	168 720
	DLS[c] = 20 ksi[d]	(0.16 to 0.501)	(1.21)	(2.13)	(1.01)	(1.18)	(1.84)	(1.46)
M-82	Fighter (A-A)	58 585	44 525	79 000	39 125	57 000	74 055	53 312
	DLS = 30 ksi	(0.15 to failure)	(0.76)	(1.35)	(0.67)	(0.97)	(1.26)	(0.91)
M-83	Fighter (A-A)	18 612	14 703	25 359	11 940	19 700	25 944	17 309
	DLS = 40 ksi	(0.15 to failure)	(0.79)	(1.36)	(0.64)	(1.06)	(1.39)	(0.93)
M-84	Fighter (A-G)[e]	268 908	302 816	395 292	396 230	342 000	496 284	368 662
	DLS = 20 ksi	(0.158 to failure)	(1.13)	(1.47)	(1.47)	(1.27)	(1.85)	(1.37)
M-85	Fighter (A-G)	95 642	73 644	99 368	84 850	90 020	131 868	91 816
	DLS = 30 ksi	(0.144 to failure)	(0.77)	(1.04)	(0.89)	(0.94)	(1.38)	(0.96)
M-86	Fighter (A-G)	36 367	23 275	29 789	23 820	30 000	45 034	29 093
	DLS = 40 ksi	(0.153 to failure)	(0.64)	(0.82)	(0.65)	(0.82)	(1.24)	(0.80)
M-88	Fighter (I-N)[f]	380 443	281 528	475 292	959 700	589 000	810 900	528 816
	DLS = 30 ksi	(0.150 to failure)	(0.74)	(1.25)	(2.52)	(1.55)	(2.13)	(1.39)
M-89	Fighter (I-N)	164 738	95 548	155 294	242 380	223 000	288 900	184 507
	DLS = 40 ksi	(0.150 to failure)	(0.58)	(0.94)	(1.47)	(1.35)	(1.75)	(1.12)
M-90	Fighter Composite	218 151	231 240	430 225	255 090	270 000	401 140	290 140
	DLS = 20 ksi	(0.153 to failure)	(1.06)	(1.97)	(1.17)	(1.24)	(1.84)	(1.33)
M-91	Fighter Composite	65 627	51 845	93 473	51 165	66 000	97 679	65 630
	DLS = 30 ksi	(0.15 to failure)	(0.79)	(1.42)	(0.78)	(1.01)	(1.49)	(1.01)
M-92	Fighter Composite	22 182	17 080	31 446	15 370	22 800	34 000	21 738
	DLS = 40 ksi	(0.15 to failure)	(0.77)	(1.42)	(0.69)	(1.03)	(1.53)	(0.98)
M-93	Transport Composite	1 359 000	2 419 020	...	1 031 200	1 470 000	3 599 000	1 780 290
	MSS[g] = 14 ksi	(0.25 to 0.54)	(1.78)	...	(0.76)	(1.08)	(2.65)	(1.31)
M-94	Transport Composite	279 000	426 870	...	348 550	257 000	628 074	318 060
	MSS = 19.6 ksi	(0.258 to 0.38)	(1.53)	...	(1.25)	(0.92)	(2.25)	(1.14)
Average (N_{pred}/N_{test}) ratio			(0.96)	(1.38)	(1.07)	(1.11)	(1.74)	(1.13)
Standard deviation			(0.36)	(0.42)	(0.33)	(0.20)	(0.42)	(0.22)

[a] 1 in. = 25.4 mm.
[b] A-A = Air-to-Air.
[c] DLS = Design limit stress.
[d] 1 ksi = 6.9 MPa.
[e] A-G = Air-to-Ground.
[f] I-N = Instrumentation and Navigation.
[g] MSS = Maximum spectrum stress.

TABLE 3—*Analytical methods and computer codes used in the round-robin predictions.*

Analytical Predictions	Prediction Method	Computer Code
JC(1)	Walker crack growth rate equation; compressive loads set to zero; tensile load retardation not accounted for	EFFGRO
CMH	root-mean-square	CYCLIF
JN	modified Elber's equation; load interaction effects accounted for by analytical closure model	FAST
WSJ	modified Forman's equation; load interaction effects accounted for by multiple-parameter yield zone model	CGR-LaRC
JR	Walker's crack growth rate equation; compressive loads set to zero; tensile load retardation effect accounted for by generalized Willenborg model	CRACKS
JC(2)	Walker's crack growth rate equation; load interaction effects accounted for by Willenborg/Chang model	EFFGRO

TABLE 4—*Summary of prediction ratios of each test case.*

Test No.	Mission Type	Test Life, cycles	N_{pred}/N_{test}
M-81	Fighter (A-A)[a] DLS[b] = 20 ksi[c]	115 700	1.47 ± 0.43
M-82	Fighter (A-A) DLS = 30 ksi	58 585	0.99 ± 0.27
M-83	Fighter (A-A) DLS = 40 ksi	18 612	1.03 ± 0.3
M-84	Fighter (A-G)[d] DLS = 20 ksi	268 908	1.43 ± 0.24
M-85	Fighter (A-G) DLS = 30 ksi	95 642	0.99 ± 0.21
M-86	Fighter (A-G) DLS = 40 ksi	36 367	0.83 ± 0.22
M-88	Fighter (I-N)[e] DLS = 30 ksi	380 443	1.60 ± 0.64
M-89	Fighter (I-N) DLS = 40 ksi	164 738	1.20 ± 0.41
M-90	Fighter Composite DLS = 20 ksi	218 151	1.44 ± 0.38
M-91	Fighter Composite DLS = 30 ksi	65 627	1.08 ± 0.31
M-92	Fighter Composite DLS = 40 ksi	22 182	1.07 ± 0.34
M-93	Transport Composite MSS[f] = 14 ksi	1 359 000	1.52 ± 0.73
M-94	Transport Composite MSS = 19.6 ksi	279 000	1.42 ± 0.51

[a] A-A = Air-to-Air.
[b] DLS = Design limit stress.
[c] 1 ksi = 6.9 MPa.
[d] A-G = Air-to-Ground.
[e] I-N = Instrumentation and Navigation.
[f] MSS = Maximum spectrum stress.

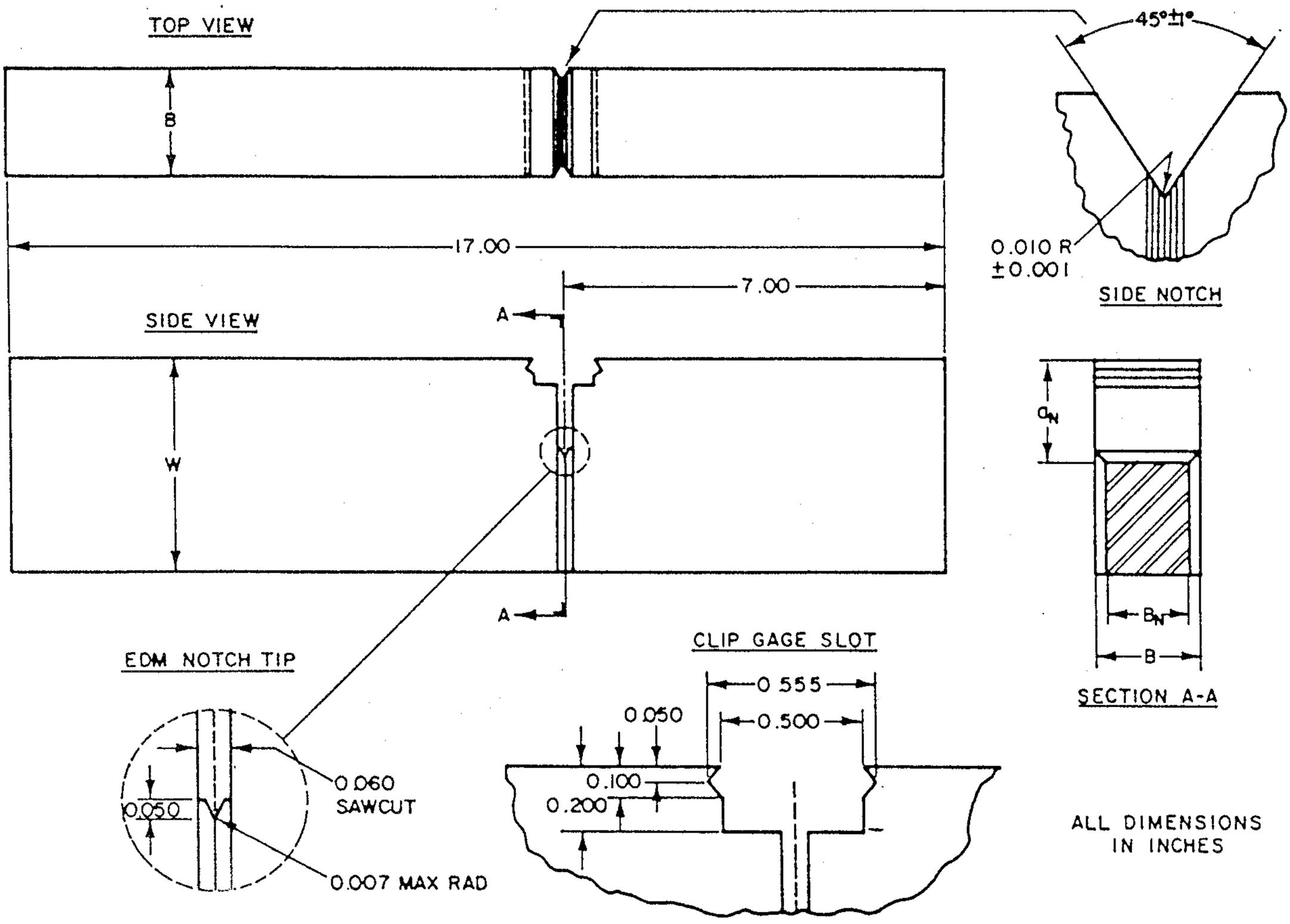


FIG. 10.1. Fatigue-cracked cantilever-beam test specimen.

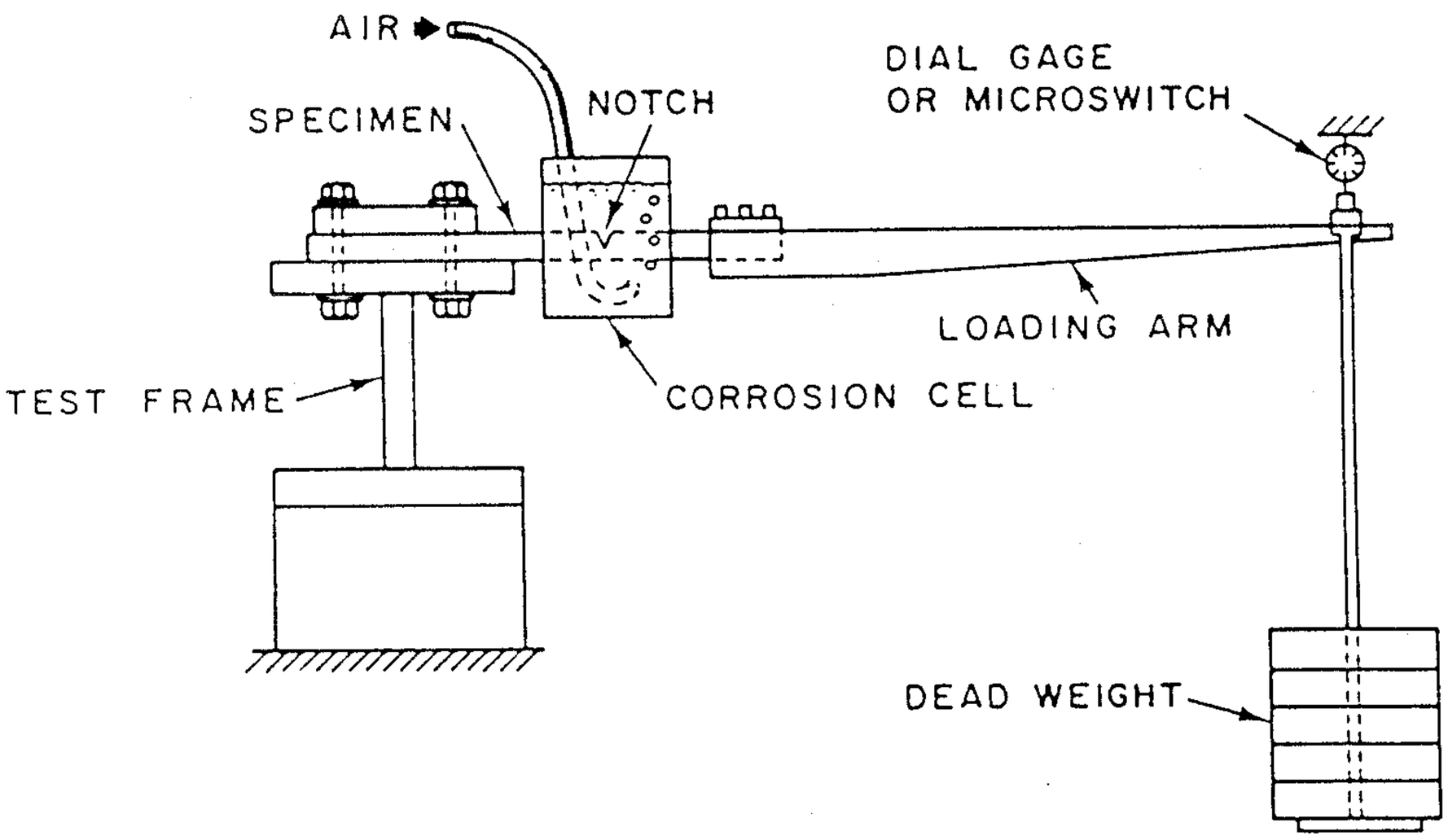


FIG. 10.2. Schematic drawing of fatigue-cracked cantilever-beam test specimen and fixtures.

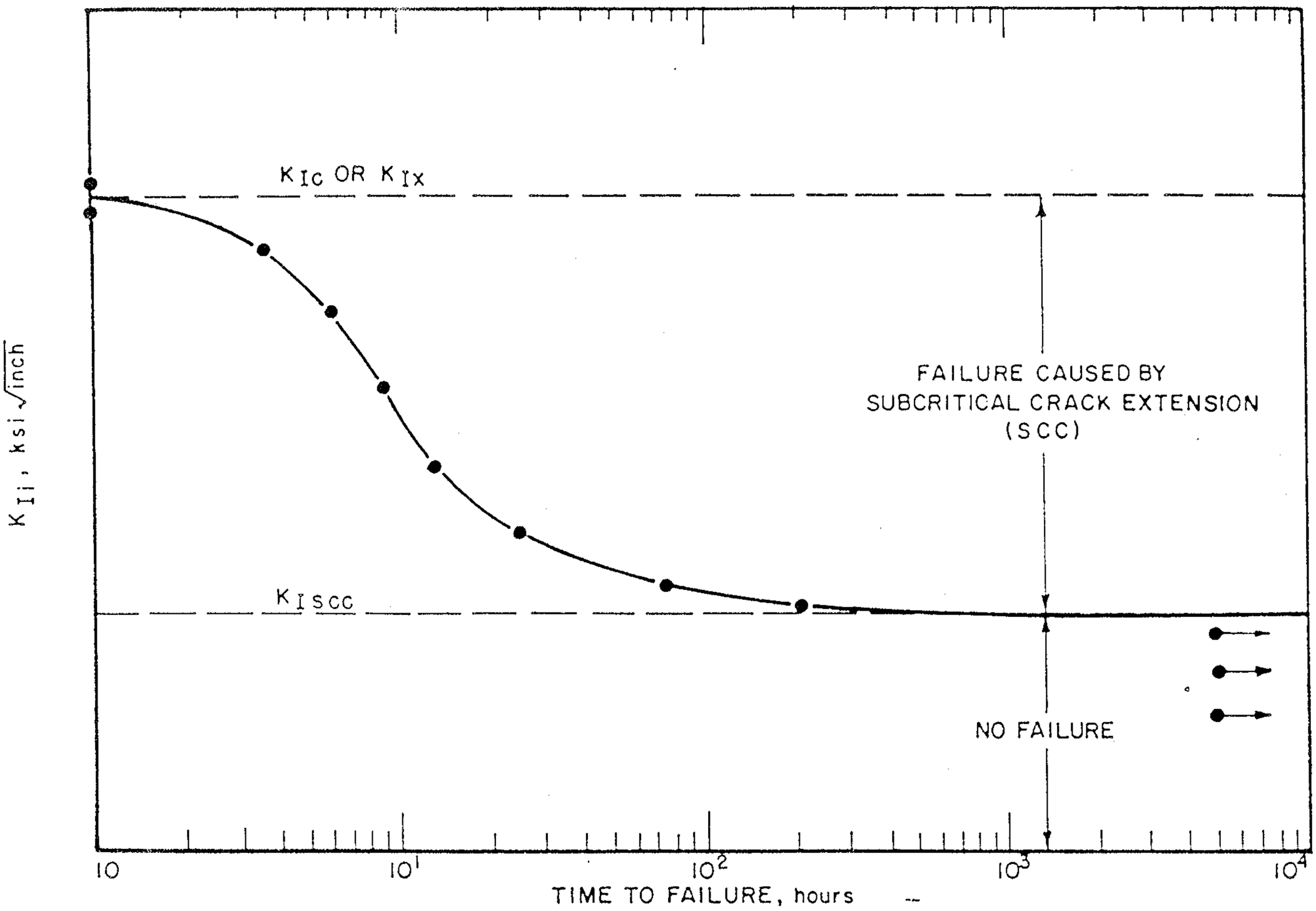


FIG. 10.3. Procedure to obtain K_{Iscc} with precracked cantilever-beam specimens.

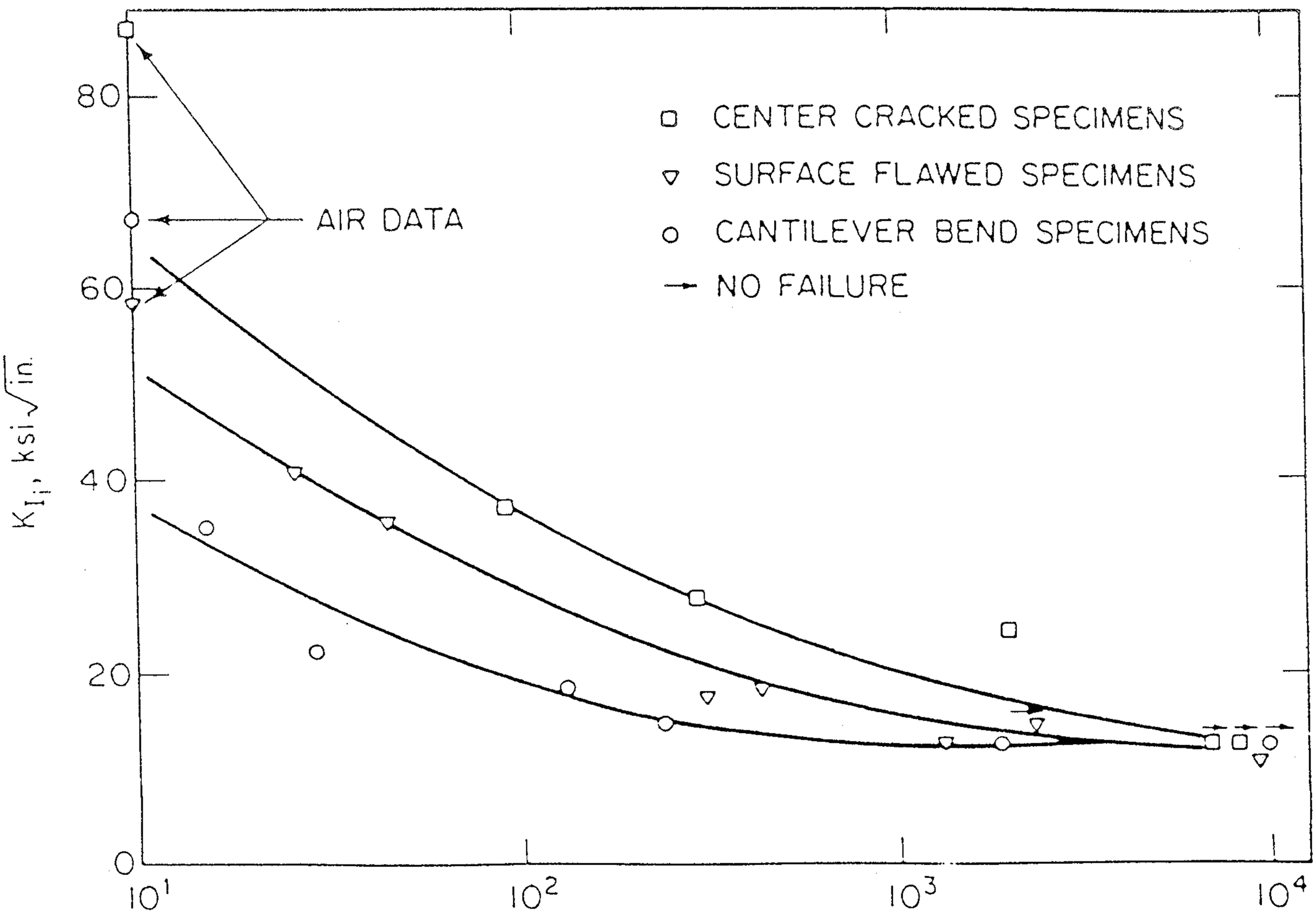


FIG. 10.8. Influence of specimen geometry on the time to failure (AISI 4340 steel).

K_{ISCC}/K_{IC} for Various Materials - Environment Systems

Material	Temp [°F]	σ_y [ksi]	Environment	K_{ISCC}/K_{IC}
6Al-4V-T_i	RT	160	Methanol	0.24
	RT	160	Freon	0.58
	RT	160	H_2O_2 (30%)	0.74
	RT	160	H_2O_2 (60%)	0.83
	RT	160	NaCl + H_2O	0.82
	RT	160	H_2O	0.80
	RT	160	He	0.90
	RT	160	Aerozine 50	0.82
	90	160	H_2O_2 (30%)	0.71
	90	160	H_2O_2 (60%)	0.75
	105	160	Mono-Hydrazine	0.75
	110	160	Aerozene 50	0.75
2219 T87 Alumina	RT	58	Air	0.96
	370	66	Liquid Hydrogen	0.82
	423	72	Liquid Hydrogen	0.85
4330	RT	205	H_2O	0.24
4340	RT	> 200	NaCl + H_2O	0.20
6Al-4V-T_i Weldments	RT	200	NaCl + H_2O (spray)	> 0.70
	RT	235	NaCl + H_2O	> 0.70
	RT	170	NaCl + H_2O	> 0.70

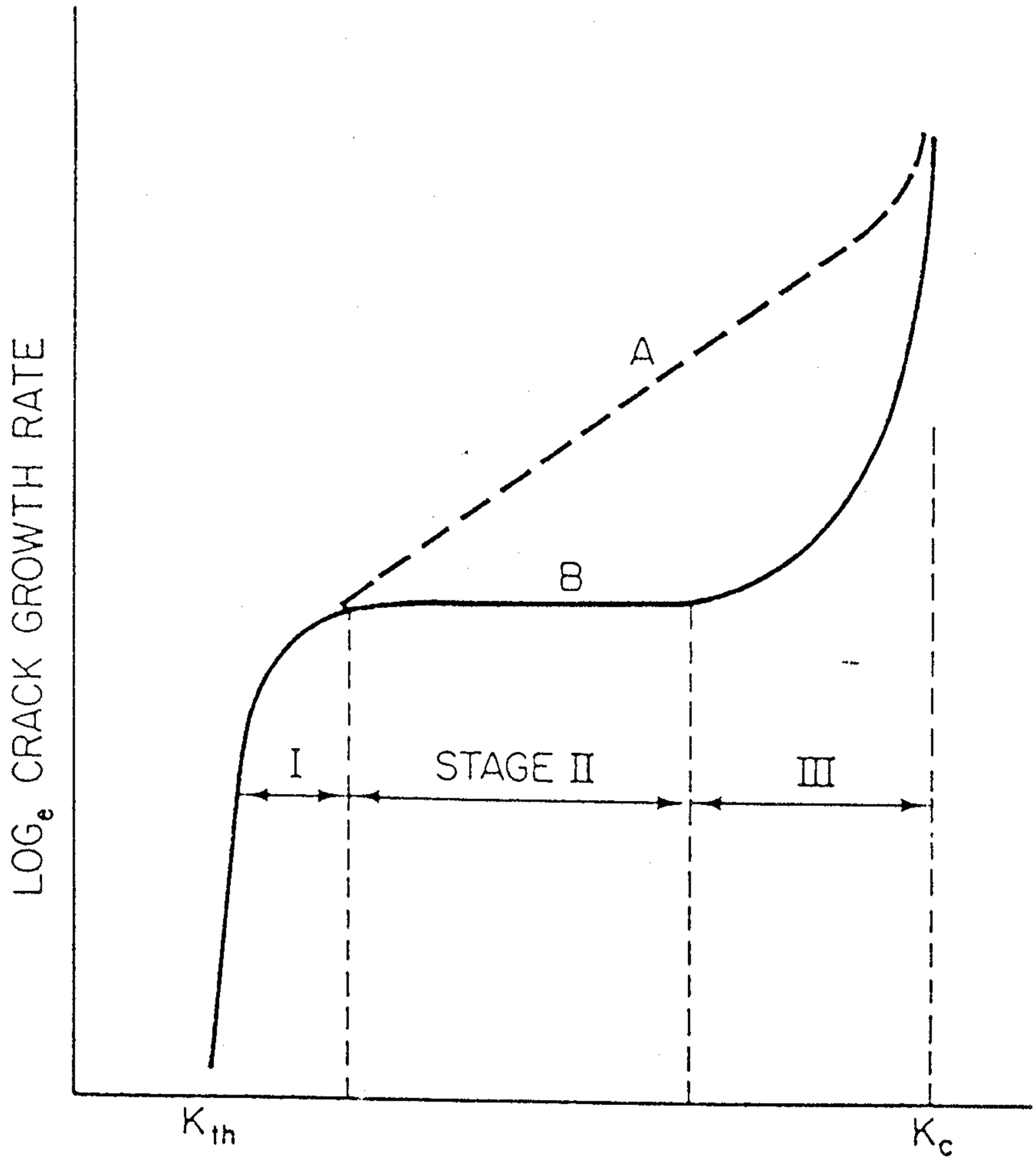


FIG. 10.17. Schematic illustration of the functional relationship between stress-intensity factor (K) and subcritical crack growth rate (da/dt).

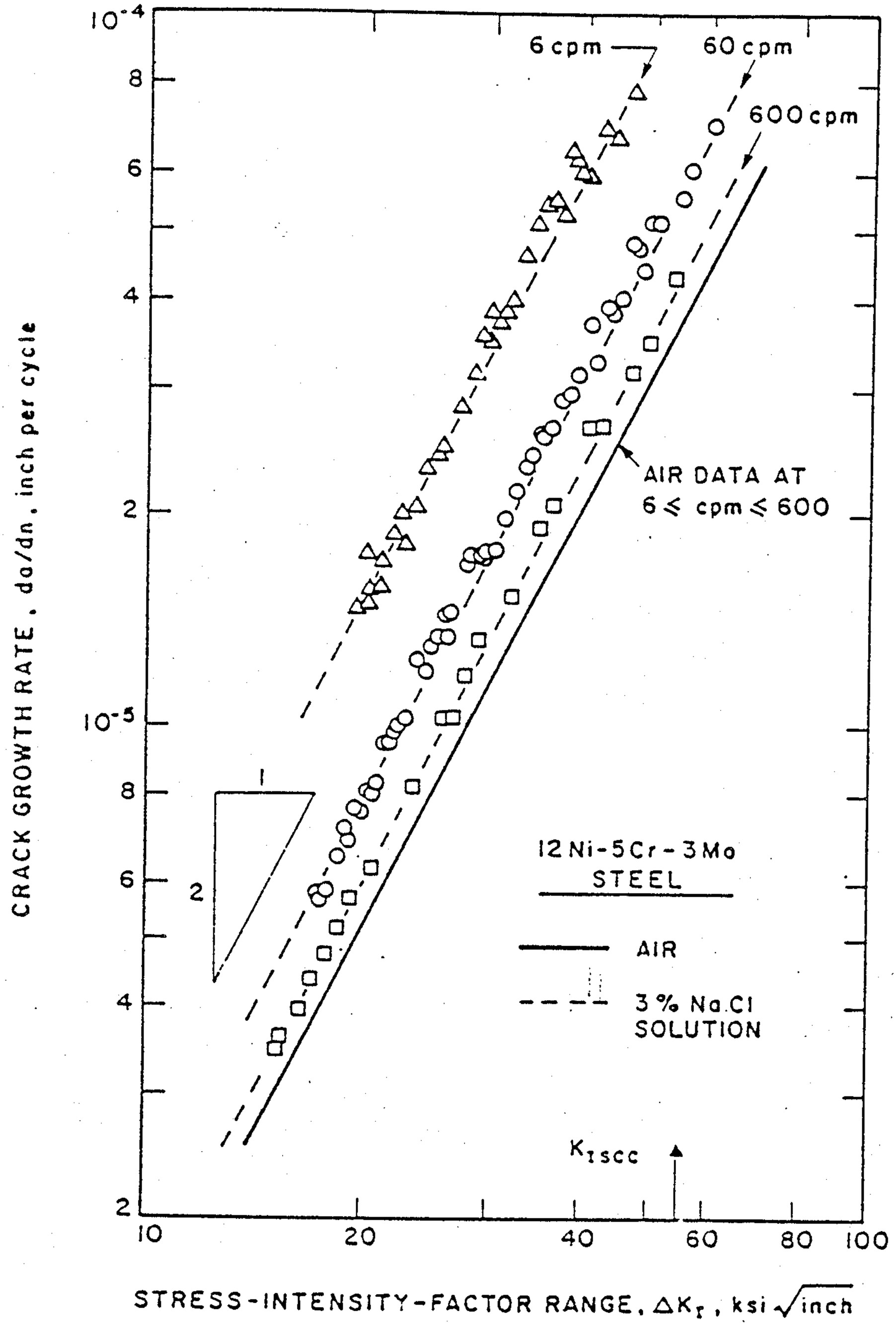


FIG. 11.2. Corrosion-fatigue-crack growth data as a function of test frequency.

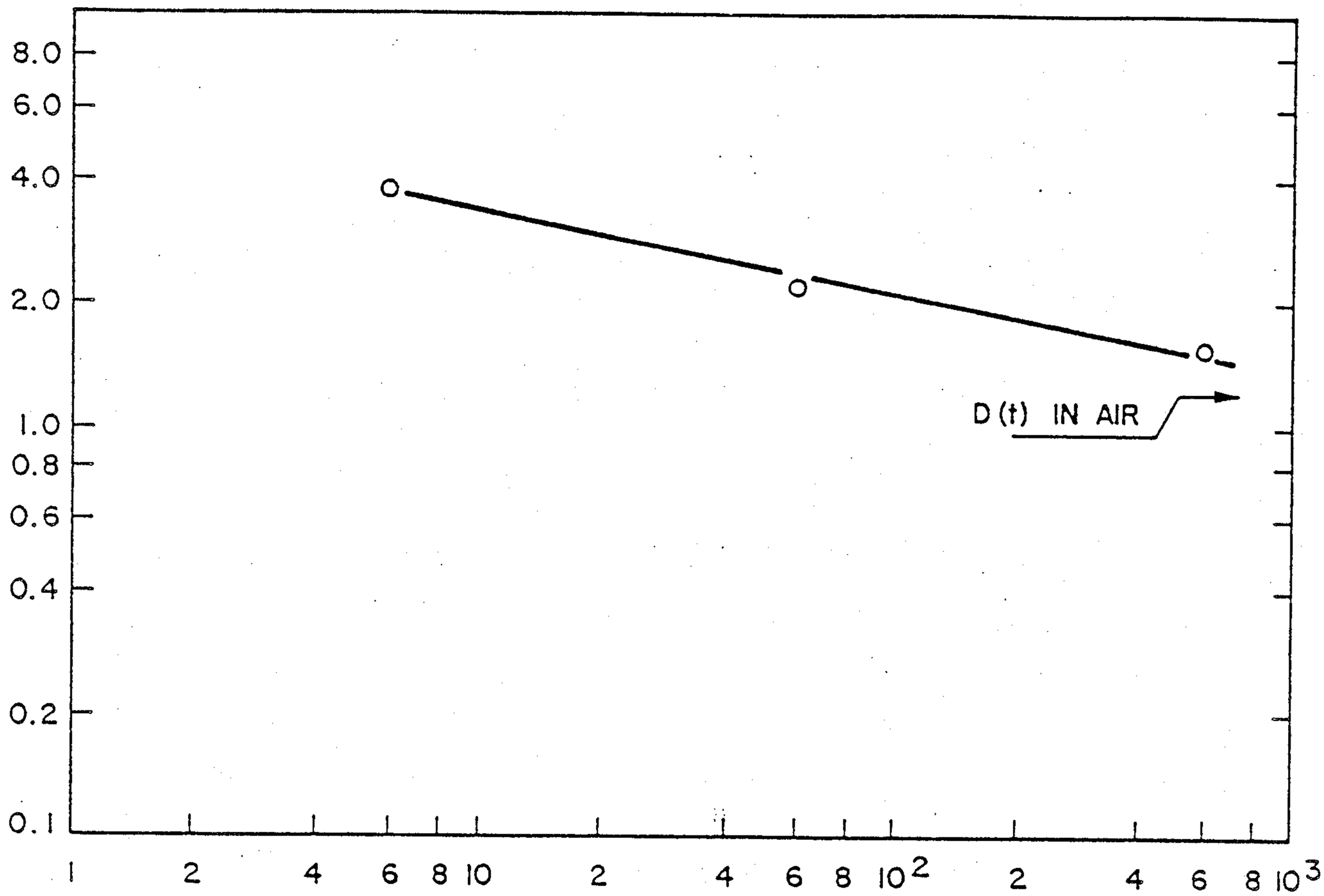


FIG. 11.3. Correlation between time-dependent function $D(t)$ and test frequency for 12Ni-5Cr-3Mo steel tested in sodium chloride solution.

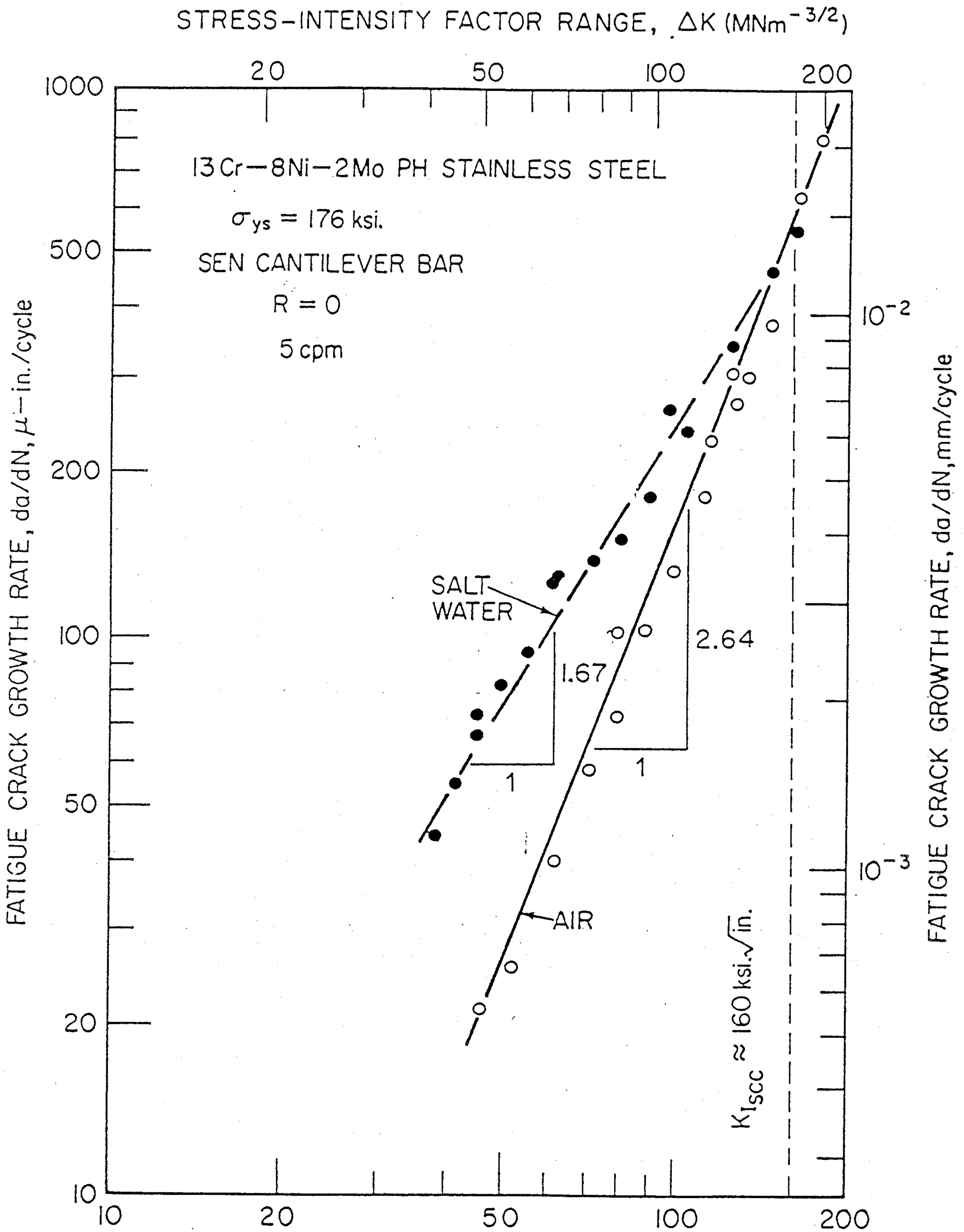


FIG. 11.4. Air and salt water fatigue crack growth rate behavior of 13Cr-8 Ni-2 Mo PH stainless steel.

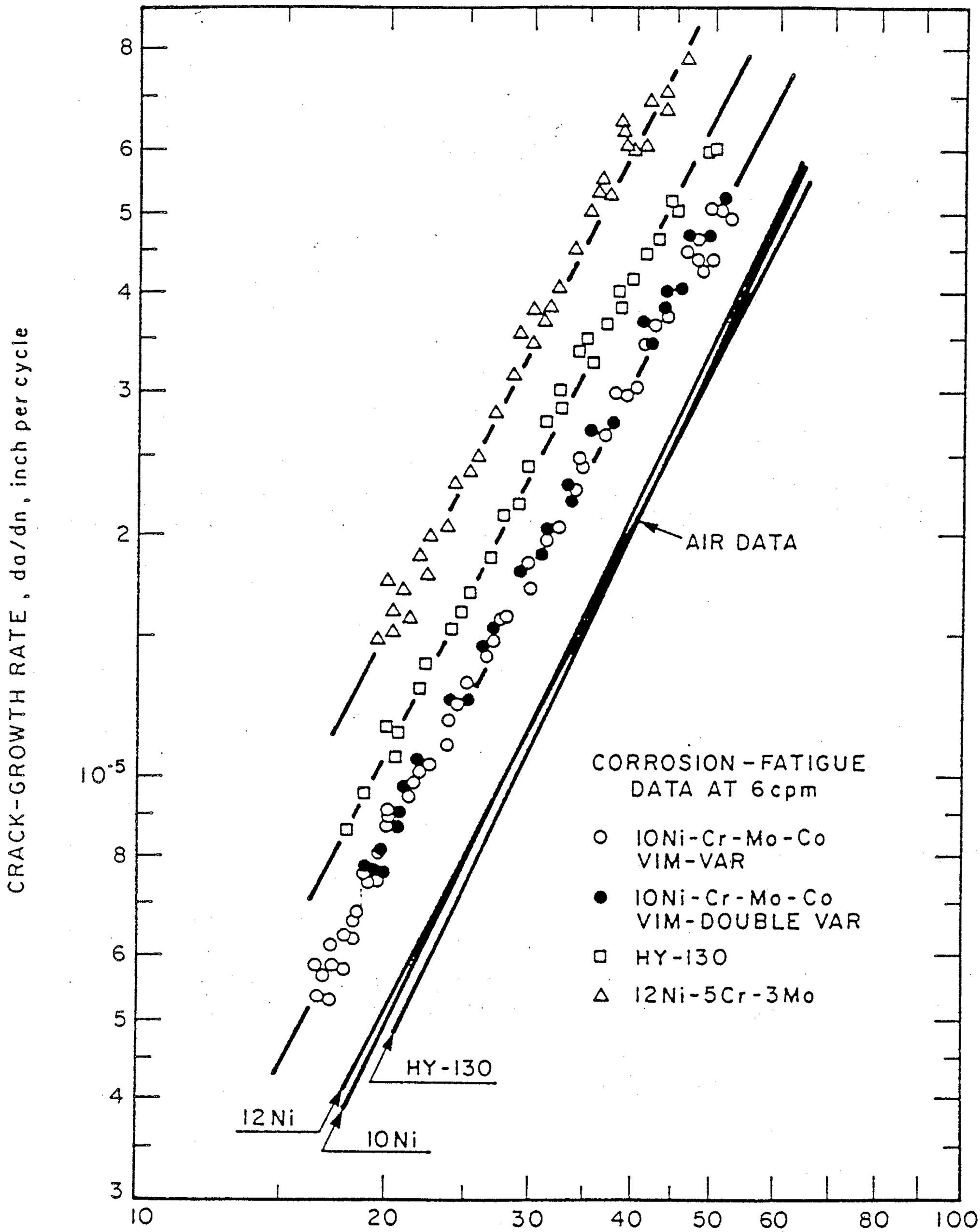


FIG. 11.5. Fatigue-crack-growth rates in air and in 3 % solution of sodium chloride below K_{Iscc} for various high-yield-strength steel.

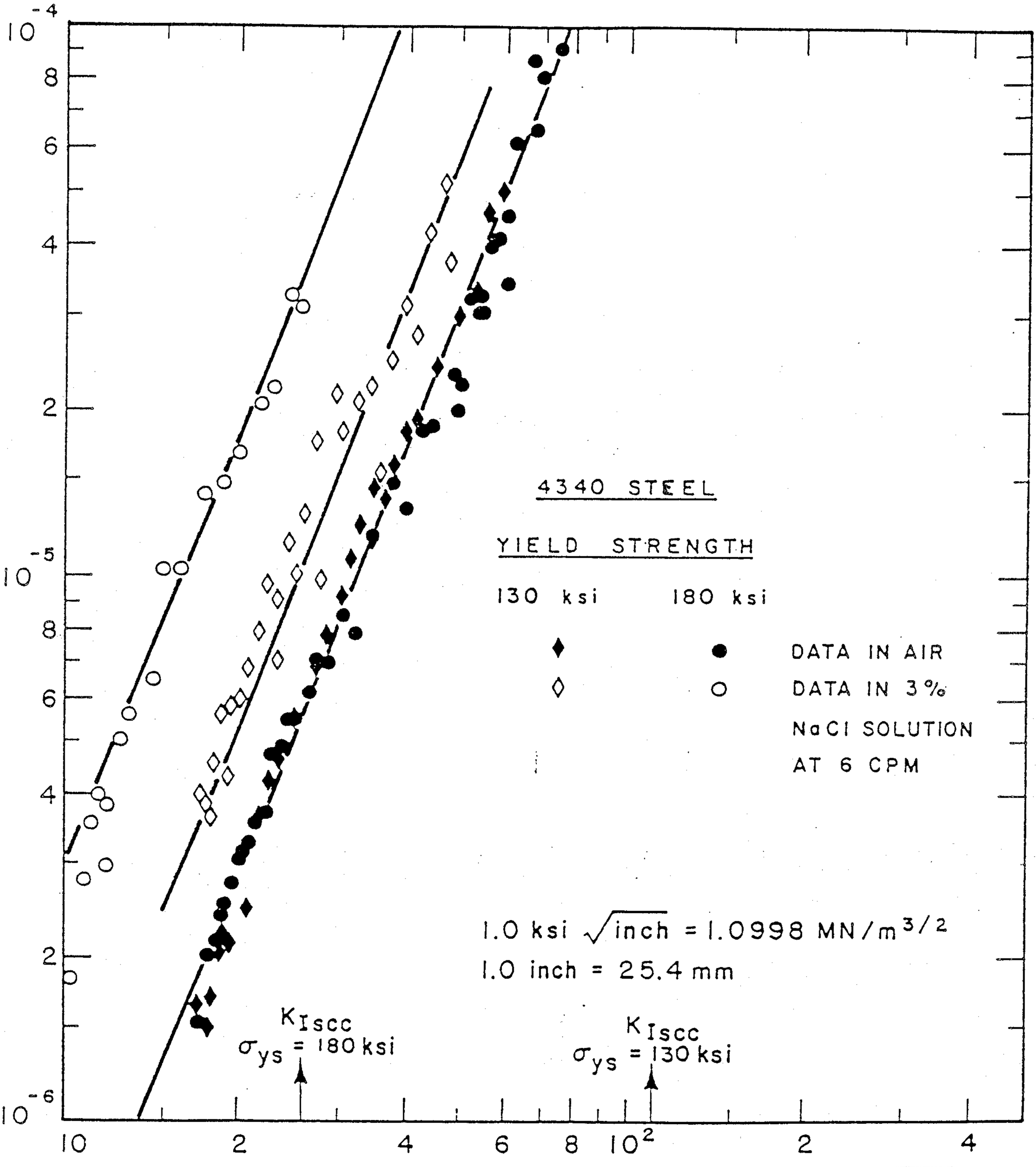


FIG. 11.6. Corrosion-fatigue-crack-growth data.

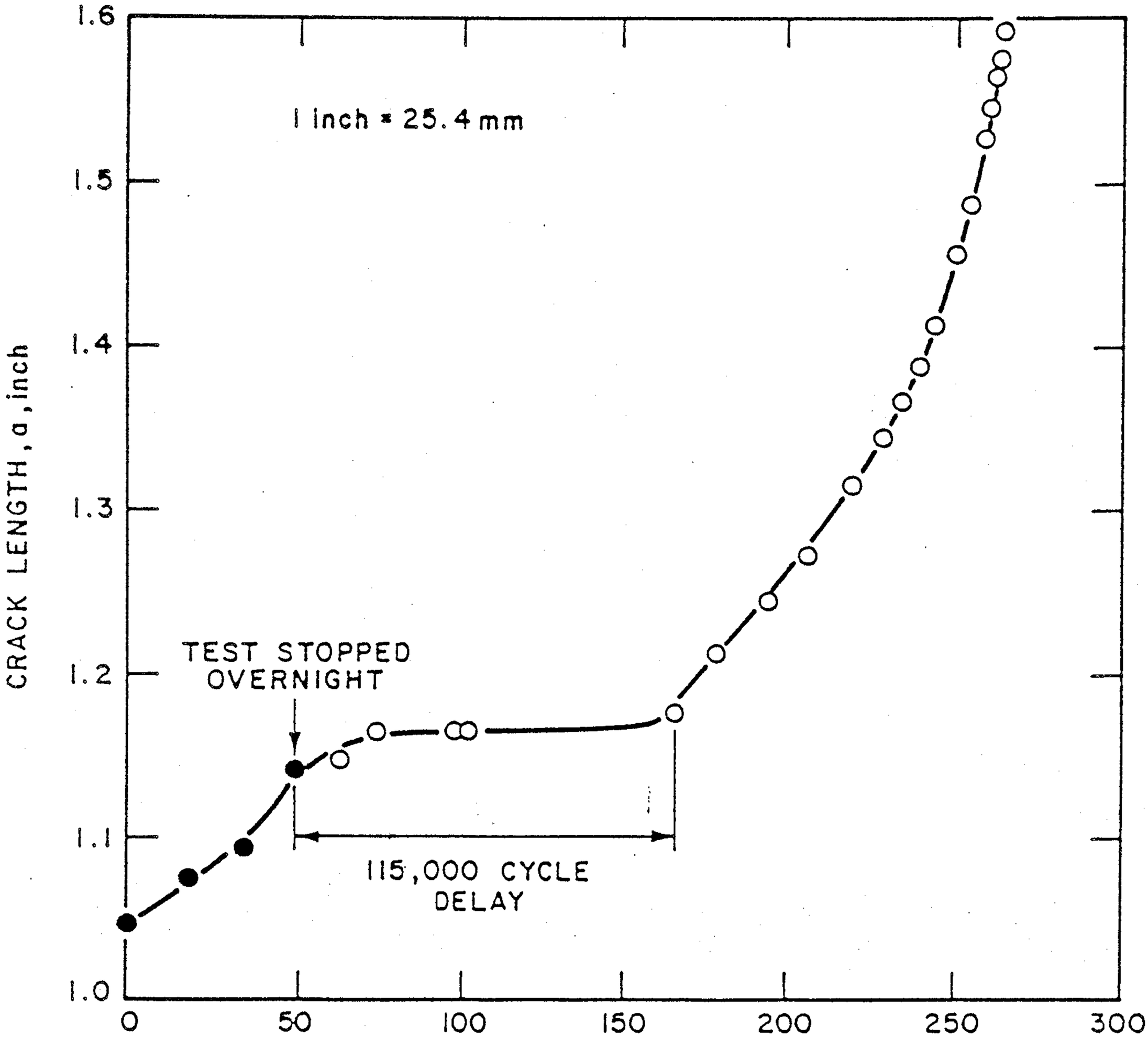


FIG. 11.21. Retardation of corrosion-fatigue-crack-growth rate under wet and dry environmental conditions for A514 Grade F steel.

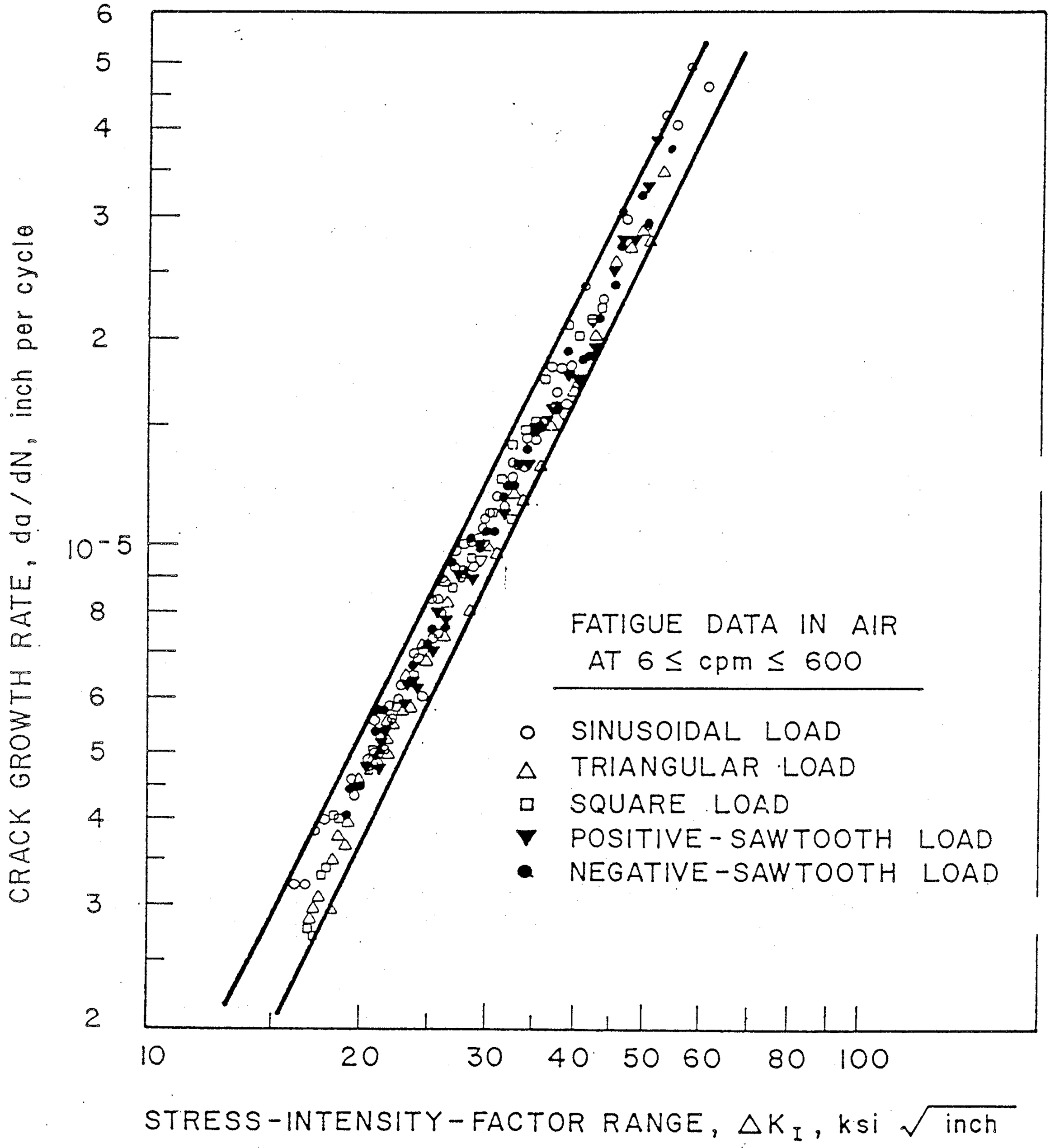


FIG. 11.22. Fatigue-crack-growth rates in 12Ni-5Cr-3Mo steel under various cyclic-stress fluctuations with different stress-time profiles.

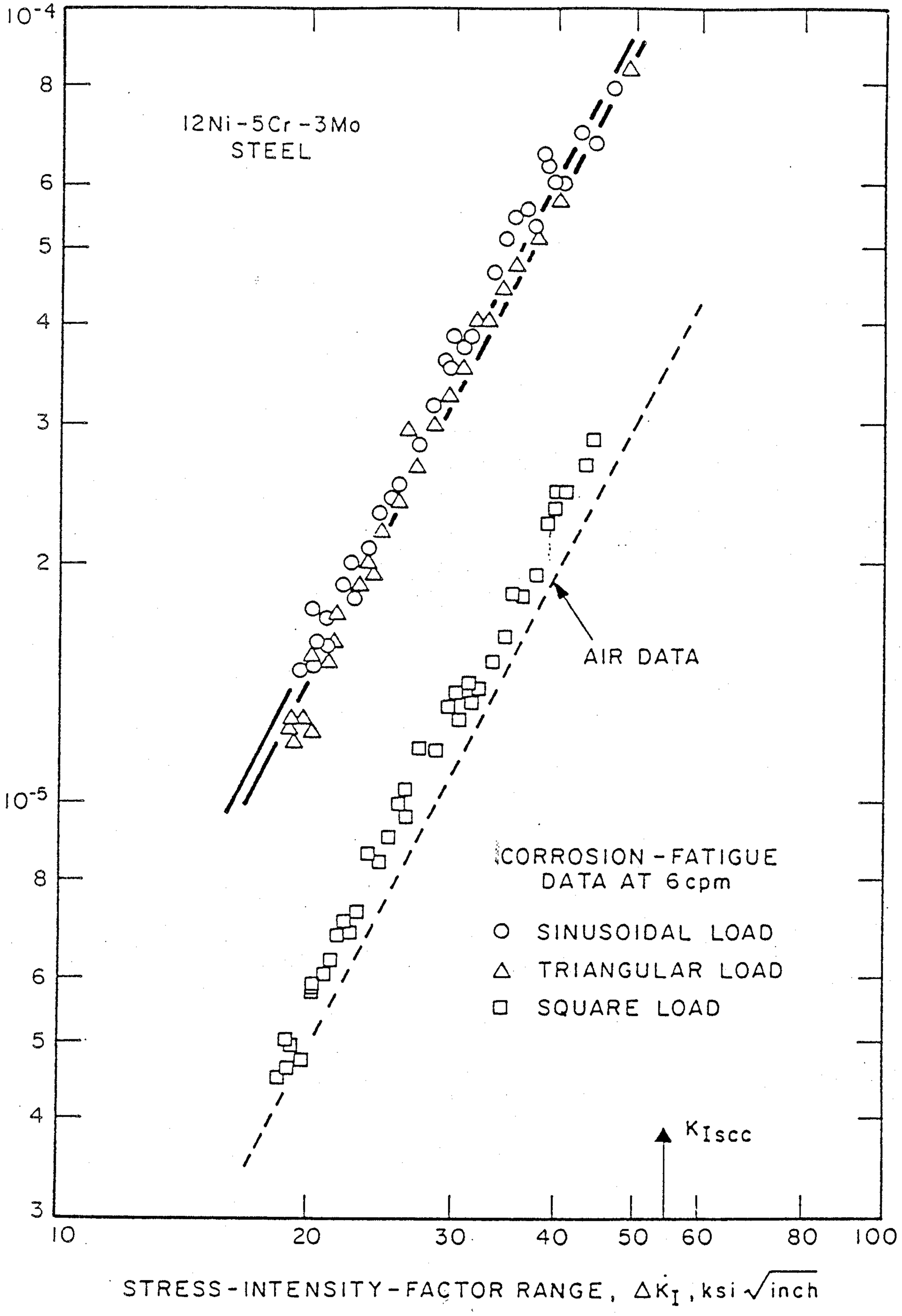


FIG. 11.23. Corrosion-fatigue-crack-growth rates below K_{Iscc} under sinusoidal, triangular, and square loads.

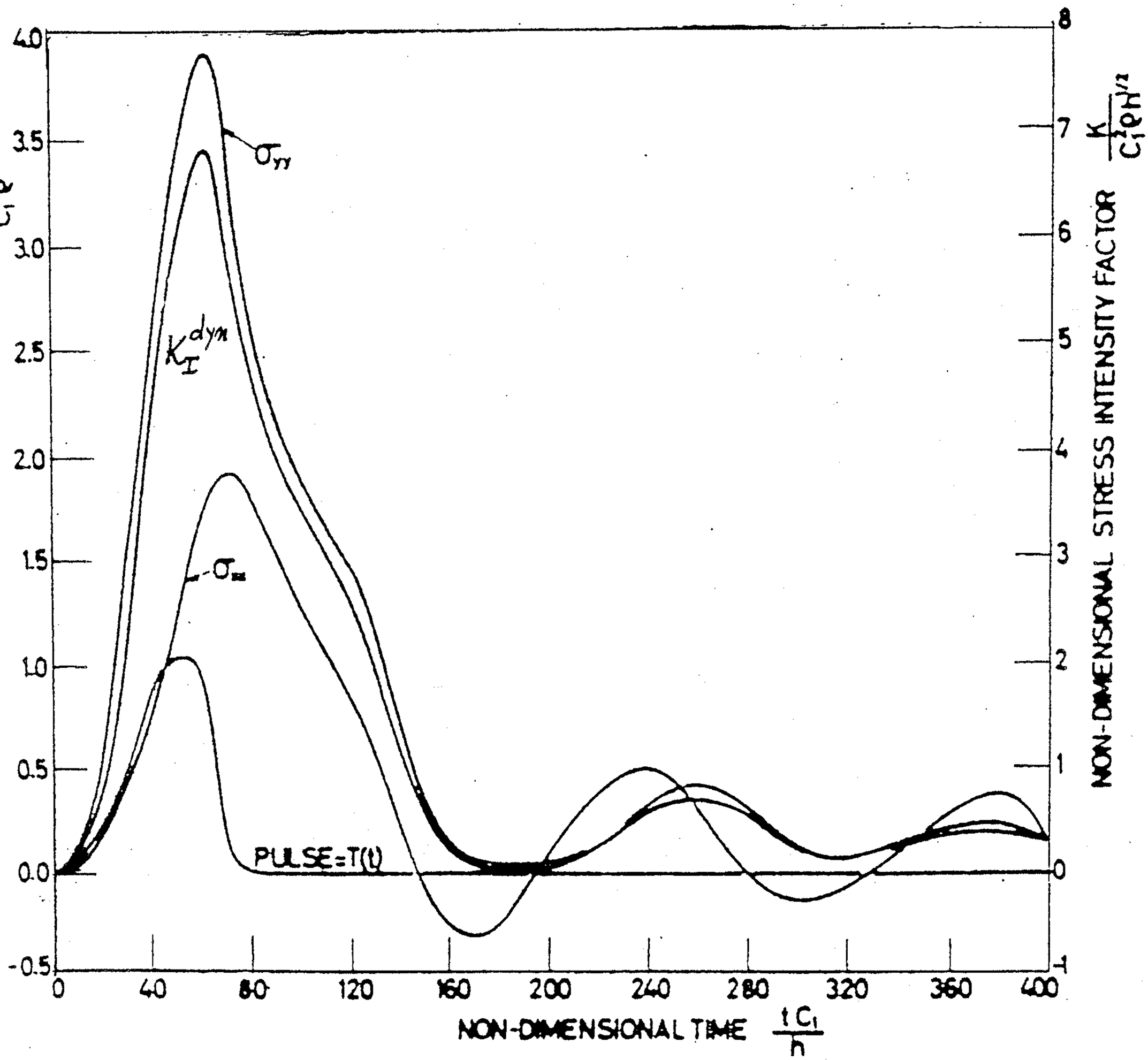


Fig. 7 Variation of Stresses Ahead of a Short Pulse Loaded Edge Crack Tip. a = 20h, L = 60h, H = 120h (see Fig. 1). Stresses are related to the point (x = a+0.5h, y=0); maximum $K_I^{stat}/C_1^2\rho h^{1/2}=8.88$.

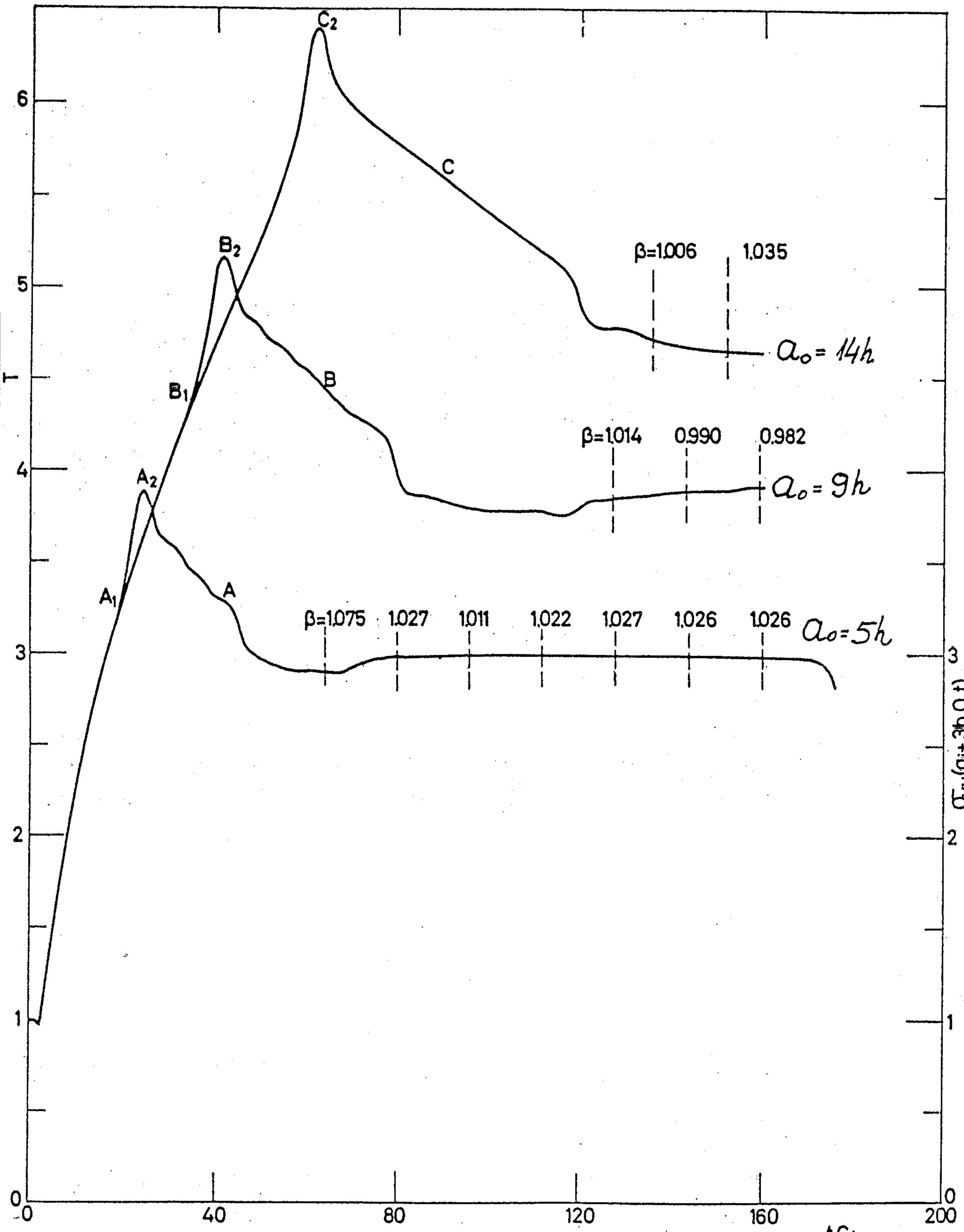


FIG. 2 NORMAL STRESSES AT THE FRONT OF THE CRACK TIP AND CRACK END SHAPES

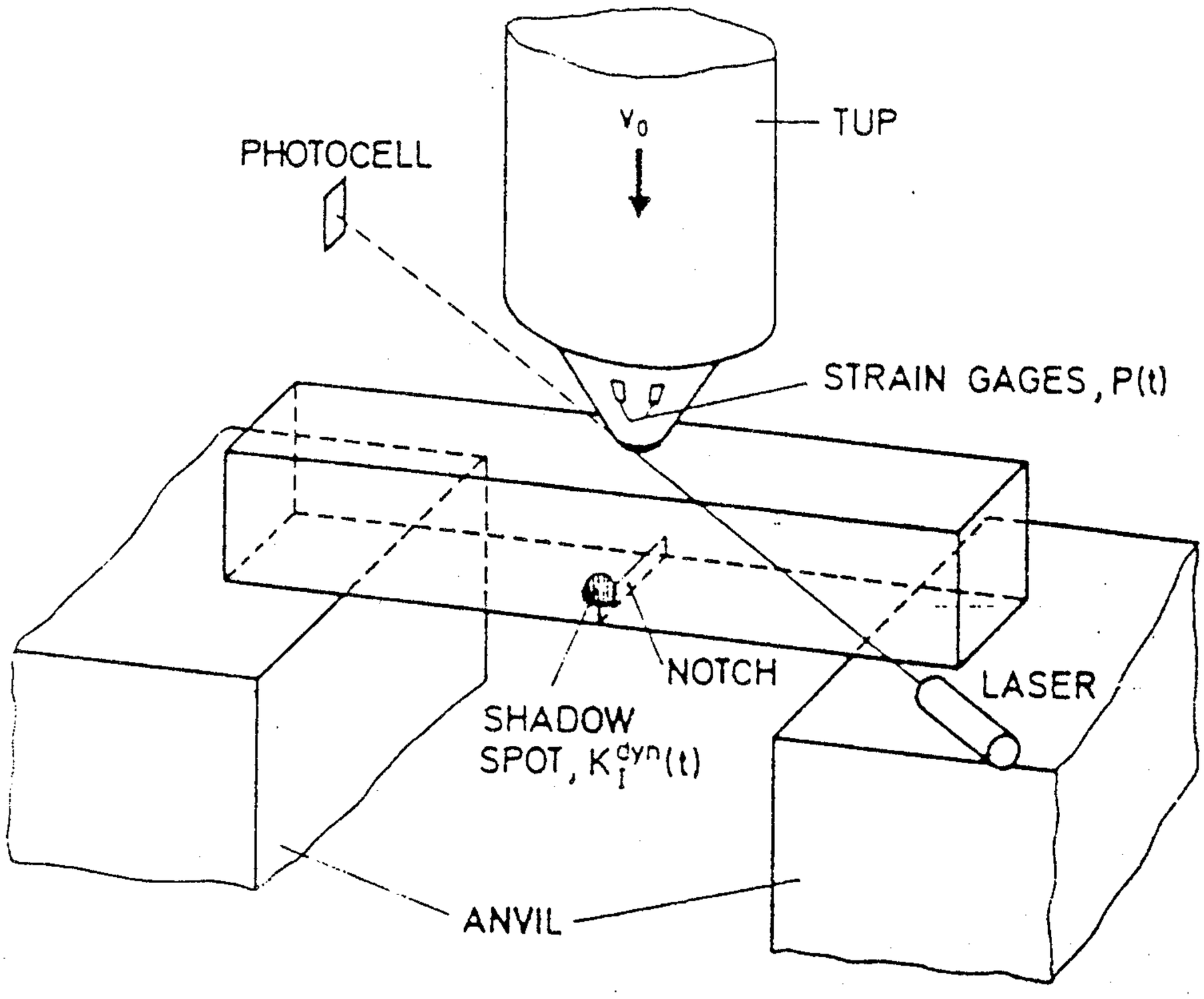


Figure 1. Experimental set up (schematically)

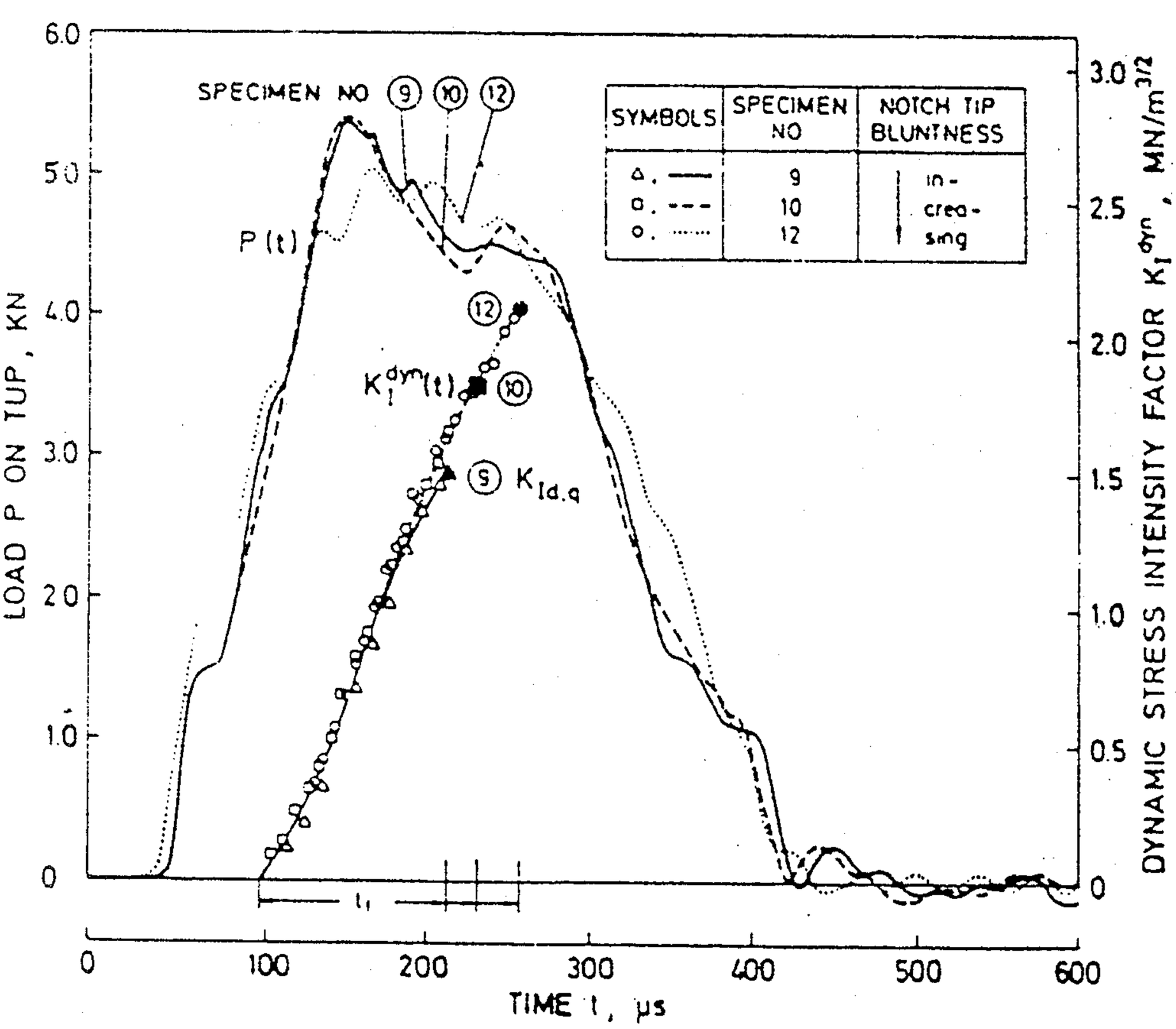


Figure 2. Comparison of the load and the stress intensity factor curves

The Spatial Distribution of the Stress Field Near the Tip of a Moving Crack

$$\sigma_{ij} = \frac{K_I^{dyn}(t)}{\sqrt{2\pi}} \cdot B(v) \cdot f_{I_{ij}}^{dyn}(r, \theta, v, c_l, c_s)$$

where:

$$B(v) = \frac{1+\alpha_s^2}{4\alpha_l\alpha_s - (1+\alpha_s^2)^2}$$

$$f_{I_{xx}}^{dyn} = (1+2\alpha_l^2-\alpha_s^2)\frac{\cos(\theta_{l/2})}{r_l^{1/2}} - \frac{4\alpha_l\alpha_s}{(1+\alpha_s^2)}\cdot\frac{\cos(\theta_{s/2})}{r_s^{1/2}}$$

$$f_{I_{xy}}^{dyn} = \frac{\sin(\theta_{l/2})}{r_l^{1/2}} - \frac{\sin(\theta_{s/2})}{r_s^{1/2}}$$

$$f_{I_{yy}}^{dyn} = -(1+\alpha_s^2)\frac{\cos(\theta_{l/2})}{r_l^{1/2}} + \frac{4\alpha_l\alpha_s}{(1+\alpha_s^2)}\cdot\frac{\cos(\theta_{s/2})}{r_s^{1/2}}$$

$$\alpha_l = \left(1-\frac{v^2}{c_l^2}\right)^{1/2} \qquad \alpha_s = \left(1-\frac{v^2}{c_s^2}\right)^{1/2}$$

$$r_l e^{i\theta_l} = \varepsilon + i\alpha_l\eta$$

$$r_l e^{i\theta_s} = \varepsilon + i\alpha_s\eta$$

$$K_I^{dyn} = k(v)\, K_I^{stat}$$

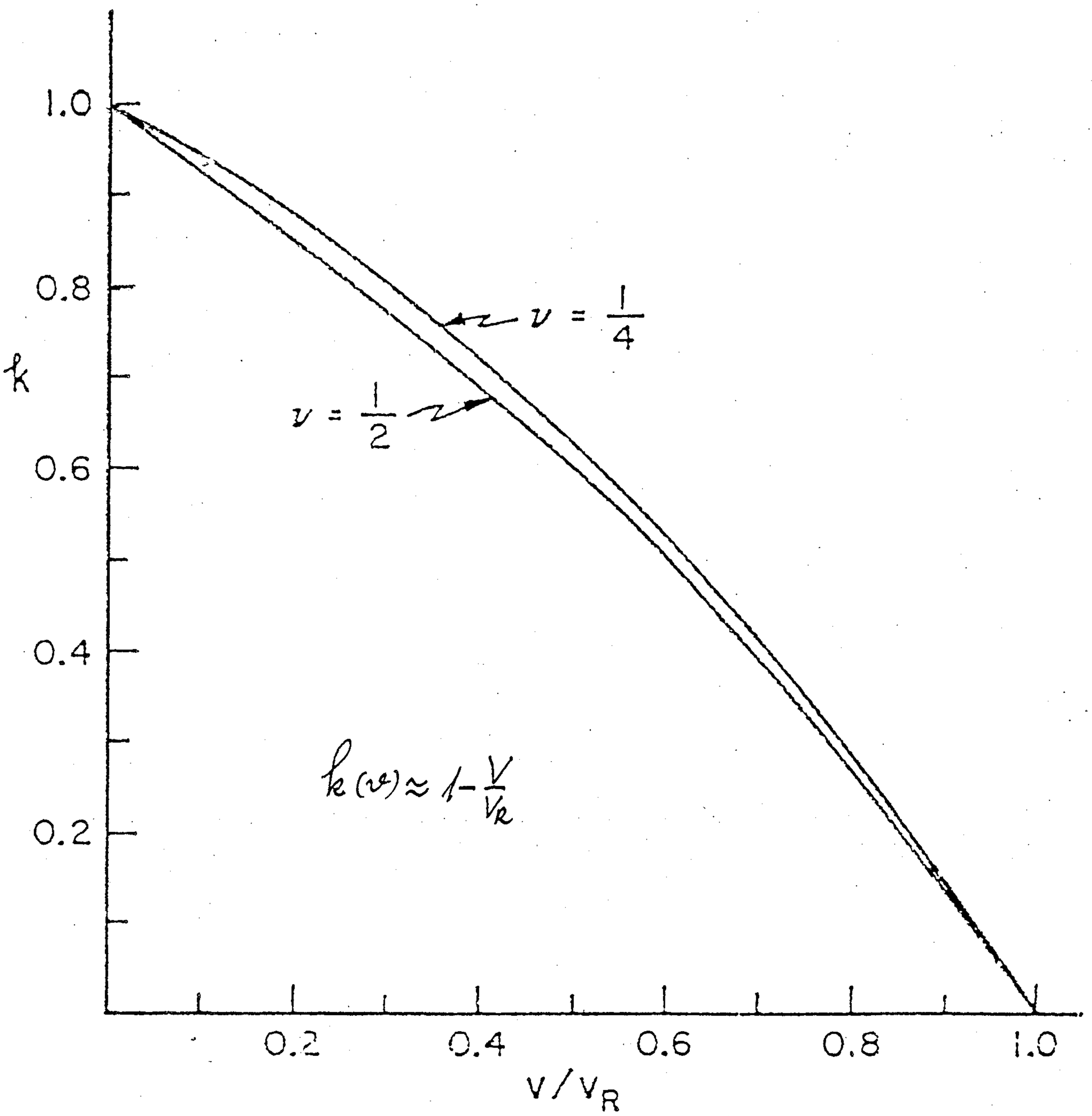
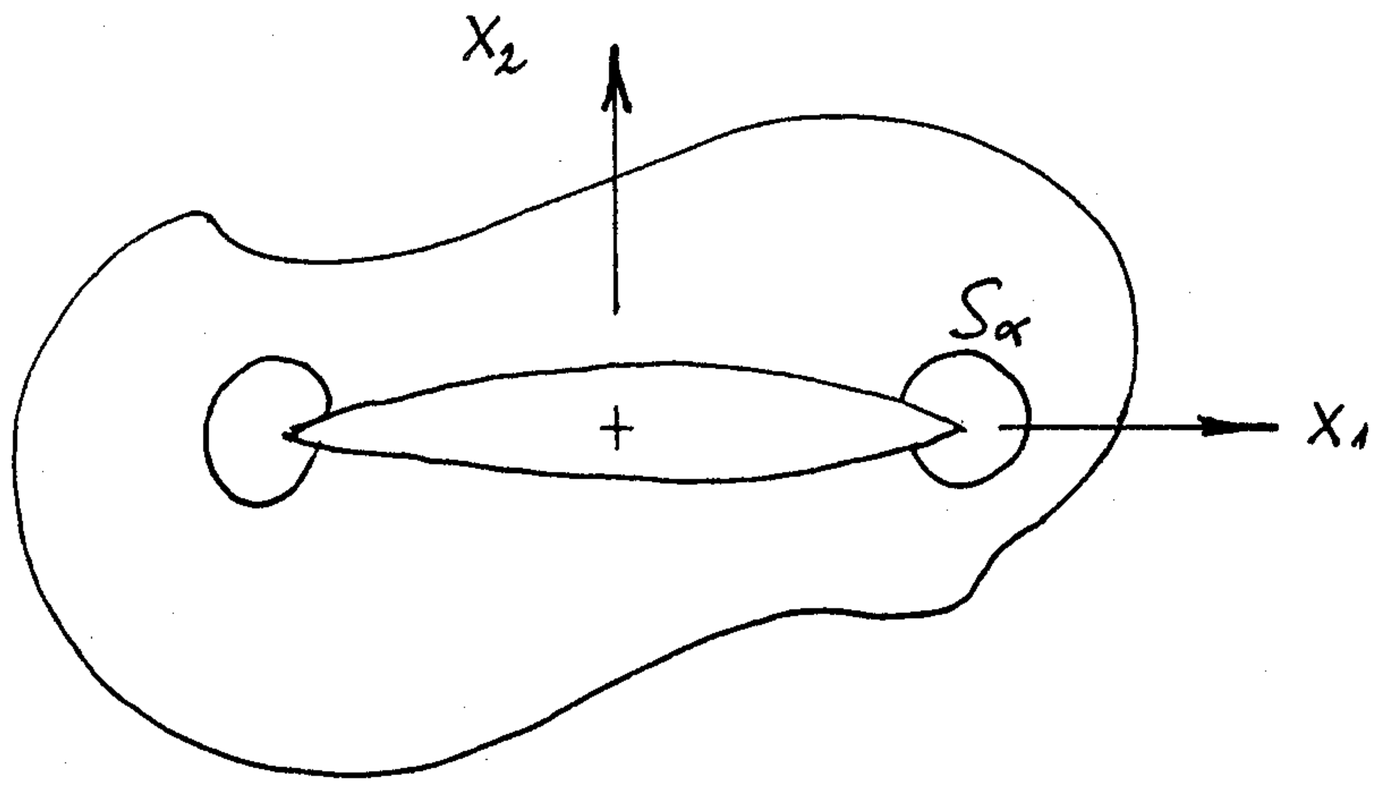


FIG. 2. The ratio of dynamic to static stress intensity factors vs. dimensionless crack speed for $\nu = 1/4, 1/2$.

The Energy Flux into a Moving Crack



$$F = \int_{S_\alpha} \left[\sigma_{ij} n_j \dot{u}_i + \frac{1}{2} \left(\sigma_{ij} u_{i,j} + \rho \dot{u}_i \dot{u}_i \right) V_x \right] dS$$

for $r \to 0$

$$F = \frac{1-\nu^2}{E} \frac{\nu^3 \alpha_1 \left(K_I^{dyn} \right)^2}{(1-\nu) c_s^2 \left[4\alpha_1 \alpha_s - (1+\alpha_s)^2 \right]}$$

$$G_{ID} = \frac{F}{V}$$

$$G_I^{dyn} = g(v)\, G_I^{stat}$$

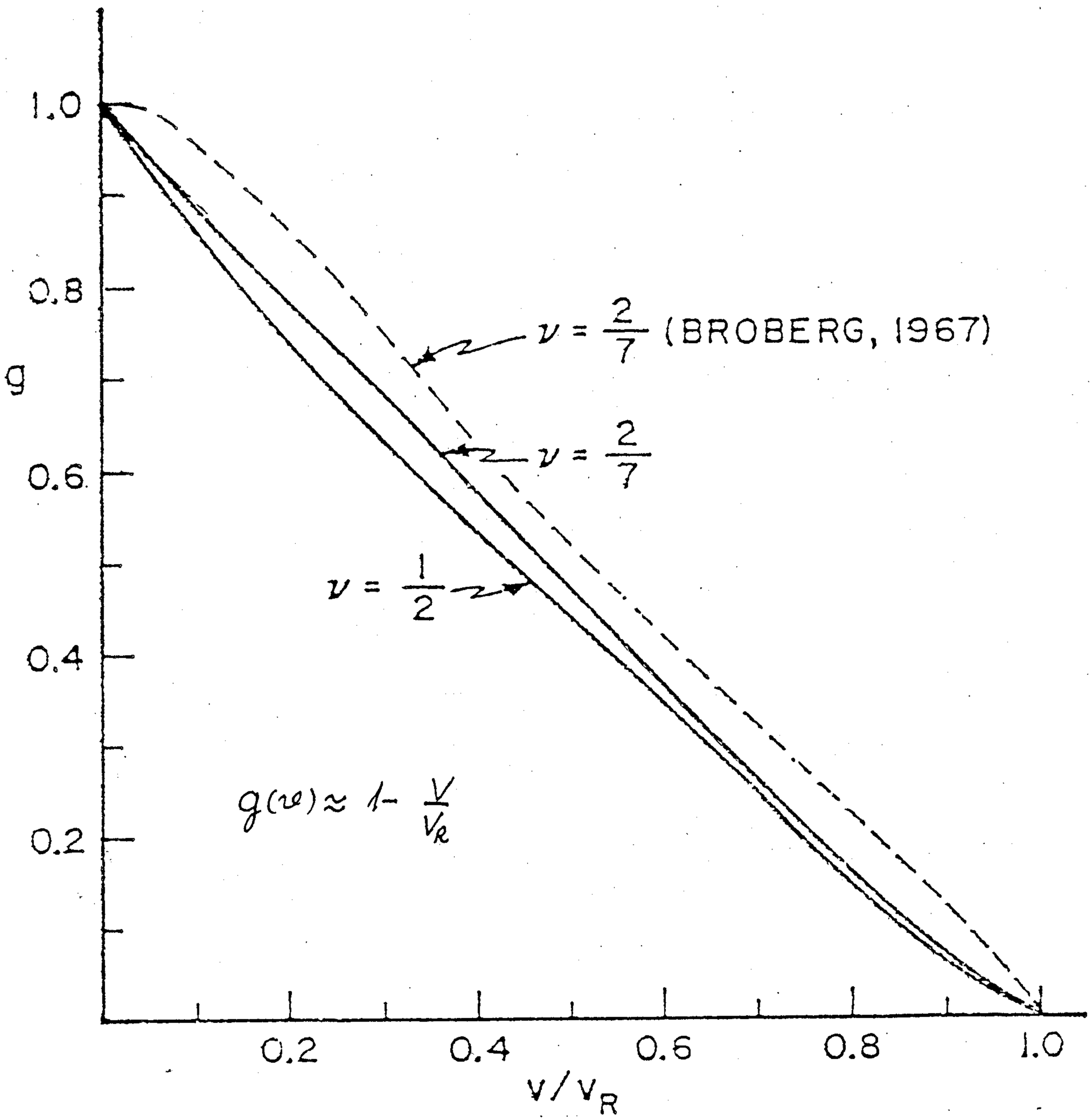


FIG. 4. The ratio of dynamic to static energy-release rates vs. dimensionless crack speed for $\nu = 2/7, 1/2$.

Static Results for the DCB Specimen

	a_o/H	$\sigma_{\eta\eta}(h/2,0)$	Jin	$K_I^{(1)}=\sigma_{\eta\eta}\sqrt{\pi h}$	$K_I^{(2)}=\sqrt{JinE}$	$K^{(1)}/K^{(2)}$	הסטיה ב- %
1	1.07087	0.64871	0.05319	0.2065	0.2036	1.0145	1.4
2	1.54748	0.39765	0.02068	0.1266	0.1269	0.9974	0.25
3	2.04724	0.25771	0.00896	0.0820	0.0835	0.9820	1.8
4	2.70866	0.15967	0.00352	0.0508	0.0524	0.9694	3.1
5	3.22835	0.11882	0.00201	0.0378	0.0396	0.9551	4.7